INSTITUTO POTOSINO DE INVESTIGACIÓN CIENTÍFICA Y TECNOLÓGICA, A.C.

Time-irreversibility indices and their application to the analysis of electrocardiograms

Tesis que presenta

Nazul Bonfilio Merino Negrete

Para obtener el grado de

Doctor en Control y Sistemas Dinámicos

Director de la Tesis:

Dr. César Octavio Maldonado Ahumada

San Luis Potosí, S.L.P., August 15, 2024

Constancia de aprobación de la tesis

La tesis **Time-irreversibility indices and their application to the analysis of electrocardiograms** presentada para obtener el Grado de Doctor en Control y Sistemas Dinámicos, fue elaborada por **Nazul Bonfilio Merino Negrete** y aprobada el **27 de agosto de 2024** por los suscritos, designados por el Colegio de Profesores de la División de Control y Sistemas Dinámicos del Instituto Potosino de Investigación Científica y Tecnológica, A.C.

Dr. César Octavio Maldonado Ahumada
Director de la tesis

Dr. Raúl Salgado García
Sinodal

Dr. Juan Gonzalo Barajas Ramírez
Sinodal

Dra. Paola Vanessa Olguín Rodríguez
Sinodal

Dr. Haret Codratian Rosu
Sinodal

Créditos Institucionales

Esta tesis fue elaborada en la División de Control y Sistemas Dinámicos del Instituto Potosino de Investigación Científica y Tecnológica, A.C., bajo la dirección del Dr. César Octavio Maldonado Ahumada.

Durante la realización del trabajo el autor recibió una beca académica del Consejo Nacional de Ciencia y Tecnología (612806) y del Instituto Potosino de Investigación Científica y Tecnológica, A. C.

Resumen

Presentamos un estudio de señales electrocardiográficas utilizando su irreversibilidad temporal. Realizamos un análisis exhaustivo de los datos clasificándolos en tres categorías diferentes, a saber, (1) la señal electrocardiográfica, (2) la señal de intervalos RR y (3) las señales de variabilidad conjunta. Se propone una técnica de codificación que nos permite un análisis conjunto de cualquier par de variables obtenidas en cada latido, a saber, la duración del latido y la amplitud de las ondas P, R y T. Nuestro método de codificación define particiones no uniformes del espacio de estados, lo que nos permite considerar las fluctuaciones típicas de la señal. Utilizamos directamente las secuencias simbólicas de las señales para construir empíricamente estimadores de irreversibilidad temporal encontrados en la literatura, a saber, el estimador de la *Tasa de Producción de Entropía*, el estimador de la *Divergencia de Kullback-Leibler* y el estimador del *Tiempo de Coincidencia*. Además, introducimos un estimador de irreversibilidad temporal, la *Función de Irreversibilidad Desfasada*.

Aplicamos nuestra metodología a cuatro conjuntos de datos, a saber, sujetos sanos jóvenes y ancianos, pacientes con fibrilación auricular y con insuficiencia cardíaca; estos datos se obtuvieron de la base de datos de libre acceso *PhysioBank*. Encontramos que al analizar la señal electrocardiográfica, es posible discriminar los cuatro grupos de pacientes utilizando los tres estimadores encontrados en la literatura. Sin embargo, en el caso de la señal de intervalos RR, no tenemos resultados concluyentes con estos estimadores, ya que no podemos distinguir el grupo de pacientes ancianos sanos de los grupos con condiciones médicas. Estos resultados mejoran cuando analizamos conjuntamente las señales de variabilidad. Por último, respaldamos nuestros resultados utilizando el análisis ROC, que demostró que nuestra metodología es eficiente hasta en el 90% de los casos cuando analizamos la señal electrocardiográfica utilizando su tasa de producción de entropía.

Palabras clave. Tasa de producción de entropía, electrocardiogramas, intervalos RR, señales de variabilidad, codificación, estimadores de irreversibilidad temporal, función de irreversibilidad desfasada, análisis ROC.

Abstract

A study of electrocardiographic signals using their time-irreversibility is presented. We achieved a comprehensive analysis of the statistical features of the data by classifying them into three different categories, namely, (1) the electrocardiographic signal, (2) *RR*-intervals signal and (3) joint variability signals. We propose an encoding technique that allows us a joint analysis of any pair of variables obtained in each heartbeat, namely, the duration of the heartbeat and the amplitude of the P, R, and T waves. Our encoding method defines partitions whose widths are not necessarily the same size, allowing us to consider the typical signal fluctuations. We directly use the symbolic sequences of the signals to empirically construct the time-irreversibility estimators found in the literature, namely, *Entropy Production Rate* estimator, *Kullback-Leibler Divergence* estimator and the *Matching Time* estimator. Additionally, we introduce an estimator for determining the time-irreversibility of a given process, the so-called *Lag Irreversibility Function*, whose main advantage is that the number of parameters to be estimated is relatively small compared to other methods.

We apply our methodology to four datasets, namely, young and elderly healthy subjects, patients with atrial fibrillation and with cardiac heart failure; these data were obtained from the free access database *PhysioBank*. We found that when analyzing the complete electrocardiographic signal, it is possible to discriminate the four groups of patients using the three estimators found in the literature. Still, in the case of the *RR*-intervals signal, we do not have conclusive results with these estimators, since we cannot distinguish the group of healthy elderly patients from the groups with medical conditions. These results improve when we jointly analyze the variability signals. Finally, we support our claim using the ROC analysis, which showed that our methodology is efficient in up to 90% of the cases when we analyze the electrocardiographic signal using its entropy production rate.

Keywords: entropy production rate, electrocardiograms, *RR*-intervals, variability signals, encoding, time-irreversibility estimators, lag irreversibility function, ROC analysis.

Contents

List of Tables

List of Figures

Chapter 1

Introduction

An intrinsic property of irreversible thermodynamic processes is the breaking of time-reversal symmetry of the microscopic trajectories, which is manifested by the entropy production of the process [1]. This feature is common in most real-life processes, such as chemical reactions [2] and living systems [3]. Then, the study and quantification of time-irreversibility in such systems might be useful for their general understanding. In particular, in biological time series, there is an increasing interest in assessing the directionality of the processes. For instance, time irreversibility in DNA sequences [4], entropy production in whole-brain models of consciousness levels [5], in Spike Trains [6], as well as, irreversibility in human heart rate analysis [7], and so on. Furthermore, time-irreversibility is important from a theoretical point of view, since it is related to the presence of non-linear correlations as well as the presence of non-Gaussian fluctuations, among other interesting properties [8]. All these characteristics of time-irreversibility as a tool for understanding systems of different natures have encouraged its study.

In this regard, several approaches have been proposed to recognize and quantify time-irreversibility in time series. The most natural way to quantify temporal irreversibility is through the comparison of the probability distribution of the trajectories of the process and its temporal reversal [9]. Perhaps the best-known quantity as a measure of time-irreversibility in discrete symbolic sequences is the Kullback-Leibler Divergence between the process forward and backward in time ([10], [11]). In [8], it is given an algorithm to detect time-irreversibility by a symbolization of the time series and comparing the frequency of words and their time-reversed counterparts. Many other indices of time-irreversibility can be used in time-series analysis, such as permutation patterns [12], visibility graphs [13], recurrence-time statistics ([14], [15]) and so on (see for instance [16] and the references therein, for a review and further details).

In this work, we are particularly interested in the time-irreversibility of electrocardiographic signals. The main idea underlying the present analysis is that cardiac activity in healthy conditions should display a more evident broken time-symmetry than in non-healthy conditions. The latter means that in healthy patients, the succession of waves, segments and intervals of the electrocardiogram have an orderly behavior such that it is possible to distinguish the *arrow of time* (see Section 3). This may not be true in non-healthy conditions where the the fluctuations of these signal components are less regular. This phenomenon might cause time-irreversibility to decrease in the presence of

diseases and aging. This behavior of temporal–irreversibility in electrocardiograms may be useful in understanding how cardiac electrical activity discloses abnormal functionality of cardiac cycle leading to diseases or heart health disorders (as actually has been reported in [7]).

On the other hand, different approaches have been proposed to test time-irreversibility in electrocardiograms ([17], [7], [18]). One of them is based on the analysis of fluctuations in the heart rate variability through *Poincaré Plots* (see Section 7.2.1). Employing these graphs, it is possible to visualize the behavior of the heartbeat data and different authors have used it to estimate the time-irreversibility from the imbalance that exists between the instantaneous accelerations and decelerations of the heart rate (see for example [18–21]). Concerning the other methods, most of them carry out an encoding of the data and statistically analyze the dissimilarities between the patterns that are formed in the original sequence and the sequence reversed in time (see for example [7], [17,22,23]). In Section 7.2 we provide a review of the state-of-the-art methodology developed so far to quantify the time-irreversibility in electrocardiograms.

In this thesis, we study the time irreversibility of the cardiac electrical activity by means of the entropy production rate in the electrocardiographic signal. We perform our analysis by segmenting the signal into three different categories, namely, (1) the electrocardiographic signal, (2) RR-intervals and (3) joint variability signals; this allowed us to have a comprehensive analysis of the statistical features of the electrocardiograms. We propose an encoding technique that allows us a joint analysis of any pair of variables obtained in each heartbeat (see Section 8.10). With this method, we derive information about the oscillation of two important signal variables in each heartbeat, namely, the duration of the heartbeat and the amplitude of the P, R, and T waves. This joint analysis is important since each variability signal represents different stages of each heartbeat. Besides, with our encoding method, we define partitions for the state space of the signals in such a way that the typical fluctuations are considered; that is, we consider partitions whose width does not necessarily have the same size. After the data encoding process is completed, we directly use the symbolic sequences of these signals to construct the entropy production estimators, assuming that the system meets the Markovian property (see Section 8.5). Next, we compute the entropy production rate from the empirically constructed estimators, namely, *Entropy Production Rate* estimator, *Kullback-Leibler Divergence* estimator and the *Matching Time* estimator. Additionally, we introduce an estimator for determining the time-irreversibility of a given process, the so-called *Lag Irreversibility Function*, whose main advantage is that the number of parameters to be estimated is relatively small compared to other methods.

We apply our methodology considering four electrocardiograms dataset. The first and second groups correspond to young and elderly subjects without cardiac conditions, respectively. The third group considered corresponds to patients with atrial fibrillation.

Finally, the fourth group is made up of patients with congestive heart failure. The four electrocardiograms groups were obtained from the free database *PhysioBank* [24]. We found that when analyzing the complete electrocardiographic signal, it is possible to discriminate the four groups of electrocardiograms dataset using the three estimators found in the literature. Still, in the case of the heart rate variability signal, we do not have conclusive results with these estimators, since we cannot distinguish the group of healthy elderly patients from the groups with medical conditions. These results improve when we jointly analyze the fluctuations in each heartbeat duration and the wave amplitudes. This joint analysis of the signals has made it possible to discriminate the group of healthy elderly subjects from the ill groups. We support our claim using the ROC analysis (see Chapter 9), in which we obtain an accuracy of above 90% in the case of the entropy production rate using electrocardiograms. Moreover, achieving that level of accuracy with our methodology has the advantage that, concerning previous works, we use up to 30 minutes of electrocardiographic signal, compared with some previous works that use up to 24 hours (see for instance [17]).

1.1 Objetives of the thesis

The main objective of the thesis is to propose a methodology to distinguish between electrocardiograms of groups of patients under different medical conditions, using the approach of time-irreversibility of the signal. Achieving this objetive through the approach proposed in this thesis, sets the following research sub-objectives:

1. *State of art*. We will present a review of the state-of-the-art methodology developed so far to quantify the time-irreversibility of electrocardiograms.

2. *Electrocardiogram encoding*. We will propose an encoding technique that considers different features of the signal, such as the duration of the heartbeats and the amplitude of the waves, which are affected when a medical condition arises.

3. *Time-irreversibility estimator*. We will use the entropy production and the Kullback-Leibler divergence in order to quantify the irreversibility degree in the ECGs. Additionally, we will introduce the Lag-Irreversibility Function, which quantifies the degree of temporal asymmetry between the probability distribution of two joint events that are lagged in time, in the sequence in natural order and in the time-reversed sequence.

4. *Construction of estimators*. This goal consists of estimating, from the signal data, the parameters of theoretical irreversibility indicators.

5. *Electrocardiogram discrimination*. We will show that the entropy production rate in electrocardiograms can be used as a tool to discriminate between electrocardiograms of different groups of patients. As well as, the Lag-irreversibility function for joint variables.

Chapter 2

Preliminaries

For this thesis to be self-contained, in this chapter we introduce some basic definitions that will serve for further analysis. It is possible to find a large amount of literature on these subjects and the interested reader may look at these topics in [25–29], for instance. First, in Section 2.1, we define stochastic processes and the strong law of large numbers. In Section 2.2 we introduce Markov processes and some of their properties. In particular, in this section we address the issue of irreversible Markov chains. Next, in Section 2.3, we discuss the symbolic representation of time series analysis and its relationship with stochastic processes. The use of the autocorrelation function as a measure of predictability in time series is addressed in Section 2.4. Finally, The Kullback-Leibler Divergence is defined in Section 2.5. We emphasize that we analyze discrete time series, and consequently, the theory provided in this chapter focuses on the case of discrete data.

2.1 Basic definitions

Definition 2.1.1 (Probability measure)**.** *Given a measurable space* $(\Omega, \mathscr{F})$*, the mapping* $\mathbb{P} : \mathscr{F} \mapsto [0, 1]$ *is a probability measure if it satisfies:*

1. $\mathbb{P}(\emptyset) = 0$, $\mathbb{P}(\Omega) = 1$;
2. $\mathbb{P}(A) \geq 0, \forall A_i \in \mathscr{F}$;
3. *For* $A_1, A_2, ...$ *with* $A_i \cap A_j = \emptyset$, $i \neq j$ *then*

$$\mathbb{P}(\cup_{i=1}^{\infty} A_i) = \sum_{i=1}^{\infty} \mathbb{P}(A_i).$$

Definition 2.1.2 (Probability space)**.** *A probability space is a three-tuple* $(\Omega, \mathscr{F}, \mathbb{P})$*, where* Ω *is a sample space,* $\mathscr{F}$ *is a* σ*-algebra of subsets of* Ω *and* $\mathbb{P}$ *is a probability measure on the measurable space* $(\Omega, \mathscr{F})$*.*

Definition 2.1.3 (Random variable)**.** *Let* $(\Omega, \mathscr{F}, \mathbb{P})$ *and* $(\mathbb{R}, \mathscr{B}(\mathbb{R}))$ *a probability space and measurable space, respectively, where* $\mathscr{B}(\mathbb{R})$ *are measurable Borel sets. A random variable over a probability space* $(\Omega, \mathscr{F}, \mathbb{P})$*, is a mapping* $X : \Omega \mapsto \mathbb{R}$ *measurable, that is,* $X^{-1}(B) \in \mathscr{F}, \forall B \in \mathscr{B}(\mathbb{R})$*.*

Given a random variable X, we can associate the *probability mass function* or *probability distribution* $p(x) = \mathbb{P}(X = x)$, which gives the probability that a random variable takes a specific value.

Definition 2.1.4 (Probability distribution)**.** *The probability distribution of a discrete random variable $p(x) = \mathbb{P}(X = x)$, is the mapping $p : \mathbb{R} \mapsto [0, 1]$, satisfying:*

1. *$p(x) \geq 0$;*
2. *$\sum_x p(x) = 1$.*

Definition 2.1.5 (Expected value)**.** *For a discrete random variable X with probability function $\mathbb{P}(X = x)$, with $i = 1, 2, ...n$, its expected value is defined as:*

$$E[X] = \sum_{i=1}^{n} x_i \mathbb{P}(X = x_i). \tag{2.1}$$

Definition 2.1.6 (Stochastic processes)**.** *Let $(\Omega, \mathscr{F}, \mathbb{P})$ be a probability space, $(\mathbb{R}, \mathscr{B}(\mathbb{R}))$ a measurable space and $T \subset \mathbb{N}$ an ordered set. A stochastic process $\mathcal{X}$, is a collection of random variables $\{X_n : n \in \mathbb{N}\}$, such that for each fixed $n \in T$, X_n is a random variable from the mapping $\mathcal{X} : T \times \Omega \mapsto \mathbb{R}$.*

Definition 2.1.7 (Almost sure convergence)**.** *Let us consider a sequence of random variable $\{X_n : n \in \mathbb{N}\}$. We say that $\{X_n : n \in \mathbb{N}\}$ converges almost surely (a.s.) to a random variable X if*

$$\mathbb{P}(\{\omega \in \Omega : \lim_{n\to\infty} X_n(\omega) \neq X(\omega)\}) = 0. \tag{2.2}$$

Equation (2.2) means that the set of events for which convergence does not occur has a measure equal to zero. We can also abbreviate this convergence as

$$\lim_{n\to\infty} X_n = X \quad a.s. \tag{2.3}$$

Definition 2.1.8 (Strong Law of Large Numbers)**.** *Let $\{X_n : n \in \mathbb{N}\}$ be a sequence of i.i.d. random variables defined on the same space, with expected value $\mu = E[X] < \infty$. Then*

$$\lim_{n\to\infty} \frac{1}{n} \sum_{j=1}^{n} X_j = \mu \quad a.s. \tag{2.4}$$

2.2 Markov processes

Definition 2.2.1 (Markov process)**.** *Consider a stochastic process $\mathcal{X} : T \times \Omega \mapsto \mathbb{R}$ defined in a probability space $(\Omega, \mathscr{F}, \mathbb{P})$, whose state space is $\mathbf{S}$ and $T \subset \mathbb{N}$. A stochastic*

process is said to be a Markov process or a Markov chain if for all $n \geq 1$ *and for all* $i_0, i_1, ..., i_n, j \in \mathbf{S}$*, it satisfies the Markov property:*

$$\mathbb{P}(X_{n+1} = j | X_n = i_n, X_{n-1} = i_{n-1}, ..., X_0 = i_0) = \mathbb{P}(X_{n+1} = j | X_n = i_n). \tag{2.5}$$

In a Markov process, the probability of knowing the future state of the process at time $n+1$ only depends on knowing the probability of being in a given state at present n. The right-hand side of Equation (2.5) is called *one-step transition probability*.

A Markov process is *stationary* or *time-homogeneous* if its transition probabilities do not depend on the time evolution, that is, for any $k \in T$, a stationary Markov process satisfies that

$$\mathbb{P}(X_{n+1} = j | X_n = i_n) = \mathbb{P}(X_{n+k+1} = j | X_{n+k} = i_n). \tag{2.6}$$

Definition 2.2.2 (Transition matrix)**.** *The transition matrix* P *of a stationary Markov process* $\mathcal{X}$*, is defined as:*

$$[P]_{i,j \in \mathbf{S}} = \mathbb{P}(X_1 = j | X_0 = i). \tag{2.7}$$

A transition matrix P describes the probabilities of moving from one state to another in a Markov process; the rows correspond to the current state ($X_0 = i$) and the columns to the future state ($X_1 = j$) of the process. A transition matrix P is a stochastic matrix if it has non-negative entries and $\sum_j p_{i,j} = 1$. The transition probability in n steps, is given by the (i, j) entry of the nth power of the transition matrix, i.e.:

$$\mathbb{P}(X_n = j | X_0 = i) = \left[P^{(n)}\right]_{i,j \in \mathbf{S}}. \tag{2.8}$$

Definition 2.2.3 (Stationary probability distributions)**.** *For a Markov process with transition probability* $P_{i,j}$*, its probability distribution* $\pi = (\pi_0, \pi_1, ..., \pi_n)$ *is stationary or invariant if*

$$\pi_j = \sum_i \pi_i P_{i,j}. \tag{2.9}$$

Equation (2.9) means that if the initial random variable X_0 has that distribution π, then the distribution of X_n is also π, that is, $\mathbb{P}(X_n = j) = \sum_i \pi_i P_{i,j}^{(n)} = \pi_j, \forall n \in \mathbb{N}$, which is a result of the fact that this distribution is independent of the time evolution. The latter can also be expressed in matrix terms by

$$\pi = \pi P^{(n)}, \forall n \in \mathbb{N}. \tag{2.10}$$

Let $\{X_n\}$ be a Markov chain realization with transition probabilities $P_{i,j}$ and stationary distribution π. Consider the process $\{Y_n\} = \{X_{m-n}\}$ for $n = 0, 1, ..., m$, that is, $\{Y_n\}$ is the original chain but seen backwards, now from time m to time 0. It turns out that this new process $\{Y_n\}$ is also a Markov chain. To see this, we must verify that, for some integer $r \in \mathbb{N}$ such that $1 \leq r < n \leq m$, it holds that

$$\mathbb{P}(Y_r = j|Y_{r-1} = i_{r-1}, Y_{r-2} = i_{r-2}, ..., Y_0 = i_0) = \mathbb{P}(Y_r = j|Y_{r-1} = i_{r-1}),$$

which, in terms of process $\{X_n\}$, can be expressed as

$$\mathbb{P}(X_{m-r} = j|X_{m-r+1} = i_{m-r+1}, X_{m-r+2} = i_{m-r+2}, ..., X_m = i_m) = \mathbb{P}(X_{m-r} = j|X_{m-r+1} = i_{m-r+1}).$$

Next, suppose that the present time is $m - r + 1$. Since $\{X_n\}$ is a Makov process, then the future time states $X_{m-r+2}, X_{m-r+3}...$ are independent of the past time state X_{m-r}. On the other hand, independence is a symmetric property, that is, if A is independent of B, then B is independent of A. This implies that past time state X_{m-r} is independent of future time states $X_{m-r+2}, X_{m-r+3}...$, which is what we wanted to verify.

One may ask whether this new process $\{Y_n\}$, which is the time reversal version of $\{X_n\}$, up to time m, is indistinguishable from $\{X_n\}$, i.e., one may wonder whether the process $\{X_n\}$ is reversible within the finite time interval $\{0, 1, ..., m\}$. In other words, we would like to know if the path probability distribution for $\{X_n\}$ y $\{Y_n\}$ coincides. The following definition of reversible Markov chains can help answer these questions.

Definition 2.2.4 (Reversible Markov processes)**.** *A Markov process with transition probabilities P_{ij} and stationary distribution π is reversible in time if for any states $i, j \in \mathbf{S}$, it satisfies that:*

$$\pi_i P_{i,j} = \pi_j P_{j,i}. \tag{2.11}$$

The Equation (2.11) is known as the *detailed balance equation*. When a Markov process does not meet the conditions of this equation, the process is said to be irreversible in time; that is, the probability distribution of the Markov process $\{X_n\}$ differs from the probability distribution of the process $\{Y_n\}$. Such processes are characterized by their entropy production rate (see Section 3.3.1).

2.2.1 Some properties of Markov processes

Definition 2.2.5 (Irreducible Markov processes)**.** *States i and j are said to be communicating if $m \geq 0$ and $n \geq 0$ exist, such that $P_{i,j}^{(m)} > 0$ and $P_{j,i}^{(n)} > 0$. A Markov chain is irreducible if $\forall i, j \in \mathbf{S}$ there exist $m \geq 0$ and $n \geq 0$ such that $P_{i,j}^{(m)} > 0$ and $P_{j,i}^{(n)} > 0$. That is, a Markov chain is irreducible if all states communicate with each other.*

Let $\{X_n\}$ be a Markov chain realization and $A \subset \mathbf{S}$. The time of first visit to set A is the random variable:

$$\mathcal{T}_A = \begin{cases} min\{n \geq 1 : X_n \in A\} & if \quad X_n \in A \quad \text{for any} \quad n \geq 0 \\ \infty & \text{other way} \end{cases} \tag{2.12}$$

When set A consists of a single state j and the chain starts at state i, the time of the first visit to state j is written $\mathcal{T}_{i,j}$. A state i is considered recurrent if there exists n

such that $\mathbb{P}(\mathcal{T}_{i,i} = n) = \mathbb{P}(X_n = i|X_0 = i) = 1$, that is, the probability of eventually returning in a finite time n to i, starting from i, is one. Similarly, a state is transient if $\mathbb{P}(\mathcal{T}_{i,i} = n) = \mathbb{P}(X_n = i|X_0 = i) < 1$.

Definition 2.2.6 (Positive recurrent Markov processes)**.** *The mean recurrence time of a recurring state j from a state i is defined as the expectation of $\mathcal{T}_{i,j}$, and is denoted by $\mu_{i,j} = E(\mathcal{T}_{i,j}) = \sum_{n=1}^{\infty} n\mathbb{P}(\mathcal{T}_{i,j} = n)$. A state i is said to be positive recurrent if $\mu_i < \infty$; is null recurrent if $\mu_i = \infty$.*

Definition 2.2.7 (Period)**.** *The period of a state i is a non-negative integer, defined as $d(i) = m.c.d.\{n \geq 1 : P_{i,i}^{(n)} > 0\}$, where m.c.d. means "greatest common factor". When $P_{i,i}^{(n)} = 0$ for all $n \geq 1$, we define $d(i) = 1$. In particular, a state i is said to be aperiodic if $d(i) = 1$. When $d(i) = k \geq 2$ it is said that i is periodic of period k.*

For an irreducible, positive recurrent and aperiodic Markov chain, its stationary distribution is unique and is given by $\pi_j = \frac{1}{\mu_j}$, which is the main statement for the *Ergodic theorem for Markov chains*, which we display below.

2.2.2 Ergodic theorem for Markov chains

Definition 2.2.8. *In a Markov chain realization $\{X_k\}$ of size n, the number of visits that a chain makes to state j, starting at state i, defines the random variable:*

$$N_{i,j}(n) := \sum_{k=1}^{n} \mathbb{1}_j(X_k), \tag{2.13}$$

where $\mathbb{1}_j(X_k)$ is a indicator function.

Theorem 2.2.1 (Ergodic theorem for Markov chains)**.** *For any states i and j of an irreducible Markov chain it holds that:*

$$\lim_{n\to\infty} \frac{N_{i,j}(n)}{n} = \frac{1}{\mu_j} \quad a.s. \tag{2.14}$$

Equation (2.14) tells us that for an irreducible Markov chain, the average time, in the limit, that the chain spends in a state j, is given by its stationary distribution $\pi_j = \frac{1}{\mu_j}$, which constitute the only solution to the system of equations $\pi = \pi P$.

2.3 Time series analysis

A discrete time series is a sequence of observed data indexed according to the order in which they were obtained in uniform time intervals, which we denote as

$$Y := \{Y_t : t \in \mathbb{N}\}. \tag{2.15}$$

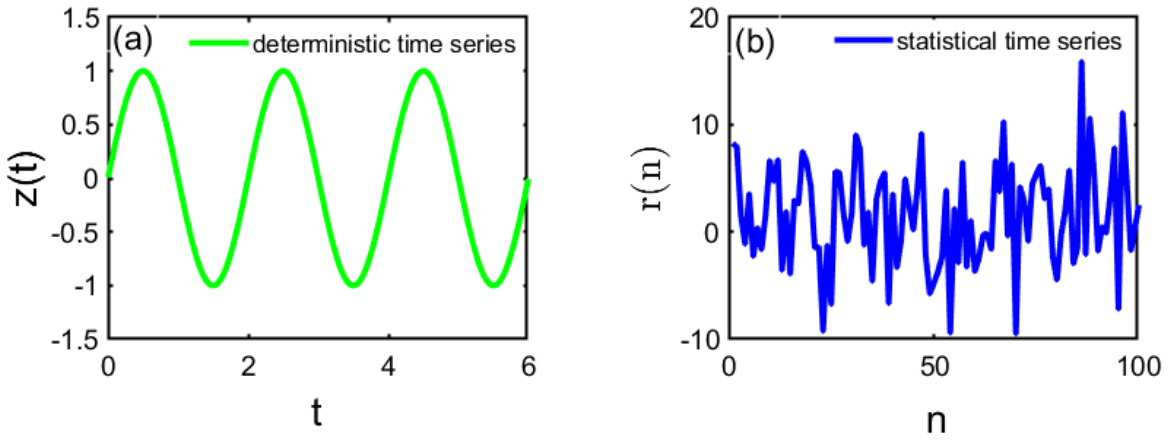

Figure 2.1: (a) Deterministic time series. The sinusoidal function $z(t)$ was simulated for a frequency $\omega = 0.5$ and $t = 6$ seconds. (b) Statistical time series. Using $\mu = 1$ and $\sigma = 5$, we generate $n = 100$ realizations $r(n)$ of the normal distribution.

For example, in the sequence $\{Y_1, Y_2, ..., Y_n\}$ formed by n consecutive values, the element Y_1 denotes the value taken by the time series at the first instant, Y_2 denotes the value taken by the time series at the second instant and Y_n denotes the value taken by the series at instant n. If the future values of a time series can be determined precisely by some mathematical function, such as $z(t) = \cos 2\pi\omega t$, we have a *deterministic time series*, that is, in a deterministic time series, it is possible to know the exact value it takes at each instant t. . When the future values of the time series can only be described by a probability distribution, such as the normal distribution $f(x) = \frac{1}{\sigma\sqrt{2\pi}} e^{-(x-\mu)^2/2^2}$, we have a *statistical time series* (STS) [35]. For example, in Figure 2.1, we show an example of a deterministic time series (a) and a statistical time series (b). In the case of Figure 2.1(a), at each instant t, it is possible to know the exact value $z(t)$ that the time series will take. On the other hand, in Figure 2.1(b), at each instant n, we generate a realization $r(n)$ of the process, that is, we only know the probability that the series takes a set of values.

In the case of STS, it is impossible to forecast the future values that the time series will take; that is, we can only know the probability that the time series will take a specific value. Therefore, an STS can be considered as a sequence of random variables indexed according to the order in which they were obtained over time. In this sense, a time series can be thought of as a realization produced by some underlying probability law $\mathbb{P}$; in other words, STS can be considered as realizations of a stochastic process [35]. This is the type of time series that we will be working within this thesis.

2.3.1 Inverse problem: symbolic representation of time series

In Figure 2.1(b), we have shown a time series generated by taking independent realizations of a normally distributed random variable. However, in real-life time series, the corresponding distribution is usually unknown. This means that we face the inverse problem: we would like to infer the law $\mathbb{P}$, from which the real-life time series was generated. This can be done using the symbolic representation of the observed sample, i.e., the time series [36]. The symbolic representation of a time series is a powerful tool that allows processing the data in a simplified way than the original data, while preserving, up to some extent, the information of interest.

Let us suppose that discrete time series $Y = \{Y_1, Y_2...Y_n\}$ takes values on a state space $\mathbf{S}$, which can be segmented into disjoint cells by $\alpha = \{A_1, A_2, ..., A_\kappa\}$, whose cells will be labeled with the elements of set $\mathcal{A} = \{1, \ldots, \kappa\}$, which we will call alphabet of size κ; that is, the symbols will indicate in which partition each data falls. This allows us to obtain a symbolic sequence $\mathbf{s}^\alpha = \{s_{i_1}, s_{i_2}, \ldots, s_{i_n}\}$ of the time series, which defines the *itinerary* of the time series visiting cells A_{i_1},A_{i_2},...,A_{i_n}. Formally, we say that $s_{i_k} = i_k$ if $y_i \in A_{i_k}$, where y_i is the value of the time series at instant i. It is essential to emphasize the fact that $\mathbf{s}^\alpha$ depends on the chosen partition α, that is, a different partition of the state space will generate a different symbolic representation [36]. This motivates introducing the following definition of *symbolic representation of time series*.

Definition 2.3.1 (Symbolic representation of time series)**.** *Let us consider a discrete time series $Y = \{Y_1, Y_2...Y_n\}$, which takes values in the state space $\mathbf{S}$. Let $\alpha = \{A_1, A_2, ..., A_\kappa\}$ be a disjoint partition of $\mathbf{S}$, whose alphabet of size κ is $\mathcal{A} = \{1, \ldots, \kappa\}$. The function $S_n^\alpha : \mathbf{S} \mapsto \mathcal{A}$, mapping each $y_i \in \mathbf{S}$ to the i-th component of its symbolic sequence $\mathbf{s}^\alpha$, is called the symbolic representation of Y with respect to the partition α.*

It turns out that the mapping S_n^α defines a stochastic process [36]. In this way, the symbolic sequences $\mathbf{s}^\alpha$ become realizations of the stochastic process of S_n^α.

2.4 Autocorrelation function

The autocorrelation refers to the cross-correlation of a signal with a version of itself as a function of a time delay. Informally, we can interpret it as a measure of the similarity between the observations of the random variable and its lagged version.

Definition 2.4.1 (Autocovariance function)**.** *The autocovariance between the random variable X_t and a copy of itself $X_{t+\tau}$ delayed τ time units, is given by [37]:*

$$\begin{aligned} \gamma(X_t, X_{t+\tau}) &:= cov(X_t, X_{t+\tau}) = E\left[(X_t - E[X_t])(X_{t+\tau} - E[X_{t+\tau}])\right] \\ &= \frac{1}{n}\sum_{i=1}^{n-\tau}\big(x_i - E[X_t]\big)\big(x_{i+\tau} - E[X_{t+\tau}]\big), \end{aligned} \tag{2.16}$$

as long as $E[X_t] < \infty$, $E[X_{t+\tau}] < \infty$, $E[X_t X_{t+\tau}] < \infty$, *where* $E[X_t]$, $E[X_{t+\tau}]$ *and* $E[X_t X_{t+\tau}]$ *denotes the expected values of the random variables* X_t, $X_{t+\tau}$ *and* $X_t X_{t+\tau}$, *respectively.*

As an interpretation, $\gamma(X_t, X_{t+\tau}) > 0$ indicates a positive dependence. This means that when the X_t values are above the mean, the $X_{t+\tau}$ values will also be higher than it; similarly, when X_t values are below the mean, so will $X_{t+\tau}$ values. When $\gamma(X_t, X_{t+\tau}) < 0$, we have a negative dependence. In this case, X_t values above the mean imply that the $X_{t+\tau}$ values are below it; likewise, X_t values below the mean imply that $X_{t+\tau}$ values are above it. In the case of $\gamma(X_t, X_{t+\tau}) = 0$, there is no linear relationship between the two variables.

Definition 2.4.2 (Autocorrelation function)**.** *The autocorrelation function (ACF) of the variables* X_t *and* $X_{t+\tau}$ *is given by [37]:*

$$\rho_\tau(X_t, X_{t+\tau}) := \frac{\gamma(X_t, X_{t+\tau})}{\sqrt{\gamma(X_t, X_t)\gamma(X_{t+\tau}, X_{t+\tau})}}. \tag{2.17}$$

The autocorrelation function satisfies the following properties:

1. If X_t and $X_{t+\tau}$ are independent, then $\rho_\tau(X_t, X_{t+\tau}) = 0$.
2. $-1 \leq \rho_\tau(X_t, X_{t+\tau}) \leq 1$
3. $|\rho_\tau(X_t, X_{t+\tau})| = 1$ if and only if there exist the constants β_1 and β_2 such that $\mathbb{P}\big(X_{t+\tau} = \beta_1 X_t + \beta_2\big) = 1$, with $\beta_1 > 0$ if $\rho_\tau(X_t, X_{t+\tau}) = 1$ and $\beta_1 < 0$ if $\rho_\tau(X_t, X_{t+\tau}) = -1$.

Due to these properties, the ACF can be interpreted as a measure of the linear predictability of the variable $X_{t+\tau}$ from X_t [37].

2.5 Entropy and Kullback–Leibler Divergence

Consider the well-known random experiment of rolling a die. Let A_1 be the event "the face of the die is greater than or equal to 3" and A_2 be the event "the face of the die is equal to 3". If we compare both events, we would be more surprised that event A_2 occurs since the probability of this event occurring ($p = 1/6$) is less than the probability of event A_1 occurring ($p = 4/6$); that is, the "amount of surprise" depends on the probability of the event occurring. The "amount of surprise" regarding the outcome of a random experiment can be quantified by a quantity known as *entropy.*

Definition 2.5.1 (Entropy)**.** *Let X be a discrete random variable with state space* $\mathbf{S}$ *and probability distribution $p(x) = \mathbb{P}(X = x)$ for all $x \in \mathbf{S}$. The entropy h of X is given by [38]:*

$$h := -\sum_{x \in \Omega} p(x) \log p(x). \tag{2.18}$$

In this equation, we will use the convention $0 \log 0 = 0$; that is, events with a probability equal to zero do not change the value of the entropy of the process. Equation (2.18) is a measure of the uncertainty of the random variable X. Intuitively, the more disordered a process is, the more significant the uncertainty regarding the value the random variable will take and, consequently, the greater the entropy. For example, for a random variable that follows a Bernoulli distribution, the entropy is at its maximum for $p = 1/2$ and decreases as p approaches 0 or 1. A concept related to the entropy of a random variable is the *relative entropy* or *Kullback-Leibler Divergence*, which measures the similarity or difference between two probability distributions.

Definition 2.5.2 (Kullback-Leibler Divergence)**.** *Let X be a discrete random variable with state space* $\mathbf{S}$*, and let $p(x)$ and $q(x)$ be two probability distributions of X. The relative entropy or Kullback-Leibler Divergence (KLD) is defined as [38]:*

$$D(p||q) := \sum_{x \in \mathbf{S}} p(x) \log \frac{p(x)}{q(x)}. \tag{2.19}$$

In this equation, we will use three conventions: (1) $0 \log \frac{0}{0} = 0$, (2) $0 \log \frac{0}{q} = 0$ and (3) $p \log \frac{p}{0} = \infty$. We have that $D(p||q) = 0$ when $p(x) = q(x)$ and $D(p||q) > 0$ when $p(x) \neq q(x)$, that is, KLD is always positive. As an interpretation, the larger the value of $D(p||q)$, the less similar the distributions $p(x)$ and $q(x)$ are; conversely, lower values of $D(p||q)$ indicate that these two distributions are more similar. In Section 3.3.3, we will see that KLD between the forward and backward paths of a process can be used to quantify its time-irreversibility.

2.6 Chapter summary

The definitions and theory presented in this chapter will serve as background to introduce the irreversibility indicators in Chapter 3 and to perform different statistical analyses. Specifically, we will use the ACF to evaluate the degree of memory of the electrocardiographic signal, which is related to the Markovianity of the process. The concept of irreversible Markov chains will allow us to define the entropy production rate of the process in Section 3.3.1. In addition, we will use the definition of relative entropy introduced in this chapter to define, in Section 3.3.3, an indicator of irreversibility, namely, the indicator of the KLD between the process and the time-reversed process.

Chapter 3

Time-irreversible processes

In this chapter we introduce the indicators of temporal irreversibility that we use for our study. First, in Section 3.1, we give a brief introduction to irreversible processes and entropy production from the point of view of classical thermodynamics. Then, Section 3.2 relates entropy production in time series and the physical mechanisms that generate them. In Section 3.3 we define some time irreversibility indices found in the literature and introduce the lag-irreversibility function. Finally, we provide two examples to illustrate the meaning of irreversible processes in Section 3.4.

3.1 Time-irreversible processes: classical thermodynamics approach

The *first law of thermodynamics* states that if work is done on (or from) a system or if it gains (or loses) heat, its internal energy will change. In other words, this law expresses that after an energy exchange, in the form of heat or work, between a system and its surroundings, the total energy of the universe remains constant (Figure 3.1). This principle can be expressed by [39]:

$$U = Q + W, \tag{3.1}$$

where U is the internal energy of the system, Q the heat it exchanges with its surroundings and W the work done by or towards the system.

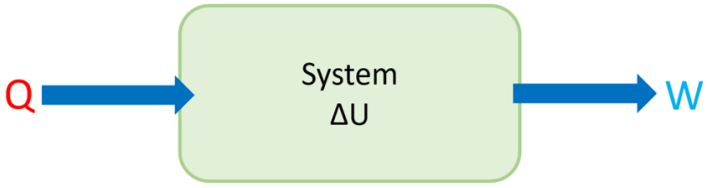

Figure 3.1: Scheme of the first law of thermodynamics. The change in the internal energy of the system is the sum of the heat and work done to or from the system. The signs of Q and W are positive when the system receives heat or work is done on it. When the system gives off heat or does work on the surroundings, the signs of Q and W will be negative.

The *first law of thermodynamics* is a universal law and no exceptions have been observed. For example, suppose that our system is an ice cube that, at an initial instant

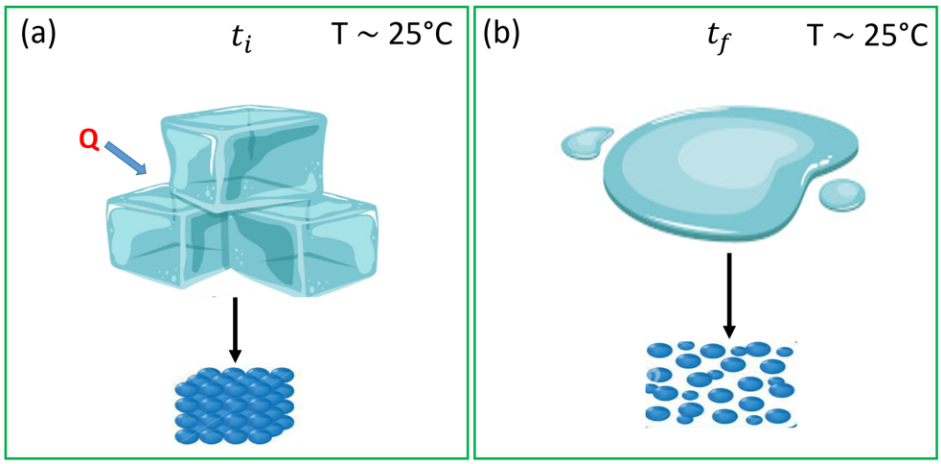

Figure 3.2: Example of an irreversible process. At the molecular level, in the solid state, water is a more ordered system compared to the liquid state. Naturally, systems tend to get disordered, that is, the system goes from a state of lower entropy to one of higher entropy. These pictures were taken from [41] and [42].

t_i, is in a room at room temperature ($T \approx 25°C$) (Figure 3.2(a)). Spontaneously, that is, without work being done towards or from the system, the ice cube will absorb heat from its surroundings, until it is in thermal equilibrium with the room and reaches the liquid state at some final instant t_f (Figure 3.2(b)). In this case, since there is no work done, the change in the internal energy of the system will be equal to the heat gained from the room, that is, $\Delta U = U_f - U_i = Q$. Once this equilibrium state is reached, the reverse process will not occur spontaneously. This means that the process is *irreversible*, since we will not observe the liquid releasing heat until the ice cube forms again. For the process to be *reversible*, that is, for the ice cube to form again, it is necessary that at the end of the reverse process, the net heat exchange between the ice cube and the room is equal to zero, which is impossible, since part of the heat transferred was lost during the heat exchange. In thermodynamics, this restriction in the direction in which the process occurs can be described in terms of the *entropy* S of the process, which is a physical quantity that measures the degree of molecular disorder of a system. In our example, our system goes from an equilibrium state A, water in a solid state, to another equilibrium state B, water in a liquid state. In the solid state, molecules exhibit a more ordered configuration than they do in the liquid state (Figure 3.2); if we define the entropy of the system in the equilibrium states A and B as S_A and S_B, we have that $S_A < S_B$, so that the entropy change $\Delta S = S_B - S_A > 0$, is positive; that is, the system went from a state of lower entropy to one of higher entropy. This happens since when a system is not in thermodynamic equilibrium, it tends to seek such a state, where the entropy is maximum ([39], [40]). To understand this positive entropy change and its relationship with the second law of thermodynamics, we will first define entropy.

In classical thermodynamics, the entropy S can be considered as differential quantities

of heat transfer divided by the temperature, by [40]:

$$dS = \frac{\delta Q}{T}, \tag{3.2}$$

since the heat Q is not a state function, δ is used instead of d, that is, δ is an inexact differential. The entropy change of a system during a process can be defined by integrating the equation (3.2), as [40]:

$$\Delta S = S_B - S_A = \int_A^B \frac{\delta Q}{T}\,. \tag{3.3}$$

On the other hand, for a cyclic process that consists of a reversible part and an irreversible part, from the Clausius inequality [40],

$$\oint \frac{\delta Q}{T} \leq 0, \tag{3.4}$$

it is possible to obtain the inequality

$$\Delta S = S_B - S_A \geq \int_A^B \frac{\delta Q}{T}\,, \tag{3.5}$$

which can be expressed in differential form as

$$dS \geq \frac{\delta Q}{T}. \tag{3.6}$$

In equation (3.6), equality is met for reversible processes and inequality for irreversible processes. This implies that, in an irreversible process, the entropy change ΔS_{irre} is greater than the integral of $\frac{\delta Q}{T}$ evaluated for that process. In the case of a reversible process, the entropy change ΔS_{rev} is equal to the integral of $\frac{\delta Q}{T}$, which represents the *entropy transfer* with heat. Therefore, the entropy change in an irreversible process is always greater than the entropy transfer, i.e. $\Delta S_{irre} > \Delta S_{rev}$. This implies that in an irreversible process, entropy is generated or produced. The entropy produced during a process is called *entropy production*, which we will denote as S_{prod}. We can deduce that the difference between the entropy change of a system and the entropy transfer, is the *entropy production*, and consequently, using equation (3.5), we can can express the entropy production as [40]:

$$S_{prod} = \Delta S - \int_A^B \frac{\delta Q}{T}\,. \tag{3.7}$$

where $\int_A^B \frac{\delta Q}{T}$ is the entropy transfer and the entropy production S_{prod} is a quantity always positive or zero. In the absence of entropy transfer, the entropy change of the system is equal to the entropy production. Additionally, entropy production is related to the *work dissipation* (W_{diss}) or *dissipation*, which we can define as the surplus of

work necessary to take a system from an equilibrium state A to an equilibrium state B, by [43]:

$$W_{diss} = W - \Delta F, \tag{3.8}$$

where $\Delta F = F_B - F_A$ is the minimum amount of work needed to take a system from state A to B. In this equation, the terms F_B and F_A are the free energy in states B and A, respectively [39]. For irreversible processes, the work dissipation is always positive, while for reversible processes it is equal to zero, that is, $W_{diss} \geq 0$. For an isothermal process (constant temperature) at temperature T, the work dissipated can be expressed in terms of entropy production, as [43]:

$$W_{diss} = TS_{prod}. \tag{3.9}$$

On the other hand, equation (3.6) is the classical expression of the *second law of thermodynamics*, which states that the change in entropy S is always greater than or equal to the heat transfer Q, divided by the equilibrium temperature T of the system; in other words, this law expresses that the amount of entropy in the universe tends to increase over time [40]. This means that the second law of thermodynamics describes the direction in which processes occur. In our example in Figure 3.2, the system spontaneously went from the solid state to the liquid state; however, the reverse process will not happen spontaneously. This change happened because there was a thermodynamic force that drove such a transformation, temperature and pressure. Other examples of thermodynamic forces could be the concentration gradient, electric potential gradient, pressure gradient, and many others, which drive different irreversible processes such as diffusion (concentration gradient) or an electric discharge (electric potential gradient). These examples of irreversible processes happen spontaneously in one direction, since when they occur, there is some loss or dissipation of energy, and therefore they produce entropy, which is proportional to the energy dissipation (equation (3.9)).

3.2 Time-irreversible processes: statistical thermodynamics approach

From a thermodynamic point of view, all natural processes are irreversible. When we want to understand, from the perspective of irreversible processes, different natural processes, it is not possible to do so using the tools of classical thermodynamics and we need to make use of the statistical definition of entropy and entropy production. This is because the tools of statistical thermodynamics of irreversible processes can be applied to the analysis of time series, which in turn can be used as graphical representations of some natural processes. In this context, the relationship between the classical thermodynamic definition and the statistical definition of the entropy production in irreversible processes

can be established through the Kolmogorov-Sinai entropy of its forward (h) and backward (h^r) trajectories, by ([44], [9]):

$$\frac{\dot{S}}{k_B} = \lim_{n\to\infty} \frac{1}{n} D_n(\mathbb{P}(x_1^n)|\mathbb{P}(x_n^1)) = (h^r - h), \tag{3.10}$$

where $\dot{S}$ is the entropy production of a thermodynamic system, k_B is the Boltzmann constant and $D_n(\mathbb{P}(x_1^n)|\mathbb{P}(x_n^1))$ is the KLD of n-strings (see equation (3.20)). $\mathbb{P}(x_1^n)$ is an abbreviated form of $\mathbb{P}(X_1^n = x_1^n)$ and denotes the probability of a realization of the process, from time 1 to n; in the next section we introduce this notation in detail. In this equation, the left-hand side is a physical quantity that defines the entropy production rate of a system at the macroscopic level, while the right-hand side is a statistical quantity that defines the entropy production rate, which depends only on the trajectory of the system $(x_1, x_2, \ldots, x_n)$ and does not take into account the physical mechanism generating the data ([44]). In this thesis, we are interested in analyzing the time-irreversibility of a process from the approach defined by the right-hand side of the equation (3.10), that is, from the observables of a process, seen as a time series. Next, we address the issue of temporal irreversibility of a process from the statistical approach, which is manifested by the time asymmetry and the entropy production rate of its trajectories.

A stationary process $\mathcal{X} := \{X_n : n \in \mathbb{N}\}$ is said to be reversible in time, if for the joint probability distribution up to time n, $\mathbb{P}(x_1^n)$ and the joint distribution of the time-reversed sequence $\mathbb{P}(x_n^1)$, it is true that ([45]):

$$\mathbb{P}(x_1^n) = \mathbb{P}(x_n^1), \tag{3.11}$$

i.e., both trajectories are equally probable for all n, which is an outcome of the fact that the trajectories of these systems do not exhibit preferential direction. In contrast, in the cases of irreversible processes, its trajectories are described by the breaking of the time-reversal symmetry or are said to exhibit *time asymmetry*. This breaking of the time-reversal symmetry is directly related to the entropy production rate at the microscopic dynamical level [46]. In addition, the *time asymmetry* quantifies the distinguishability between the process paths and their time reversal, which is an interpretation of an irreversible process. Therefore, the main characteristic of irreversible processes is their preferred direction and their proficiency in discerning the *arrow of time* ([10], [43], [47]).

When equation (3.11) is not met in the context of irreversible processes, we ask whether general methods exist to estimate the temporal asymmetry or the entropy production rate, since these quantities are essential for quantifying how far from thermodynamic equilibrium a system is. In this regard, different approaches have been proposed to address the problem of estimating these quantities, such as permutation patterns, ternary coding, micro-scale trends, visibility graphs, and some others; for a review see [16]

and the references therein. Therefore, in order to test and quantify the time-irreversibility of the process under study in this thesis (see methodology Section **??**), we consider three indices of irreversibility found in the literature, namely, *entropy production rate*, the *Kullback-Leibler divergence* between the forward and backward process and the *matching time*. Furthermore, we introduce the *Lag-irreversibility function*, as index of time irreversibility in time series. Next, in Section 3.3, we introduce each of these indices.

3.3 Time-irreversibility indices

The entropy production rate quantifies how far a system is from equilibrium. It is well known that a Bernoulli process is reversible and thus can be seen as in equilibrium; also, Markov processes are reversible whenever they are in detailed balance [9]. In [48], the entropy production rate was defined for general stochastic processes and dynamical systems at the level of their trajectories. Here, we assume that our data sequences are produced by a discrete stationary Markov chain that is not in detailed balance.

We will begin by providing useful definitions to introduce the indices. Let $\mathcal{X} = \{X_n : n \in \mathbb{N}\}$ be a discrete-valued stationary process generated by the law $\mathbb{P}$, which takes values from the *state space* $\mathbf{S} = \{s_1, s_2, ..., s_\kappa\}$. A realization of length n of process $\mathcal{X}$ will be denoted as $x = x_1, x_2, x_3, \cdots, x_n$, which one can write as a sequence in $\mathbf{S}^n$. Next, let $k < n$ be a positive integer; the chain of the first k symbols of x is denoted as x_1^k. A finite string $a_1^k := a_1 a_2 a_3 \cdots a_k$ comprised of k symbols will be called either k-word or k-block. We say that the k-word "occurs" at the j-th site of x, if $x_j^{j+k-1} = a_1^k$. We will denote by X_1^n the process up to time n and X_n^1 will denote the process reversed in time, analogously, we write x_1^n for a realization of the process and x_n^1 for its corresponding time-reversed realization. For convenience, we will denote the probability of the realization x_1^n, as $\mathbb{P}(x_1^n)$ instead of $\mathbb{P}(X_1^n = x_1^n)$. Analogously, the probability of sequence $\mathbf{s} = s_1 s_2 \dots s_n$ will be denoted as $\mathbb{P}(\mathbf{s})$.

3.3.1 Entropy production rate

Let $\mathcal{X}$ be a Markov process with transition matrix $[P_{i,j}]_{i,j\in\mathbf{S}} = \mathbb{P}(X_m = s_j | X_{m-1} = s_i)$ and a finite state space $\mathbf{S}$. Let us consider the finite sequence $\mathbf{s} = s_1 s_2 \dots s_n$, which represents the trajectory of the process. The invariant probability of the process visiting the state s_i is given by $\pi_i := \pi(s_i)$, which is the i-th entry of the eigenvector π defined as $\pi = P\pi$. This invariant probability vector π is unique for an ergodic Markov process that is irreducible, aperiodic and positive recurrent. We have that π and P are independent of time when the Markov process $\mathcal{X}$ is stationary. Due to the Markov property, the probability $\mathbb{P}(\mathbf{s})$ of the sequence $\mathbf{s}$ is [2]:

$$\mathbb{P}(\mathbf{s}) = \mathbb{P}(s_1 s_2 \dots s_n) = \mathbb{P}(s_1)\mathbb{P}(s_2|s_1)\mathbb{P}(s_3|s_2)...\mathbb{P}(s_n|s_{n-1}) \tag{3.12}$$

The entropy of the sequence $h(\mathbf{s})$ and the time-reversed one $h^r(\mathbf{s})$ are given by [2]:

$$h(\mathbf{s}) = -\sum_{i,j} \mathbb{P}(s_i)\mathbb{P}(s_j|s_i) \ln \mathbb{P}(s_j|s_i), \tag{3.13a}$$

and

$$h(\mathbf{s}^r) = -\sum_{i,j} \mathbb{P}(s_j)\mathbb{P}(s_i|s_j) \ln \mathbb{P}(s_i|s_j), \tag{3.13b}$$

respectively. For a discrete stationary Markov process, its *Entropy Production Rate* (EPR) can be estimated as [2]:

$$e_p := h(\mathbf{s}^r) - h(\mathbf{s}) = \frac{1}{2}\sum_{i,j} \Big[\mathbb{P}(s_i)\mathbb{P}(s_j|s_i) - \mathbb{P}(s_j)\mathbb{P}(s_i|s_j)\Big] \ln \frac{\mathbb{P}(s_i)\mathbb{P}(s_j|s_i)}{\mathbb{P}(s_j)\mathbb{P}(s_i|s_j)} \geq 0, \tag{3.14}$$

where $\mathbb{P}(s_i) = \pi_i$ and $\mathbb{P}(s_j) = \pi_j$.

3.3.2 Matching time

As stated by Gaspard in [2], in Markov processes the EPR can be obtained as the difference between the time-reversed and standard entropies, $e_p = h^r - h$ (see equation (3.14)). Accordingly, this difference between the entropy rate in the time-reversed sequence and the entropy rate in the original sequence, can be used as an index of temporal irreversibility. On the other hand, it is possible to derive expressions for the entropy rate h and the time-reversed entropy rate h^r, based on *matching times* (MT) [49].

For a finite realization $x = x_1, x_2, ..., x_n$, of a process $\mathcal{X}$, the *matching time* L_n^+ is defined as [4]:

$$L_n^+(x) := \min\{\ell : x_1^\ell \neq x_k^{k+\ell-1}, \forall k = 1, 2, ..., n-\ell+1\}. \tag{3.15}$$

Analogously, the *reversed matching time* L_n^- is defined as [4]:

$$L_n^-(x) := \min\{\ell : x_\ell^1 \neq x_k^{k+\ell-1}, \forall k = 1, 2, ..., n-\ell+1\}. \tag{3.16}$$

It turns out that matching time L_n^+, obeys the strong law of large numbers when $n \to \infty$ [50], in the sense that:

$$\frac{L_n^+}{\log(n)} \longrightarrow \frac{1}{h} \qquad a.s. \tag{3.17}$$

Correspondingly, the reversed matching time L_n^-, obeys the strong law of large numbers when $n \to \infty$, in the sense that:

$$\frac{L_n^-}{\log(n)} \longrightarrow \frac{1}{h^r} \qquad a.s. \tag{3.18}$$

Equations (3.17) and (3.18) suggest that the entropy rate h and the time-reversed entropy rate h^r can be estimated by means of:

$$\widehat{h} = \frac{\log(n)}{L_n^+}, \tag{3.19a}$$

and

$$\widehat{h}^r = \frac{\log(n)}{L_n^-}, \tag{3.19b}$$

respectively. In Ref. [4], the author derives estimators of h and h^r from the *matching times* (MT) and estimates the EPR as $M = h^r - h$. In Section 4.2 we describe the estimation procedure.

3.3.3 Kullback-Leibler Divergence

As we saw in Section 2.5, KLD is a tool that can measure the difference between two probability distributions. The latter is a consequence of the *Chernoff-Stein lemma* (see Theorem 11.8.3 in [38]), which states that the probability of incorrectly assigning the distribution $p(x)$ to the sequence $\{X_i : 1 \leq i \leq n\}$, when its true distribution is $q(x)$, is proportional to $e^{-nD(p||q)}$. As an interpretation, the larger the value of KLD, the easier it is to distinguish between the two probability distributions; conversely, lower values of KLD indicate that it is more difficult to distinguish between the two probability distributions.

In this thesis, we are interested in the KLD between the process forward and backward in time, which gives its EPR in the case of Markov processes; in [10], the authors provide a broader discussion of KLD and its relationship with EPR. From a practical point of view, probability distributions are constructed from the data, with which we can directly estimate the KLD. Given a process $\mathcal{X}$ with trajectory $x = x_1, x_2, \cdots, x_n$, one can define the n-block KLD of the process, with respect to its time reversal, as follows [9]:

$$D_n(\mathbb{P}(x_1^n)|\mathbb{P}(x_n^1)) = \sum_{x_1 x_2 \cdots x_n} \mathbb{P}(x_1^n) \ln \frac{\mathbb{P}(x_1^n)}{\mathbb{P}(x_n^1)}. \tag{3.20}$$

The EPR is given by the limit:

$$D = \lim_{n\to\infty} \frac{1}{n} D_n(\mathbb{P}(x_1^n)|\mathbb{P}(x_n^1)), \tag{3.21}$$

and it exists for almost every realization of the process whenever it is an ergodic process. Equation (3.21) has been used for estimation of the entropy production rate or as an index of irreversibility in [9, 10].

3.3.4 Lag-irreversibility function

As we mentioned above, the main problem in evaluating time-irreversibility in time series is the finiteness of the sample. Here, we propose an index for determining the time-irreversibility of a given process, the *Lag Irreversibility Function*, whose main advantage is that the number of parameters to be estimated is relatively small compared to other methods (see [16]). Let $\mathcal{X} = \{X_n : n \in \mathbb{N}\}$ a discrete-valued stationary process generated by the law $\mathbb{P}$ as defined previously, and let $\tau \in \mathbb{N}$ be a non-negative integer. Let us consider the joint probability function of two events that are τ-lagged in time, $\mathbb{P}(X_n = x_i; X_{n+\tau} = x_j)$, and equivalently in the backward process, $\mathbb{P}(X_n = x_j; X_{n+\tau} = x_i)$. Equation (3.11) implies that if the process $\mathbb{P}$ is irreversible, the joint probability function of the forward and backward process will follow the asymmetry property [51]:

$$\mathbb{P}(X_n = x_i; X_{n+\tau} = x_j) \neq \mathbb{P}(X_n = x_j; X_{n+\tau} = x_i). \tag{3.22}$$

Equation (3.22) motives the next definition of *pairwise reversibility*.

Definition 3.3.1. *We say that a stochastic process $\mathcal{X} = \{X_n : n \in \mathbb{N}\}$ is pairwise reversible if for all $\tau \in \mathbb{N}$, we have that [51]:*

$$\mathbb{P}(X_n = x_i; X_{n+\tau} = x_j) = \mathbb{P}(X_n = x_j; X_{n+\tau} = x_i). \tag{3.23}$$

Otherwise, we say that the process is pairwise irreversible.

A natural way to evaluate the pairwise irreversibility is to compute the KLD between the joint probability $\mathbb{P}(X_n = x_i; X_{n+\tau} = x_j)$ and $\mathbb{P}(X_n = x_j; X_{n+\tau} = x_i)$, which leads to the following definition of the *Lag Irreversibility Function*.

Definition 3.3.2. *Let $\mathcal{X} = \{X_n : n \in \mathbb{N}\}$ a discrete-valued stationary process generated by the law $\mathbb{P}$. We define the Lag Irreversibility (LI) Function, $L(\tau)$, as the Kullback-Leibler Divergence between the joint probability $\mathbb{P}(X_n = x_i; X_{n+\tau} = x_j)$ and $\mathbb{P}(X_n = x_j; X_{n+\tau} = x_i)$, [51] as:,*

$$\begin{aligned} L(\tau) &:= D_\tau\big(\mathbb{P}(X_n = x_i; X_{n+\tau} = x_j) \,||\, \mathbb{P}(X_n = x_j; X_{n+\tau} = x_i)\big) \\ &= \sum_i \sum_j \mathbb{P}(X_n = x_i; X_{n+\tau} = x_j) \log\left(\frac{\mathbb{P}(X_n = x_i; X_{n+\tau} = x_j)}{\mathbb{P}(X_n = x_j; X_{n+\tau} = x_i)}\right). \end{aligned} \tag{3.24}$$

The LI function can be described as a two-point statistic time-irreversibility index, which measures the breaking of the time-symmetry of the process probability distribution $\mathbb{P}(X_n = x_i; X_{n+\tau} = x_j)$ of two events that are τ-lagged in time, regarding the probability distribution $\mathbb{P}(X_n = x_j; X_{n+\tau} = x_i)$ of the process reversed in time. However, in some cases, although the process is irreversible, it may exhibit pairwise symmetry between these probability distributions, resulting in the process being pairwise-reversible. The

latter might suggest that the property of lag-reversibility is less stringent than the general condition of reversibility defined in equation 3.11. Therefore, the question of whether the pairwise-reversibility criterion defined by equation (3.23) is equal to the general reversibility criterion defined by equation 3.11, remains open [51].

3.4 Some examples of time-reversible and irreversible processes

We provide two examples to illustrate the meaning of irreversible processes. The first is a Markov process whose EPR can be obtained explicitly; that is, we know the probability law $\mathbb{P}$ of the process and we can generate realizations of it, which can be displayed as time series. The second example is a time series, representing the opposite case; that is, the probability law $\mathbb{P}$ generating the realization displayed as a time series is unknown.

In the first example, when we know the law $\mathbb{P}$ that generates the process, we can directly use the equation (3.14) to obtain the exact value of the EPR of the process. The second example is more complex because we first need to obtain the symbolic representation of the time series, from which it is possible to construct time-irreversibility estimators. In Chapter 4 we introduce the corresponding estimators of the irreversibility indices we presented above and we show how to construct them directly from symbolic sequences, using a numerical example.

Example 3.4.1. *Let us consider a Markov chain whose EPR can be obtained explicitly. Let* $S := \{1, 2, 3\}$ *be the state space of the discrete-time Markov chain with stochastic matrix* $\mathbf{A} : S \times S \to [0, 1]$*, defined by*

$$\mathbf{A} = \begin{pmatrix} 0 & p & 1-p \\ 1-p & 0 & p \\ p & 1-p & 0 \end{pmatrix}, \tag{3.25}$$

where p *is the probability to jump from one node to the next one and* $(1-p)$ *to go backwards (see Figure 3.3). This matrix is doubly stochastic and the unique invariant probability vector is given by* $\pi = (\frac{1}{3}, \frac{1}{3}, \frac{1}{3})$*. The corresponding EPR of this process is given by:*

$$
\begin{aligned}
e_p(p) = \frac{1}{2}\Bigg\{ & \left[\left(\frac{1}{3}(1-p) - \frac{1}{3}p\right)\ln\frac{\frac{1}{3}(1-p)}{\frac{1}{3}p}\right] + \left[\left(\frac{1}{3}(p) - \frac{1}{3}(1-p)\right)\ln\frac{\frac{1}{3}(p)}{\frac{1}{3}(1-p)}\right] \\
& + \left[\left(\frac{1}{3}(p) - \frac{1}{3}(1-p)\right)\ln\frac{\frac{1}{3}(p)}{\frac{1}{3}(1-p)}\right] + \left[\left(\frac{1}{3}(1-p) - \frac{1}{3}p\right)\ln\frac{\frac{1}{3}(1-p)}{\frac{1}{3}p}\right] \\
& + \left[\left(\frac{1}{3}(1-p) - \frac{1}{3}p\right)\ln\frac{\frac{1}{3}(1-p)}{\frac{1}{3}p}\right] + \left[\left(\frac{1}{3}(p) - \frac{1}{3}(1-p)\right)\ln\frac{\frac{1}{3}(p)}{\frac{1}{3}(1-p)}\right]\Bigg\} \\
= \frac{1}{2}\Bigg\{ & 3\left[\frac{1}{3}(1-p) - \frac{1}{3}(p)\ln\frac{\frac{1}{3}(1-p)}{\frac{1}{3}p}\right] + 3\left[\frac{1}{3}(p) - \frac{1}{3}(1-p)\ln\frac{\frac{1}{3}(p)}{\frac{1}{3}(1-p)}\right]\Bigg\} \\
= \frac{1}{2}\Bigg\{ & \left[\ln\frac{1-p}{p} - 2p\ln\frac{1-p}{p}\right] + \left[2p\ln\frac{p}{1-p} - \ln\frac{p}{1-p}\right]\Bigg\} \\
= (2p-1)\ln p - (2p-1)\ln(1-p) & = (2p-1)\left[\ln p - \ln(1-p)\right] \\
& = (2p-1)\ln\left(\frac{p}{1-p}\right), \quad (3.26)
\end{aligned}
$$

which is obtained directly from equation 3.14 and the probabilities given by the transition matrix 3.25. From the equation 3.26 it is clear the process is reversible, i.e., $e_p = 0$, only for the case $p = 1/2$, and irreversible otherwise. The number p can be thought as a parameter that quantifies the degree of irreversibility of the process.

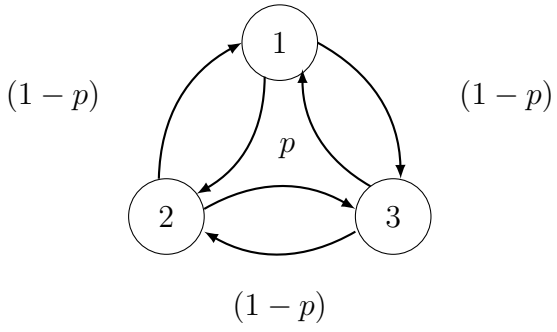

Figure 3.3: Three-states Markov chain cycle

Example 3.4.2. *Let us consider the time series generated by an irreversible process depicted in Fig. 3.4(a). If we compare the original trajectory (graph in blue) with its version reversed in time (graph in red), we can distinguish the direction of the arrow of time; we can distinguish that there is a change in the pattern that the trajectory follows since the original trajectory is in the form of stairs that are inclined towards the*

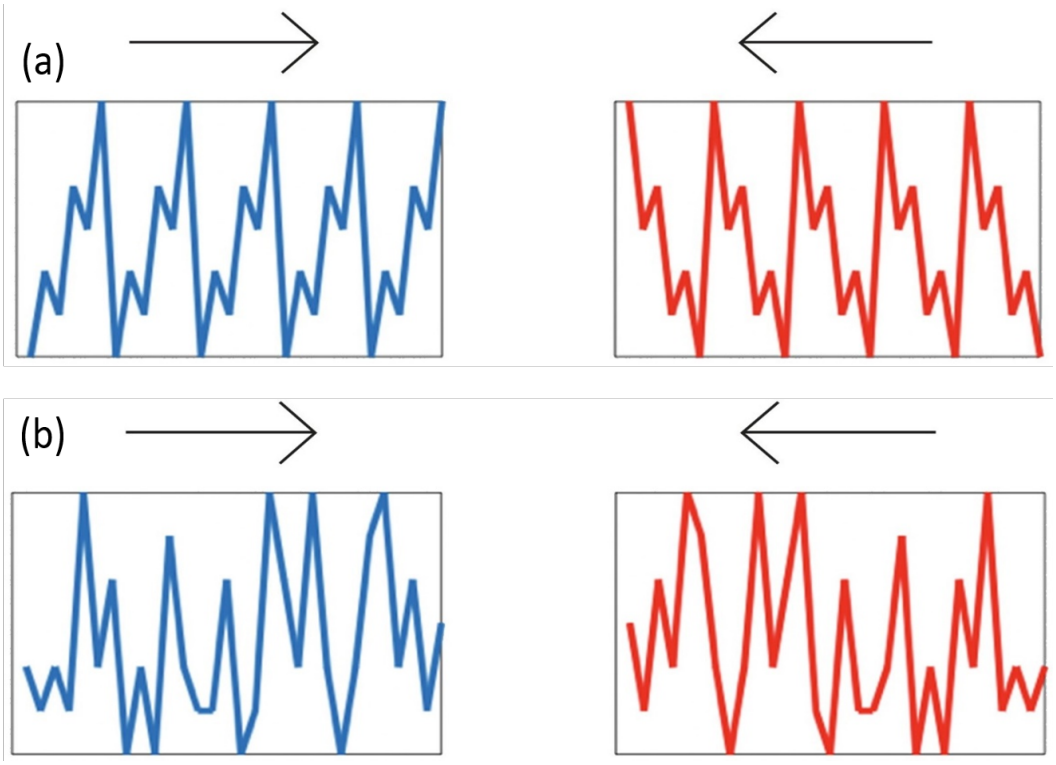

Figure 3.4: (a) Trajectory of a time series generated by an irreversible process; it is clear to distinguish the direction of the arrow of time. (b) Trajectory of a time series generated by a reversible process; the direction of the arrow of time is not clear.

right-hand side, while in the trajectory reversed in time, we see that these stairs appear inclined in the opposite direction. This means that the time series exhibits temporal asymmetry and suggests that it has a positive entropy production rate.

Let us consider the time series generated by a reversible process depicted in Fig. 3.4(b). If we compare the original trajectory (graph in blue) with its version reversed in time (graph in red), in this case, it is not clear to distinguish the direction of the time arrow, it seems that we are observing the same pattern of behavior in both cases. This means that the time series preserves its time-reversal symmetry, that is, the probability distribution of the process and its time-reversed version satisfy equation (3.11)*. The latter implies that it has an entropy production rate equal to zero.*

As we mentioned before, in this case, to estimate the EPR of the process, an alternative to do so is to obtain the symbolic representation of the time series, from which we can construct the irreversibility estimators.

3.5 Chapter summary

In this chapter we have defined different irreversibility indices found in the literature and we have introduced the *lag irreversibility function*. However, when we want to

use these tools to estimate the temporal irreversibility in time series generated by real life systems, the parameters of these indicators are not known exactly and we have to estimate them from the time series data. In this regard, in Chapter 4, we will introduce the estimators of the different irreversibility indicators discussed in this chapter. In particular, these estimators will be based on empirically estimating the probabilities of the events in the symbolic sequences.

Chapter 4

Estimators of time-irreversibility indices

In Section 3.3, we discussed different temporal irreversibility indices, namely, the *Entropy Production Rate*, the *Kulback-Leibler Divergence*, the *Matching Time* and the *Lag-Irreversibility Function*. This chapter introduces the corresponding estimators of those irreversibility indices in an analogous way to the "plug-in" estimators for the entropy rate as in [52]; that is, we construct empirical probabilities from the data. For this purpose, we assume that the samples are produced by a Markov chain whose transition matrix is unknown, but that can be estimated directly from the trajectories. In particular, when introducing each estimator, we provide an example to illustrate the general idea of the estimation procedure. Next, we test these estimators using time series coming from Markov chain models. We introduce these irreversibility estimators using the notation described in Chapter 3.

4.1 Entropy production rate empirical estimator

Let $\mathbf{S} = \{s_1, s_2, ..., s_\kappa\}$ be the state space of a discrete Markov chain $\mathcal{X}$ with a finite realization $x = x_1, x_2, ..., x_n$ of size n. We say that the process at time i is at the state s_j if $x_i = s_j$. So, for every $j = 1, \ldots, \kappa$, and a given n, we define the *empirical frequency* of the state s_j in a typical sequence x of size n, as follows [53]:

$$f(s_j; x_1^n) := \sum_{i=1}^{n} \chi_{s_j}(x_i), \tag{4.1}$$

where $\chi_{s_j}(\cdot)$ is the indicator function of s_j. Moreover, for $i = 2, \ldots, n$, the transition probabilities $\mathbb{P}(x_i = s_j | x_{i-1} = s_k)$, are estimated using the empirical probabilities from the sequence x of size n, and thus defined by [53]:

$$\widehat{P}_n(s_j|s_k) = \frac{1}{f(s_k; x_1^n)} \sum_{i=2}^{n} \chi_{s_j}(x_i) \cdot \chi_{s_k}(x_{i-1}). \tag{4.2}$$

In other words, in a sequence of length $n = 20$, the empirical transition probability from state s_k to state s_j, is obtained by dividing the number of transitions from state s_k to state s_j by the empirical frequency of state s_k. For example, let us consider the

sequence $x = 2\,3\,1\,211212\,33\,2122\,3\,1\,2\,3\,2$ (with $n = 20$), the empirical probability of transitions from state 3 to state 1 is $\widehat{P}_n(1|3) = \frac{2}{5}$, since state 3 appears five times (blue shaded text) and make two transitions to the state 1 (green shaded text).

The empirical conditional probabilities obtained with equation (4.2), are used to estimate the $\widehat{e}_p$ by directly plugging them into equation (3.14), giving the following expression [53]:

$$\widehat{e}_p := \frac{1}{2}\sum_{j,k}\left[\widehat{\pi}_k\widehat{P}_n(s_j|s_k) - \widehat{\pi}_j\widehat{P}_n(s_k|s_j)\right]\ln\frac{\widehat{\pi}_k\widehat{P}_n(s_j|s_k)}{\widehat{\pi}_j\widehat{P}_n(s_k|s_j)}, \tag{4.3}$$

where $\widehat{\pi}$ represents the left eigenvector of the empirical transition matrix $\widehat{P}_n$ (corresponding to the eigenvalue 1).

4.2 Matching time estimator

In [49], Kontoyiannis and Antos introduced an estimator of entropy rate based on *Matching Times* (MT) (see Section 3.3.2). On the other hand, in [4], the authors propose a procedure to estimate the matching time from the symbolic sequences of the system, whose lengths are not necessarily uniform. Let us assume we have the set $\mathscr{M} := \{\mathbf{x}_i : |\mathbf{x}_i| = n_i, 1 \leq i \leq m\}$, which is made up of m finite samples sequences, each with a different length n_i and coming from the process $\mathscr{X}$. Let $\mathscr{I} := \{n_i : 1 \leq i \leq m\}$ be the collection of all lengths n_i of the sequences. By applying the equations (3.15) and (3.16), each sequence in $\mathscr{M}$ yields a sample of its corresponding matching time ℓ^+ and a sample of the reversed matching time ℓ^-, respectively. In addition, the collection of all the outcomes of applying equation (3.15) to each sequence in $\mathscr{M}$, that is, all the resulting matching times ℓ_i^+, can be expressed as [4]:

$$\mathscr{L}^+ := \{\ell_i^+ = L_{n_i}^+(\mathbf{x}_i) : \mathbf{x}_i \in \mathscr{M}, 1 \leq i \leq m\}. \tag{4.4}$$

Equivalently, using equation 3.16 for each sequence in $\mathscr{M}$, we can obtain the collection of matching times of the time-reversed process, denoted as [4]:

$$\mathscr{L}^- := \{\ell_i^- = L_{n_i}^-(\mathbf{x}_i) : \mathbf{x}_i \in \mathscr{M}, 1 \leq i \leq m\}. \tag{4.5}$$

For example, let us consider the set $\mathscr{M} := \{\mathbf{x}_1, \mathbf{x}_2\}$, where $\mathbf{x}_1 = 122\,2\,32122313322$ ($n = 15$) and $\mathbf{x}_2 = 211\,31\,32122222133112$ ($n = 19$). In the case of $\mathbf{x}_1$, we have $\ell^+ = 4$ and $\ell^- = 3$ since the blocks 1222 (green shaded text) and 221 (blue shaded text) appear once, respectively. For $\mathbf{x}_2$ the parameters are $\ell^+ = 3$ and $\ell^- = 5$ since the blocks 211 (green shaded text) and 13112 (blue shaded text) appear once, respectively. Now we can build the sets $\mathscr{I} := \{15, 19\}$, $\mathscr{L}^+ = \{4, 3\}$ and $\mathscr{L}^- = \{3, 5\}$.

Up to this point, it is possible to define the estimators for the entropy rate h and the time-reversed entropy rate h^r, for a set of m samples, as [4]:

$$\widehat{h} = \frac{\frac{1}{m}\sum_{j=1}^{m}\log(n_j)}{\frac{1}{m}\sum_{j=1}^{m}\ell_j^+}, \tag{4.6a}$$

and

$$\widehat{h}^r = \frac{\frac{1}{m}\sum_{j=1}^{m}\log(n_j)}{\frac{1}{m}\sum_{j=1}^{m}\ell_j^-}, \tag{4.6b}$$

respectively, where $n_i \in \mathscr{I}$, $\ell_i^- \in \mathscr{L}^-$ and $\ell_i^+ \in \mathscr{L}^+$. Given the process $\mathcal{X}$, equations (4.6a) and (4.6b) provide us with the estimators of the entropy rate of its symbolic sequence (h) and of its time-reversed symbolic sequence (h^r), which were defined in equation (3.19). The EPR of the process can be estimated by [4]:

$$\widehat{M} := \widehat{h}^r - \widehat{h}. \tag{4.7}$$

4.3 Kullback–Leibler Divergence empirical estimator

Let s_1^k be a k-block and s_k^1 its reversed order version. We define the empirical probability of the block s_1^k in the sequence x of size n, as follows [53]:

$$f(s_1^k; x_1^n) := \frac{1}{n-k+1}\sum_{i=1}^{n-k+1}\chi_{s_1^k}(x_i^{i+k-1}). \tag{4.8}$$

Analogously, equation (4.8) is used for the empirical probability of the reversed block s_k^1.

For example, for the sequence $x = 21\,132\,111212\,132\,33\,132\,21\,231\,2$ ($n = 25$), for $k = 3$, let us consider the randomly chosen k-block $s_1^k = 132$ and its reversed order version $s_k^1 = 231$. Then, the empirical probability of s_1^k and s_k^1 are given by $f(s_1^k; x) = \frac{3}{23}$ and $f(s_k^1; x) = \frac{1}{23}$, respectively.

Equation (4.8) provides us with the empirical probabilities of the k-blocks that will be used to estimate the KLD, by substituting them directly into the equation (3.20), which in turn yields [53]:

$$\widehat{D}_{n,k} := \sum_{s_1^k \in \mathbf{S}} f(s_1^k; x_1^n)\ln\frac{f(s_1^k; x_1^n)}{f(s_k^1; x_1^n)}. \tag{4.9}$$

In an ergodic process, for each k and for almost every realization, the empirical probability $f(s_1^k; x_1^n)$ of each k-block converges to its theoretical probability $\mathbb{P}(s_1^k)$ when the size of the sequence x goes to infinity (see [54]). So, one must have that $\lim_{n\to\infty}\widehat{D}_{n,k} =$

$D_k(\mathbb{P}(s_1^k)|\mathbb{P}(s_k^1))$, where the expression in the right-hand side is (3.20), and is obtained as the limit of the empirical frequencies. Furthermore, for an ergodic process it is known that the EPR is given by the limit [9]:

$$D = \lim_{k\to\infty} \frac{D_k\big(\mathbb{P}(s_1^k)|\mathbb{P}(s_k^1)\big)}{k}. \tag{4.10}$$

Moreover, one can take the two limits at once $k(n) \to \infty$, by choosing $k \sim \log(n)$. This holds by the Ornstein-Weiss theorem (see [54], for a reference). This gives us the mathematical foundations for the consistency of this estimator.

Let us remember that $s_1^k \in \mathbf{S}^n$ is one of all possible words of size k that can be formed from the state space $\mathbf{S}$. When $k = 3$, we have 3 possible cases [22]: (1) blocks like "222", which are read the same regardless of whether the process runs forward or backward in time and we will call them *homogeneous words*; (2) words like "121", which, as in the previous case, are read the same regardless of the direction of the time arrow and we will call them *symmetric words*; (3) the remaining words, like "213", which we will call *asymmetric words*. In the case of homogeneous and symmetric words, we will have $\ln \frac{f(s_1^k;x_1^n)}{f(s_k^1;x_1^n)} = 0$, since $f(s_1^k;x_1^n) = f(s_k^1;x_1^n)$, that is, these words do not contribute to the quantity defined in equation (4.9). The above implies that the time-irreversibility of the process is related to the probability distribution of asymmetric words.

4.4 Lag irreversibility function estimator

The empirical LI function estimator is defined by the empirical joint probability of the variables x_n and $x_{n+\tau}$, both in the original and time-reversed sequences. We assume that an unknown process produces these variables, but that they can be estimated directly from the trajectories. Let $x = x_1, x_2, \ldots, x_n$ be a realization of the stationary process $\mathcal{X} = \{X_t : t \in \mathbb{N}\}$, with state space $\mathbf{S} = \{s_1, s_2, ..., s_\kappa\}$. The joint probability functions $\mathbb{P}(x_t = s_i; x_{t+\tau} = s_j)$ and $\mathbb{P}(x_t = s_j; x_{t+\tau} = s_i)$, can be estimated by means of:

$$\widehat{P}(x_t = s_i; x_{t+\tau} = s_j) = \frac{1}{n-\tau}\sum_{t=1}^{n-\tau} \chi_{s_i}(x_t)\chi_{s_j}(x_{t+\tau}), \tag{4.11a}$$

and

$$\widehat{P}(x_t = s_j; x_{t+\tau} = s_i) = \frac{1}{n-\tau}\sum_{t=1}^{n-\tau} \chi_{s_j}(x_t)\chi_{x_{s_i}}(x_{t+\tau}), \tag{4.11b}$$

respectively, where $\chi_s(x)$ is the indicator function for the state s.

For example, let us consider the sequence $x =$ 1 32 3 3 1 1 2 3 1 12 3 21 1 1211 ($n = 20$). For $\tau = 3$, the joint probability that at instants t and $t+\tau$ the process is in states 1 and 3 (blue shaded text), respectively, is $\widehat{P}(x_t = 1; x_{t+\tau} = 3) = \frac{3}{17}$; for the time-reversed version (green shaded text) we have that $\widehat{P}(x_t = 3; x_{t+\tau} = 1) = \frac{2}{17}$.

Equations (4.11a) and (4.11b) give us the empirical joint probability that we use to estimate $L(\tau)$, by directly substitute them in Equation (3.24), which yields [51]:

$$\widehat{L}(\tau) = \sum_{s_i} \sum_{s_j} \widehat{P}(x_t = s_i; x_{t+\tau} = s_j) \log \left[\frac{\widehat{P}(x_t = s_i; x_{t+\tau} = s_j)}{\widehat{P}(x_t = s_j; x_{t+\tau} = s_i)} \right] \tag{4.12}$$

4.5 Numerical example

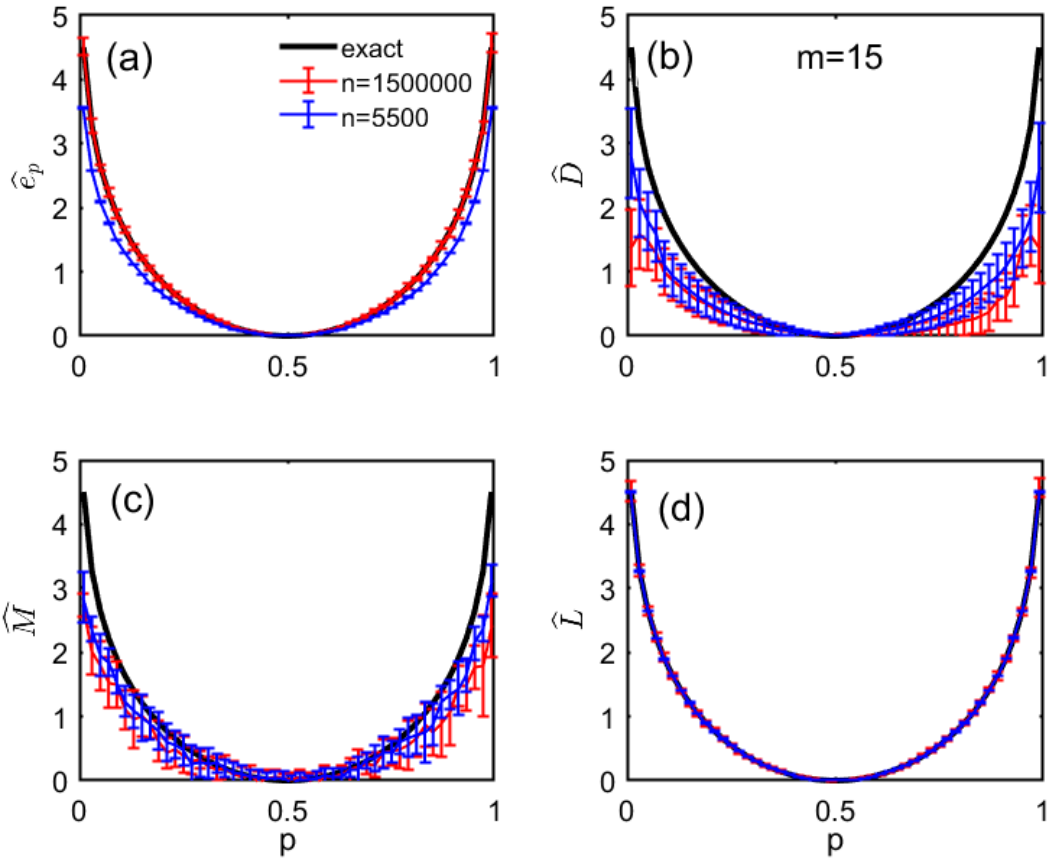

Figure 4.1: Exact values of the entropy production rate is depicted in the solid black line. Its empirical estimations are shown in red and blue colors for samples of size $n = 5500$ and $n = 1500000$, respectively, for the four estimators discussed, namely, $\widehat{e}_p$, $\widehat{D}$, $\widehat{M}$ and $\widehat{L}$.

In order to assess the performance of the estimators defined in the previous section, we performed numerical simulations of the three-states Markov chain with transition matrix $\mathbf{A}$, defined by the equation (3.25) in Section 3.4. Firstly, we generate $m = 15$ realizations of length $n = 5,500$ and $n = 1,500,000$, which corresponds to the length of the real samples we will use in Section **??**; we do this for each value of p coming from the interval $[0.01, 0.99]$. Next, For every sequence $x = x_1, x_2, ..., x_n$, we used the

equations (4.3), (4.10), (4.7) and (4.12) to empirically construct the time-irreversibility estimators defined in this chapter. Afterwards, we compared the results derived from these estimators and the exact value of the EPR using the equation 3.26. In Figure 4.1 we show these quantities as a function of p.

In Figure 4.1, we depict the exact value of the EPR and the average value of the estimates, as well as their respective error bars. We observe that while the estimators $\widehat{e}_p$ and $\widehat{L}$ give the best approximations of the EPR (Figures 4.1(a) and 4.1(d)), the $\widehat{D}$ and $\widehat{M}$ estimators underestimates it (Figures 4.1(b) and (c)). We will use the same methodology to analyze the electrocardiographic signal using the different irreversibility estimators. Afterwards, we will use the significant values of these estimators to discriminate between groups of healthy patients and those with medical conditions.

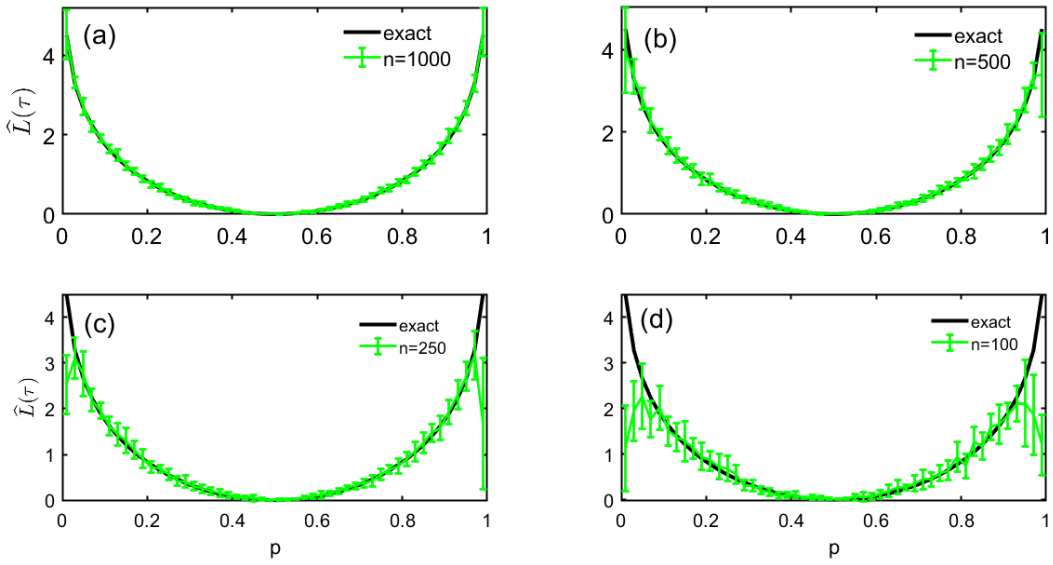

Figure 4.2: Exact values of the entropy production rate and...

As we saw in Figure 4.1(d), the $\widehat{L}$ estimator yields a good estimate of the EPR of the process for $n \geq 5500$. In order to numerically find minimum values of n for which such behavior can be observed, we now perform additional estimations for $n < 5500$. Specifically, in Figure 4.2 we show the results for $n = 1000$, $n = 500$, $n = 250$ and $n = 100$, since for $1000 < n < 5500$, the estimator $\widehat{L}$ exhibits results similar to those shown for $n \geq 5500$. In Figure 4.2(b) ($n = 500$), we can observe that while the average estimated EPR value still remains close to the exact value, the error bars grow as p moves away from $p = 1/2$. In Figure 4.2(c) ($n = 250$), we can notice that the error bars are even larger and that the average estimated EPR value is less accurate than in the case corresponding to $n = 500$. For $n = 100$, we can see that the estimated average value of the EPR departs significantly from the exact value and that the error bars are large.

For the case of the $\widehat{e}_p$ estimator, we follow the same procedure described in the previous paragraph, obtaining similar results. When comparing both estimators, we see

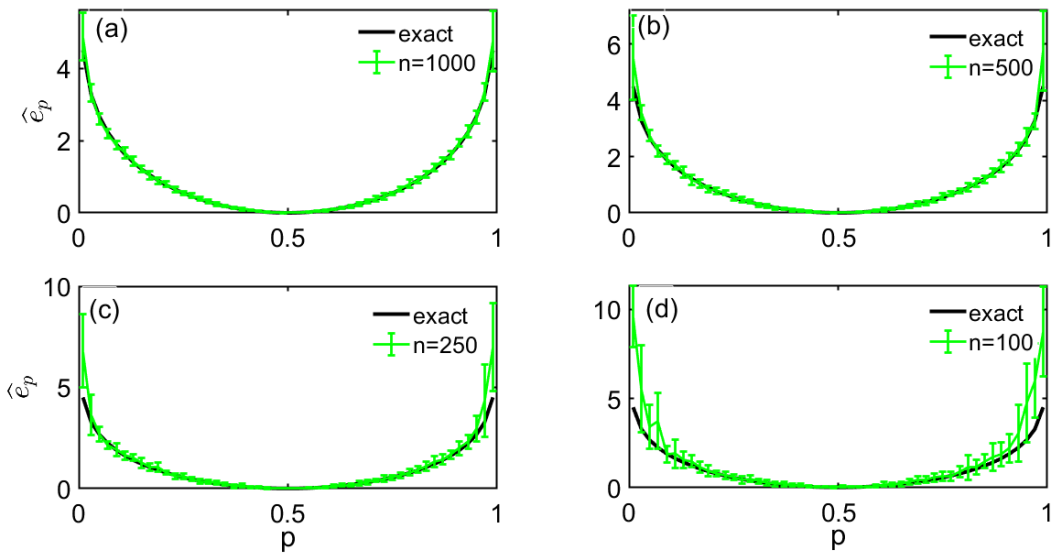

Figure 4.3: Exact values of the entropy production rate and...

that when $n = 250$, in the case of $\widehat{e}_p$, the estimated average value moves away faster from the exact value, with respect to that obtained with $\widehat{L}$.

These numerical results allow us to suggest that with values of $n \geq 1000$ we can have results similar to those obtained when n is large, using both estimators. Additionally, we can see that the $\widehat{L}$ estimator works better when we have short sequences, since for $n = 250$, the average value of $\widehat{L}$ remains closer to the exact value of the EPR, with respect to what is obtained with the $\widehat{e}_p$ estimator.

4.6 Chapter summary

In this chapter we have introduced irreversibility estimators, which can be implemented using directly the symbolic sequence of the data. According to the numerical results shown in Figure 5, in Markov processes, these estimators give a good approximation of the EPR. In Section 8.8, we give a more specific description of the estimation procedure for time series analysis. We then use these estimators to estimate the EPR in the electrocardiographic signal.

Chapter 5

Electrocardiography

This Chapter introduces the basic concepts for the study and interpretation of electrocardiograms. First, in Section 5.1, we define electrocardiograms as a recording of cardiac electrical activity and the medical significance of each component in the signal are discussed in Section 5.2. The main characteristics of a normal electrocardiogram are introduced in Section 5.3. In Section 5.4, we discuss *Heart Rate Variability* and its use in detecting medical conditions. Finally, we give a description of *Atrial Fibrillation* (Section 5.6) and *Congestive Heart Failure* (Section 5.5), which are medical conditions that we will be working on within Chapter 10.

5.1 Electrocardiograms

An *electrocardiogram*, abbreviated as ECG, is a recording of the *cardiac electrical activity* (CEA), whose x- and y-axes represent time (in s) and electrical potential (in mV), respectively (see Figure 5.1). This recording is obtained through an electrocardiograph, placing electrodes in specific areas of the body of a patient, according to Einthoven's triangle. By using various combinations of these electrodes, twelve different CEA recordings are obtained, called *electrocardiographic leads* [55]; in this thesis, we will always be working with lead II.

The different upward and downward curvatures that an ECG trace takes are called waveforms. These waveforms repeat periodically from one heartbeat to the next and have been arranged alphabetically as P, Q, R, S, T, and U. For lead II, a normal ECG consists of a P wave, a QRS complex, a T and a U wave; the QRS complex is made up of Q, R, and S waves, while the small U wave usually is invisible. The QRS complex appears as its main and most dominant pattern in a normal cardiac cycle (see Figure 5.1). The "flat" sections between the above mentioned waveforms are called *segments* and *intervals* (see Section 5.3). Each of these waveforms, segments and intervals on the ECG represents electrical pulses from the atria and ventricles, as we describe in Section 5.2 ([55]). Another essential feature of each cycle is the RR interval, which defines the heart rate and is the distance between two consecutive peaks of the R wave (see Section 5.4).

Nowadays, electrocardiographic devices allow the digitization of electrocardiograms, which simplifies their computational analysis through discrete time series of the form

$x = (x_1, \ldots, x_N)$. We give further details about the databases used in this thesis in Section 8.2.

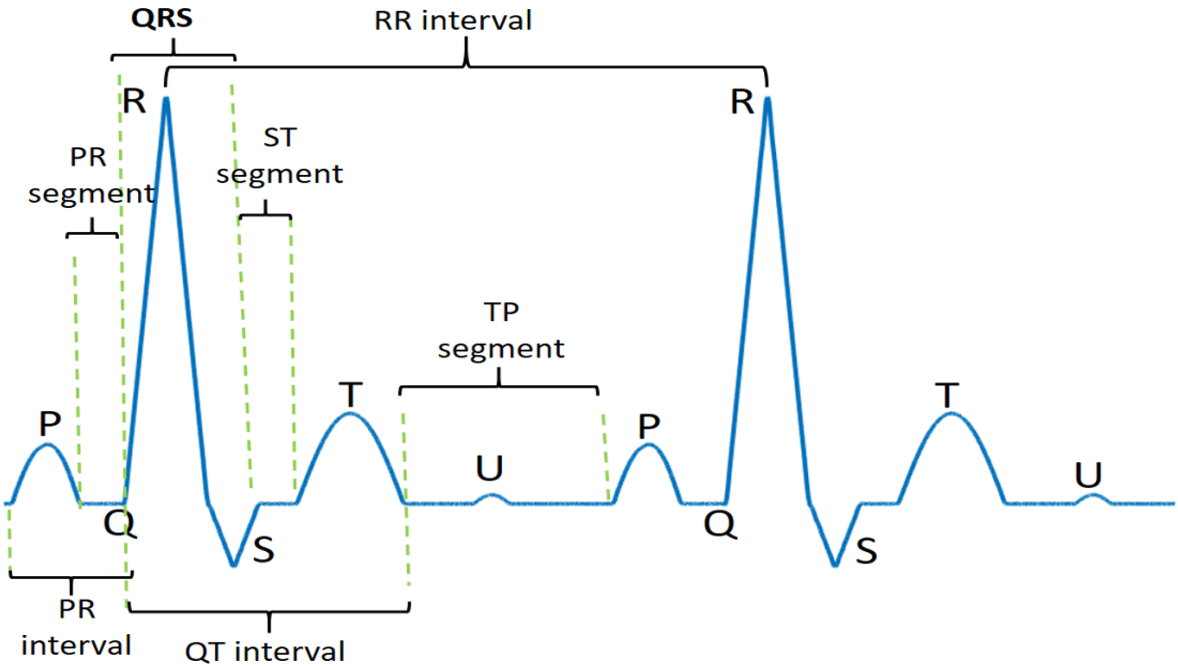

Figure 5.1: Schematic diagram of an electrocardiogram. A normal electrocardiogram is made up of the P, Q, R, S, T and U waveforms, which represent the ordered spread of electrical stimuli through the atria and ventricles. The P, R, T and U waveforms are in the form of convex curves, while the Q and S waveforms are found as concave curves. This electrocardiogram was artificially generated using the algorithm proposed in [56].

5.2 Cardiac cycle

At resting conditions, the cells of the muscle tissue of the heart, or *myocardium*, are polarized. This means that myocardial cells carry electrical charges, with the outside of the cell positively charged and the inside negatively charged (Figure 5.2(a)); this electric charge gradient is approximately 90 mV. When cells receive an electrical stimulus (**e**), this produces a difference in electrical voltage, which in turn causes an electrical current that spreads throughout the cell and initiates *depolarization* (Figure 5.2(b)). Then, when depolarization is complete, the cell is positively charged on the inside and negatively charged on the outside (Figure 5.2(c)). Finally, *repolarization* begins when the completely depolarized cell begins to return to the resting state, causing a small area on the outside of the cell to become positive again, which in turn causes the repolarization current to spread throughout the cell (Figure 5.2(d)). The repolarization process ends when the cell is completely repolarized, that is, the outside of the cell is positively charged and the inside is negatively charged [55].

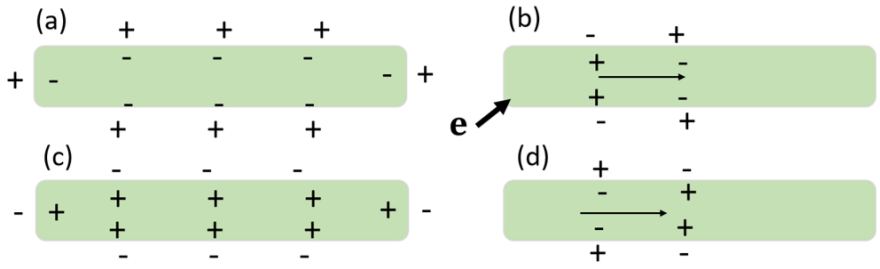

Figure 5.2: Scheme of depolarization and repolarization. From the electrical point of view, we can consider that the cardiac cycle has four stages: polarized cardiac muscle tissue (a), onset of depolarization (b), complete depolarization (c) and onset of repolarization (d). The polarized state of the cells at the beginning of the cardiac cycle is due to differences in the concentration of ions inside and outside the cell, with the inside of the cell membrane being negative in relation to the outside. The electrical charge gradient between the inside and outside of the cell is 90 mV, which is the action potential that triggers each cardiac cycle.

On the other hand, the depolarization and repolarization of cardiac tissue is associated with the contractions of the chambers that make up the heart. Although the heart has four chambers, from an electrical point of view, it can be considered that it only has two, the *atria* and the *ventricles*, since the left and right atria contract simultaneously (depolarization), as do both ventricles (see Figure 5.3). The muscle mass of the atria is small compared to that of the ventricles, so the electrical variation accompanying atrial contraction is weaker than the electrical variation due to ventricular contraction [57].

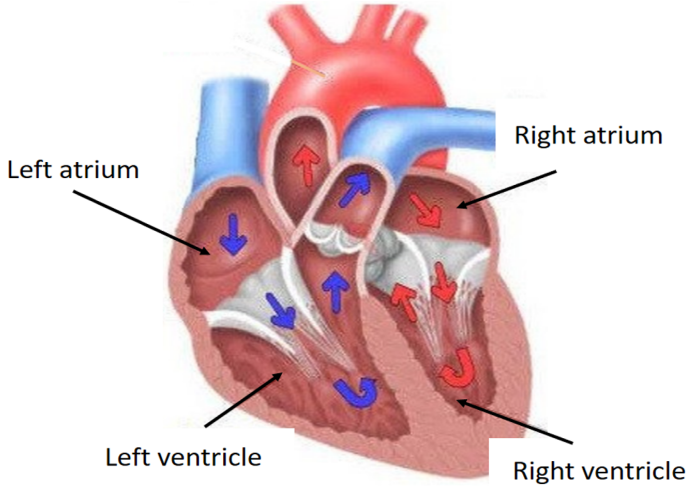

Figure 5.3: Chambers of the heart. The heart comprises four chambers: the right and left atria and the right and left ventricles. The atria are located at the top of the heart, with an atrium on each side, and are responsible for receiving blood flow. The ventricles are located at the bottom of the heart and are responsible for discharging blood from the heart. This picture was taken from [58].

In a normal cardiac cycle, the electric firing begins in a particular area of the right

atrium called the "sinoatrial node" (Figure 5.4(a)). Depolarization then spreads through the atrial muscle fibers, generating the P wave (Figure 5.4(b)). After that, to complete atrial depolarization, the depolarization wave travels very quickly through a specialized conduction tissue, called the bundle of His, thus generating the PQ segment (Figure 5.4(c)). Afterwards, the electrical impulse propagates through the ventricular muscle, at the same time that atrial repolarization begins, which generates the QRS complex (Figure 5.4(d)). When ventricular depolarization is being completed, the ST segment is generated (Figure 5.4(e)). Finally, ventricular repolarization begins, forming the T wave (Figure 5.4(f)) [57].

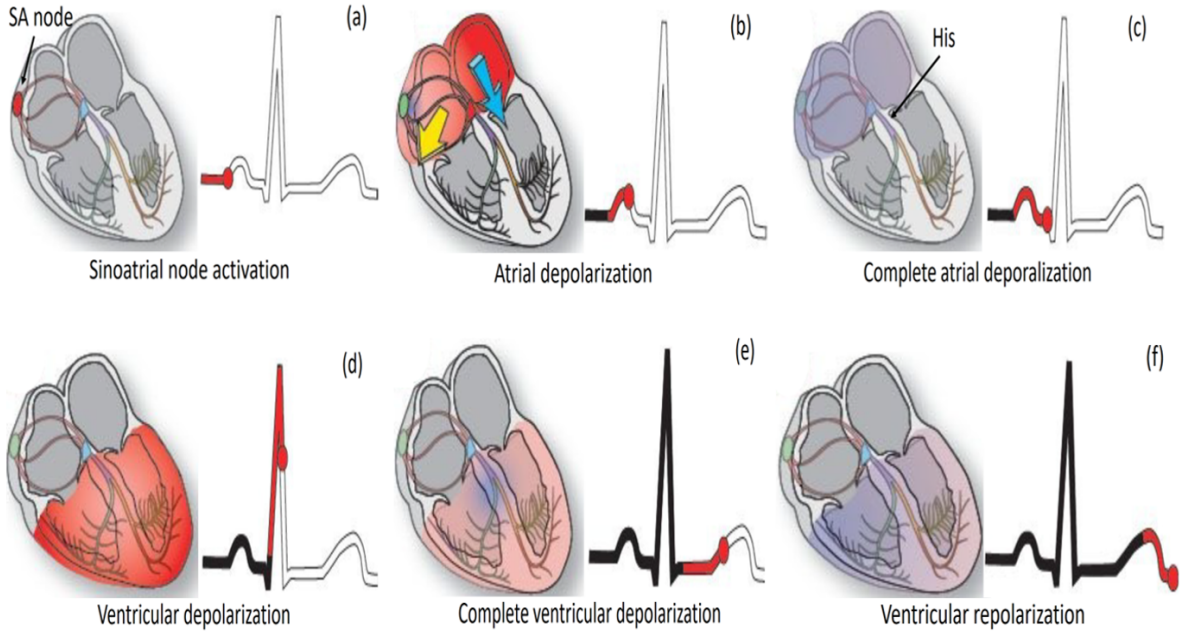

Figure 5.4: Cardiac cycle. The cardiac cycle is a sequence of events that occur in strict order, related to the flow of blood through the chambers that make up the heart, atria and ventricles. The alternating contraction and relaxation of these chambers, as a consequence of the spread of the electrical current through the cardiac tissue, is recorded in the form of deflections (waveforms) and flat areas (intervals and segments) of the electrocardiogram. These pictures were taken from [57].

We point out that in the previous paragraph, we omitted specific information on the different stages of the cardiac cycle, which would allow us to have a more detailed description of it (function of the atrioventricular node, depolarization of the atrioventricular septum, sinoatrial node-atrioventricular node-bundle of His interaction, division of the bundle of His, isovolumetric contraction, absolute refractory period, etc.). However, this general description of the process provides us with sufficient information to address the problem of analyzing electrocardiograms using the temporal irreversibility approach (see Chapter 8). In other words, up to this point, we know that an electrocardiogram is a graphic representation of a directional process, which consists of an ordered succession

of waves and segments, which are repeated in each heartbeat; any alteration in this pattern of behavior could imply the presence of a medical condition.

5.3 Characteristics of a normal electrocardiogram: waveforms, segments and intervals

As we saw in the previous Section (5.2), an electrocardiogram, broadly speaking, records two events. The first of them is depolarization, that is, the directional propagation of electrical stimuli through the myocardium. The second event recorded in the electrocardiogram is repolarization, that is, when the stimulated heart muscle returns to the resting state. These two depolarization and repolarization processes are responsible for the waveforms, segments and intervals in the ECG (see Figure 5.1) [55]. Next, we give more detailed information on the components of the ECG.

In Table 8.1, we summarize the biomedical meaning of each wave, as well as the respective values of durations (s) and amplitudes (mV). In relation to the U waveform (see Figure 5.1), which is a small, flattened wave that sometimes appears before the next P waveform and after the T waveform, although it represents the final phase of ventricular repolarization, its exact mechanism is unknown [57].

Regarding the flat zones of the electrocardiogram, that is, the segments and intervals, although they do not represent any electrical change, their correct interpretation is also essential for the analysis of electrocardiograms. A *segment* refers to the portion of the electrocardiogram bracketed by the end of one wave and the beginning of the next. Similarly, an *interval* is a portion of the electrocardiogram that includes at least one entire waveform (see Figure 5.1) [55]. In Table 5.2, we show a summary of each of the segments and intervals of the ECG, which will help us define our variability signals in Section 8.4.

Waveform	Duration (s)	Amplitude (mV)	Description
P	$0.08 - 0.11$	less than 0.25	Atrial depolarization
QRS	$0.06 - 0.11$	less than 3.5	Ventricular depolarization
T	less than 0.20	$0.20 - 0.30$	Ventricular repolarization
U	$0.06 - 0.09$	less than 0.1	Final phase of ventricular repolarization

Table 5.1: Parameters of ECG waveforms. Each waveform in the electrocardiogram is defined in a well-specified interval of duration and electrical potential. Any alteration in this pattern of behavior could indicate the presence of medical conditions ([55], [57]).

Perhaps the best known interval is the RR interval, since it is used to measure heart rate (see Section 5.4). Another important component is the TP segment, representing the

electrical resting state and is used as a *baseline* reference (see Figure 5.1). This segment evaluates changes in ST and PR segments when there are medical conditions. Additionally, when the electrocardiographic signal is under noisy conditions and interferences such as *baseline wandering* appear (see Section 6.1), the TP segment is used to assess the deviation of the ST and PR segments.

	Description
PR segment:	from offsets of the P wave to onsets of the QRS complex.
ST segment:	from offsets of the QRS complex to onsets of the next T wave.
TP segment:	from offsets of the T wave to onsets of the P wave.
PR interval:	from the onsets of the P wave to the onsets of the QRS complex.
QRS interval:	from the onsets to the offsets of the same QRS complex.
QT interval:	from the onsets of the QRS complex to the offsets of the T wave.
RR interval:	from the peak on a given QRS complex to the corresponding point on the next.

Table 5.2: Segments and intervals of the electrocardiographic signal. Although these components in the electrocardiogram do not represent the spread of the electrical charge directly, the order in which each interval and segment appears is useful for analyzing electrocardiograms, since they allow the beginning and ending points of each waveform to be identified [55].

5.4 Heart rate variability

Heart Rate Variability (HRV) refers to the oscillation in RR_i intervals duration between two consecutive heartbeats (see Figure 5.5). With this signal it is possible to analyze the status of the *autonomic nervous system* (ANS), which is in charge of regulating cardiac activity, through a balance between the *sympathetic nervous system* (SNS) and the *parasympathetic nervous system* (PNS), the two components of the ANS ([59], [60], [61]). An increase in the activity of the SNS or a decrease in the activity of the PNS, results in an acceleration of the heart rate. Conversely, a low SNS activity or high PNS activity results in a deceleration of the heart rate [62]. On the other hand, this balance does not imply that the two branches of the ANS contribute equally in each heartbeat since this balance can change to either of the two branches under different conditions in each heartbeat, which gives rise to an imbalance between accelerations and decelerations of the heart rate [63].

The HRV has different uses for monitoring and studying biomedical conditions, such as type 1 diabetes [64], myocardial infarction [65], ventricular tachycardia [66], early detection of sudden cardiac death [67], among others. These features we can

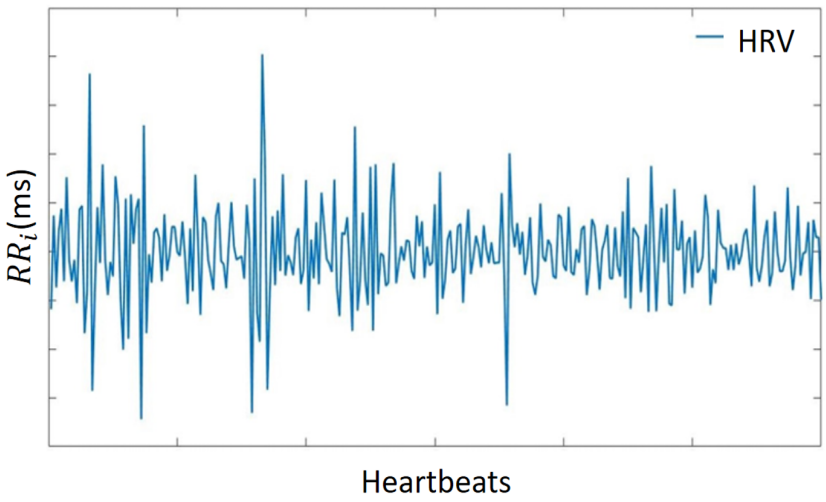

Figure 5.5: Heart rate variability. Fluctuations in time intervals between one heartbeat and another are inherent to the heart rhythm, since the heart, even under normal conditions, does not function as a metronome.

find in the HRV for the analysis of ECGs have encouraged their study using different methodologies (see [68] for a review). In this thesis, we analyzed the HRV using the temporal irreversibility approach, with the aim of discriminating between groups of healthy young and elderly patients from those under medical conditions, specifically, congestive heart failure and atrial fibrillation. We will talk about these medical conditions in Sections 5.5 and 5.6.

5.5 Congestive Heart Failure

Congestive Heart Failure (CHF) occurs when the ventricular walls become weak, damaged, or thickened, disrupting the normal function of the heart, causing a buildup of blood in the veins, lungs, abdomen, liver, and other parts of the body. Over time, CHF weakens and enlarges the ventricles, so they send insufficient amounts of blood to the body.

In the case of lead II, when CHF occurs, we can observe that there is a higher voltage in the P wave, with a value greater than 0.25 mV, as a consequence of an enlargement of the right atrial chamber. Another effect of CHF is an enlargement of the left atrial chamber, which we can verify when the P wave has a duration greater than 120 ms and exhibits 2 peaks separated by 40 ms, with an M-like morphology (see Figure 5.6).

5.6 Atrial Fibrillation

Atrial Fibrillation (AF) occurs when the electrical signal is generated in different

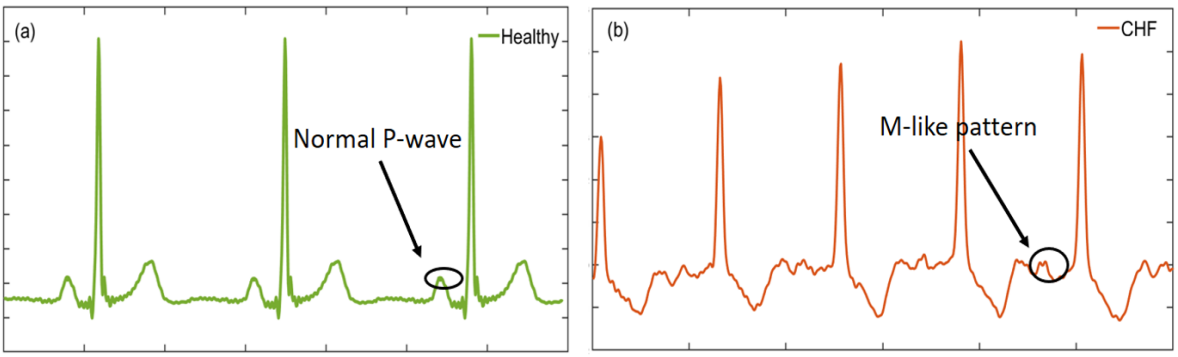

Figure 5.6: Congestive Heart Failure. The M-like pattern of the P wave is a consequence of the enlargement of the left branch of the atria.

parts of the atria and not normally in the SA node, causing rapid depolarization of the atria, making the atrial chambers rapidly contract and become disordered, that is, they "vibrate" or "fibrillate". This causes the atria to not be able to pump blood adequately and not emptying completely. During this irregular heart beating process it can be observed [55]:

- There is no clear formation of the P wave.
- Absence of baseline.
- Variable ventricular rate.
- The frequency of the fibrillatory waveforms can achieve up to 300 to 600 per minute.

All the characteristics of this arrhythmia affect the normal rhythm of the heart. Furthermore, fibrillatory waves can mimic or resemble the P wave, which can lead to erroneous diagnosis (see Figure 5.7).

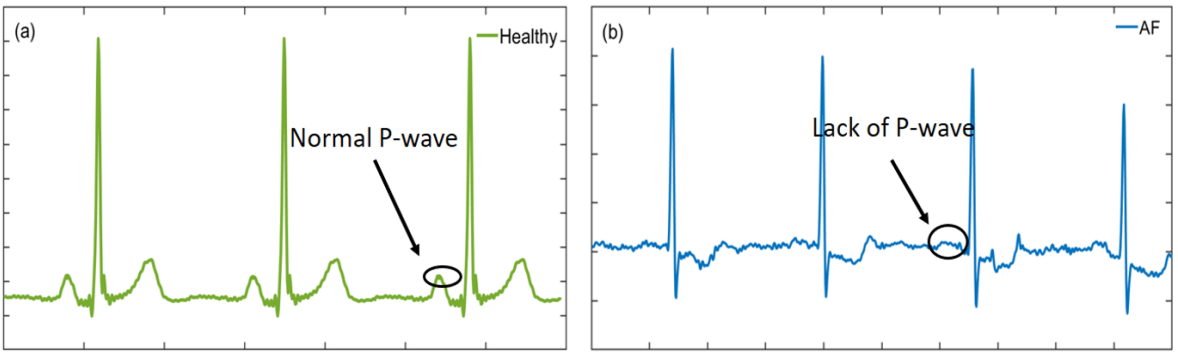

Figure 5.7: Atrial Fibrillation. This arrhythmia is characterized by the contraction and relaxation of the atria occurring in a disorganized manner, the absence of the P wave and disturbed baseline.

5.7 Chapter summary

In this chapter we have given a brief description of electrocardiograms, as well as their interpretation based on their different components (waveforms, segments and intervals). In summary, we know that electrocardiograms are an orderly succession of waveforms, segments and intervals, which appear in a strict order, which is repeated in each heartbeat, unless there is some medical condition that alters such behavior. However, in addition to medical conditions, this cyclic and orderly behavior can be altered by the presence of noise in the signal, which is the subject of Chapter 6. In addition, in Chapter 7 we will see that the orderly behavior of the electrocardiographic signal is related to its time-irreversibility.

Chapter 6

Electrocardiogram preprocessing: signal noise removal

In the data preprocessing stage, noise removal in the electrocardiographic signal plays a vital role in subsequent analysis, such as obtaining variability signals (Section 8.4) and the encoding process (Section 8.6). In this Section, we provide the theoretical framework for noise removal in electrocardiograms using the wavelet transform approach.

On the other hand, there is a large amount of literature on the use of the wavelet transform for the denoising process in electrocardiograms (see [32] for review) and there are powerful software packages for its implementation. Here, we merely present fundamental concepts for the processing of electrocardiograms using the wavelet transform, with which we also introduce the terminology and notation that we will use later in Section 8.3, where we perform the denoising of the signal, using the software package *Wavelet Signal Denoiser* for MATLAB.

6.1 Noise in electrocardiograms

The electrocardiographic signal is composed of signals of different frequencies, of which a certain range of frequencies is due to the normal functioning of the heart. Specifically, the frequency range of the P and T waves is between 0.5 and 10 Hz, while the frequency range of the QRS complex is between 4 and 20 Hz. In this context, signal noise refers to signals from high and low frequencies that do not correspond to cardiac electrical activity. The different sources of noise that the signal can present corrupt the signal and prevent its correct analysis. Therefore, removing noise in the data is a vital part of the preprocessing stage [30]. Noise sources include low (respiratory movement and muscle noise) and high frequency (equipment power line) signals, which can appear in combination (see Figure 6.1) [31]. Next, we describe the different noise sources.

6.1.1 Electric line noise

This type of noise is produced by medical equipment and occurs due to the influence of the electromagnetic field of the devices. Since its frequency range is between 50 and 60 Hz, this noise spectrum does not overlap with the frequencies of the electrocardiographic

signal, and therefore, does not distort it, which in turn makes its removal relatively easy [31].

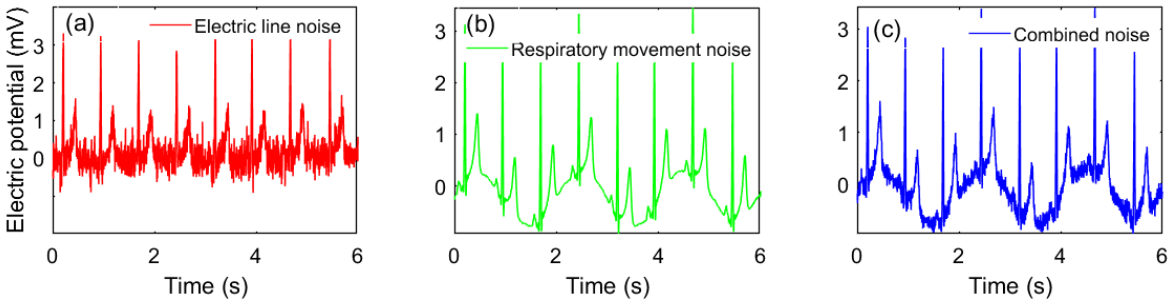

Figure 6.1: Some types of noise in the electrocardiographic signal. Among the different types of noise that affect the signal, low-frequency noise is the most difficult to process.

6.1.2 Electrode Contact Noise

This noise originates as a result of the loss of contact between the measuring device and the skin, and is usually an intermittent noise. The frequency content of this type of noise is around 60 Hz [30].

6.1.3 Muscle noise

This type of noise, whose frequency content is around 10 Hz, is due to the contraction of skeletal muscles and occurs when the patient moves, which is most evident in two cases. The first of them is during stress tests through physical examinations, which causes intense muscle contractions. The second case is during prolonged electrocardiographic recordings, such as ambulatory electrocardiography. In this case, the noise level will depend on the activity level [31].

6.1.4 Base Line Wander

Baseline wandering refers to the deviation of the PR and ST segments with respect to the TP segment, which can interfere with the reading of the electrocardiogram. For example, due to this deflection, the peak of the T wave could be higher than the R peak, causing the T peak to be detected as R peak. Therefore, this type of noise, whose frequency range is between 0.15 and 0.3 Hz, must be removed before signal analysis. This interference can be due to different sources such as movement, breathing and exercise [30].

6.2 Noise removal in electrocardiograms

6.2.1 Backgrounds: Fourier Transform

Definition 6.2.1 (Fourier Transform)**.** *The Fourier Transform (FT) of a time-dependent function $f(x)$ is given by*

$$F[f(t)](\omega) = \int_{-\infty}^{\infty} f(t)e^{-i2\pi\omega t}\, dt, \tag{6.1}$$

where ω is the frequency of the complex exponential function and $f(t)$ has to be integrable in the sense of the Lebesgue integral.

The FT decomposes a signal into its constituent frequencies and their respective amplitudes. For example, Figure 6.2(b) graphs the frequency spectrum of the signal $f(t) = \sin 2\pi\omega_i t$ (Figure 6.2(a)), whose parameter ω_i varies according to:

$$\omega_i = \begin{cases} 4 & if \quad 0 \leq t \leq 0.5 \\ 60 & if \quad 0.5 < t < 0.6 \\ 12 & if \quad 0.6 \leq t \leq 1 \end{cases}$$

In Figure 6.2(b) we can see that the FT gives information about the different frequencies that make up the signal but does not provide information about the location of these frequencies in the signal. Therefore, the main disadvantage of FT is the lack of ability to provide information about when, in time, the signal components appear. On the other hand, data of biomedical origin, such as electrocardiograms, are characterized by high-frequency components of short duration and components of lower frequency but of long duration. Therefore, to analyze these signals, we need tools that provide good resolution in both, the time and frequency domain [34]. In this context, it is possible to analyze this type of signal using the *wavelet transform* (WT) approach, which provides signal information at different time and frequency resolutions.

6.2.2 Wavelet transform

Definition 6.2.2 (Continuous Wavelet transform)**.** *The Continuous Wavelet transform (CWT) of a signal $f(t)$ is given by [32]:*

$$W(s,\tau) = \int_{-\infty}^{\infty} f(t)\psi\big(\frac{t-\tau}{s}\big)\, dt, \tag{6.2}$$

where $\psi(\frac{t-\tau}{s})$ is called mother wavelet*, s is scale or dilation parameter and τ is the location parameter of the wavelet. The word "mother" means that this function is used as a model for generating the other window functions during the analysis.*

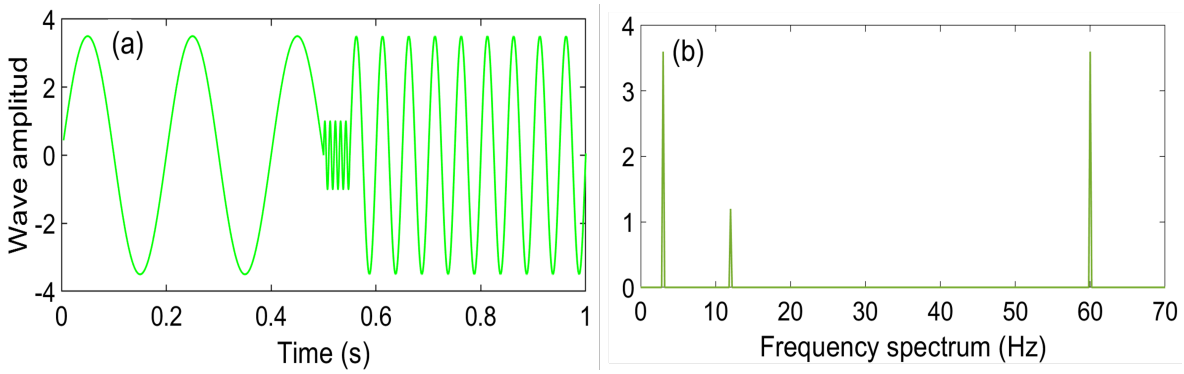

Figure 6.2: (a) Simulation of the signal $f(t) = \sin 2\pi\omega_i t$, whose values ω_i vary in different time windows. (b) Frequency spectrum of $f(t)$. The FT allows us to know the different frequencies that make up a signal, but not their location.

Analogously to FT, the WT decomposes a signal into a set of wavelet signals obtained from the mother wavelet, by means of dilations and contractions that depend on the parameter s, as well as displacements in time that depend on the parameter τ. Since the relationship between the frequency ω of the signal and the parameter s is $s = \frac{1}{\omega}$, then, for large values of parameter s (i.e., $s > 1$ and $0 < \omega < 1$), we have more low-frequency information; conversely, for small values of s (i.e., $0 < s < 1$ and $\omega > 1$), we can better analyze the information from high frequencies. In this way, one of the key advantages of WT over FT, is the temporal resolution; that is, it captures frequency information and its respective location in time. The other advantage is the multiresolution; that is, compression and dilation of the parameter s, allow the signal to be analyzed on a wide set of scales

Regarding the practical aspects of implementing the WT, that is, when we deal with discrete time series, it is possible to implement the *Discrete Wavelet transform*, which we define below.

Definition 6.2.3 (Discrete Wavelet transform)**.** *The Discrete Wavelet transform (DWT) of a discrete signal $f(t)$ is given by [32]:*

$$C(a,b) = \sum_{z=1}^{Z} f(t_z)\psi\Big(\frac{t_z - b}{a}\Big), \tag{6.3}$$

where $\psi\big(\frac{t-b}{a}\big)$ is the discrete mother wavelet, a represents the scaling parameter, b the translation parameter and Z is is the number of samples taken from the signal for discretization.

Estimating the wavelet coefficients, i.e., the $C(a,b)$, for all possible scales would generate a large amount of data and is computationally expensive. Therefore, sets of scales and translations based on powers of base two yield more optimal and precise

results; that is, the parameters a, b are chosen according to $a = 2^j$ and $b = 2^j k$, for $j, k \in \mathbb{N}$ ([32], [33]).

6.2.3 Selecting mother wavelet

In the process of denoising electrocardiograms using WT, the choice of the appropriate mother wavelet is essential, since the transform coefficients contain important information about the signal, and if the choice of the mother wavelet is optimal for a given signal, this leads to maximizing the values of the transform coefficients; that is, vital signal information will be preserved when reconstructing the signal. In [33], the authors present a procedure for mother wavelet selection and use it for noise elimination in electrocardiograms. The results show that their procedure allows the signal to preserve essential signal information, so that it can be used for analysis and diagnosis. In Table 6.1 we show the types of basic mother wavelet functions and their respective order, with which optimal results are obtained for both noise elimination and signal reconstruction, according to the authors in [33].

Mother Wavelet	Order
Daubechies	4,6,8,10,12.
Symmlet	4,5,6,7,8.
Coiflet	1,2,3,4,5.
Battle–Lemarie	1,3,5

Table 6.1: Some type of Mother Wavelet basis function applied for denoising of the ECG signal.

6.2.4 Noise removal

Filtering noise in a signal using WT consists of three general stages: (1) take the DWT of a noisy signal, (2) filter the values of the transform coefficients using a threshold, eliminating the coefficients whose values are less than the threshold and (3) obtain the inverse WDT, with which it is possible to reconstruct the signal. Perhaps the best-known threshold value selection procedure is based on Stein's unbiased risk estimator, which provides an indication of the precision of an estimator [33].

The three stages of signal processing using WT can be viewed as a process of *multilevel decomposition* of the signal. Given a signal $f(t)$, first, a high-pass filter and a low-pass filter are used, with which the transform coefficients are obtained. The coefficients of the low pass filter are called *approximation coefficients* (A_1) and the coefficients of the high pass filter are called *detail coefficients* (D_1) (see Figure 6.3). Half of the samples are discarded after filtering, according to the Nyquist criterion. For the

next level of decomposition, subband A_1 is filtered using the same technique to produce narrower subbands, A_2 and D_2. Following the same filtering process iteratively, we have a set of approximation coefficients A_n and detail coefficients D_n at the end of the process.

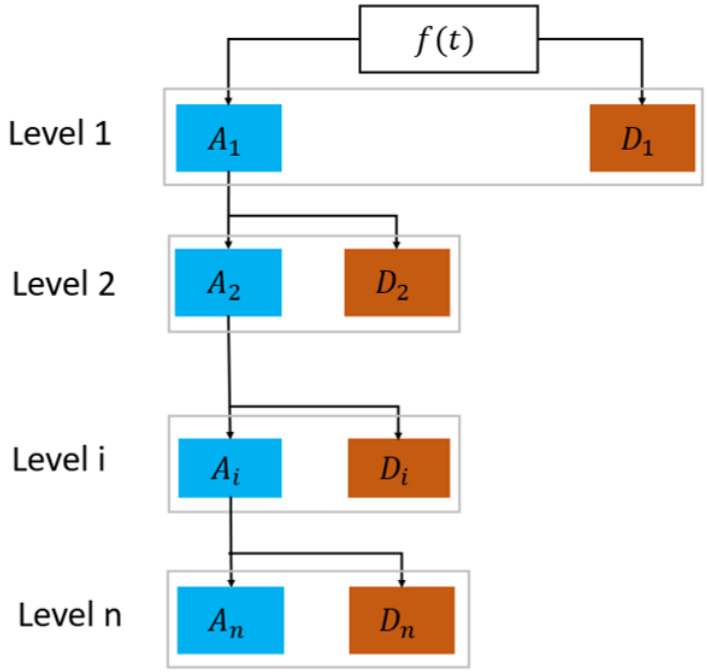

Figure 6.3: Multilevel decomposition scheme.

As an example of multilevel decomposition using WT for noise removal in ECG, Figure 6.4 graphs the decomposition of an electrocardiographic signal for 3 levels of decomposition of its detail coefficients and approximation coefficients; in the case of approximation coefficients, we only show level 3. The detail coefficients at levels 1, 2 and 3 show the high frequencies, that is, the noise in the signal. At level 3 of the approximation coefficients, which correspond to the outputs of the low-pass filter, we can observe that the information of interest in the signal is preserved, that is, we can easily find the waves and segments of the ECG.

6.3 Chapter summary

In this chapter we have described the general procedure for noise elimination in electrocardiograms. The methodology described is based on an algorithm that uses WT as a denoising tool. In Section 8.3, we will use this methodology for ECG denoising. As we will see in the results shown in that section, this process allows preserving the components of interest in the signal, such as the onset and peak of each waveform, as well as keeping the isoelectric line unaltered.

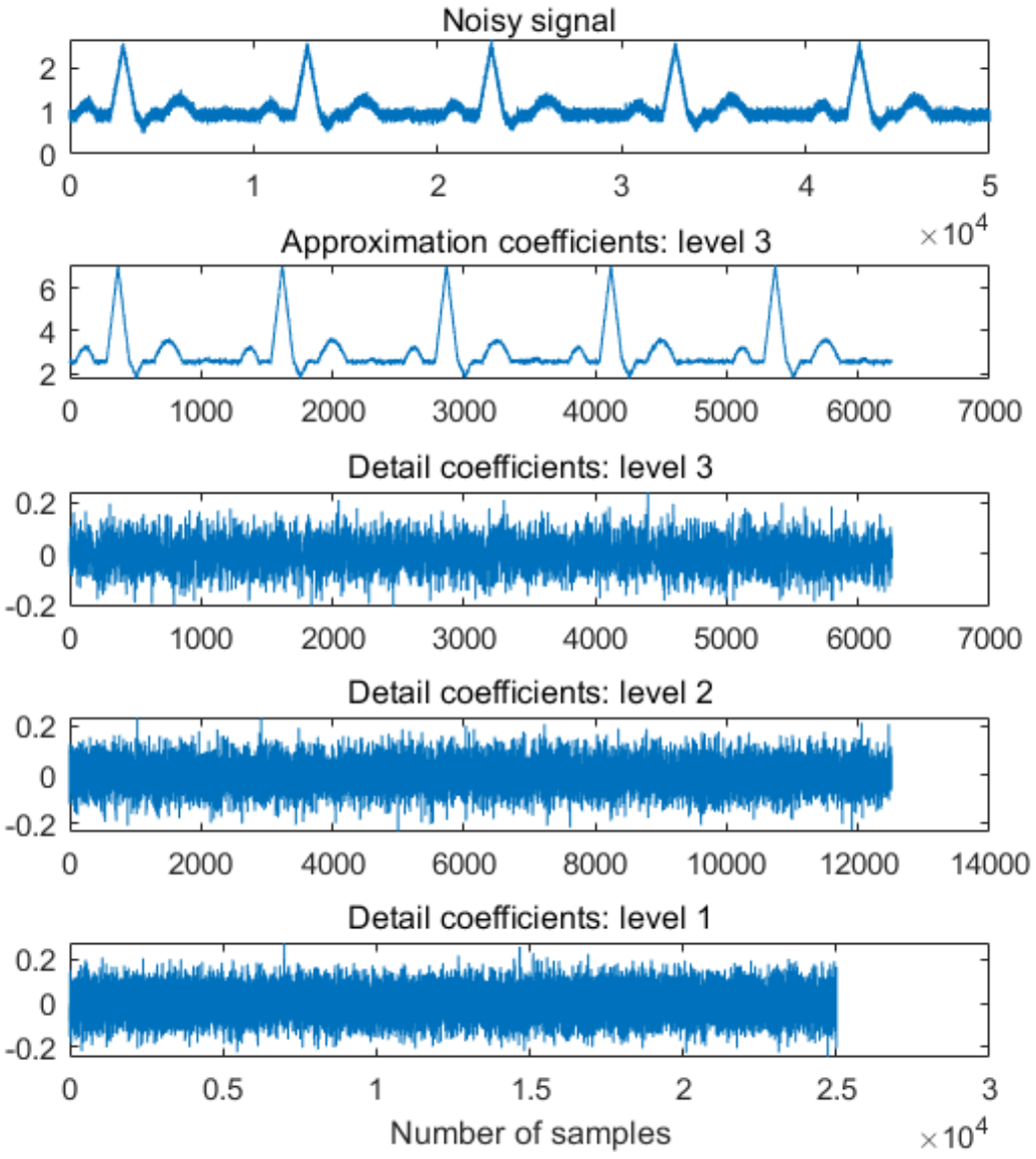

Figure 6.4: Multilevel decomposition of the electrocardiographic signal, using the order 8 Symlet wavelet. At each level of decomposition, half of the samples are discarded, according to the Nyquist criterion. That is, as the original signal has 50000 samples, in the first level of decomposition we have 25000 samples, while in the second level of decomposition, we have 12500 samples and so on.

Chapter 7

Irreversibility and electrocardiograms

In this chapter we address the underlying idea of analyzing temporal irreversibility in the electrocardiographic signal as a tool to discriminate between groups of patients under different medical conditions. First, in Section 7.1, we analyze electrocardiograms as a time series that exhibits an ordered pattern of behavior, which is related to the irreversibility of the CEA. This characteristic, in turn, can be quantified by different indicators of irreversibility. In Section 7.2.1, we give an introduction to Poincaré plots and their usefulness for quantifying irreversibility in electrocardiograms. Next, we make a general review of previous research where electrocardiograms are analyzed with the time-irreversibility approach and make a comparison between them.

7.1 Time asymmetry of the electrocardiographic signal

To address the issue of temporal irreversibility in the signal, we will consider an artificially generated electrocardiogram, which simulates the behavior of a normal electrocardiogram, that is, of a healthy subject (Figure 7.1). A normal electrocardiogram consists of an ordered succession of waves and segments that are repeated in each cardiac cycle, unless there is some medical condition that alters it (Figure 7.1(a)). If we write the signal as a symbolic sequence representing the succession of waveforms in a normal electrocardiogram ($\omega_H = \{PQRSTPQRST...PQRST\}$) and compare it with the time-reversed sequence ($\omega_H^r = \{TSRQPTSRQP...TSRQP\}$), we can notice that there is a change in the pattern with which the symbol strings appear regarding the original sequence (Figure 7.1(b)), that is, we can straightforward distinguish the change in the direction of the arrow of time between both sequences. This means that the time series exhibits time asymmetry, which is an indicator of the time-irreversibility of the process generating the electrocardiogram (CEA) and this irreversibility can be measured by means of its EPR. Additionally, let us denote with subscripts unhealthy conditions, such as P_2 portrays the P waveform altered by the presence of some medical disorder. Let us suppose that the trajectories of an electrocardiogram of an unhealthy patient and its version reversed in time are described by the sequences $\omega_{UH} = \{P_2Q_3RS_2T_3PQ_2RST_2...P_2Q_3RS_3T_2\}$ and $\omega_{UH}^r = \{T_2S_3RQ_3P_2, T_2SRQ_2P, ..., T_3S_2RQ_3P_2\}$, respectively (Figure 7.2). Here, since the sequences represent a more disordered system, it is less accessible to distinguish the

change of the arrow of time when comparing both sequences.

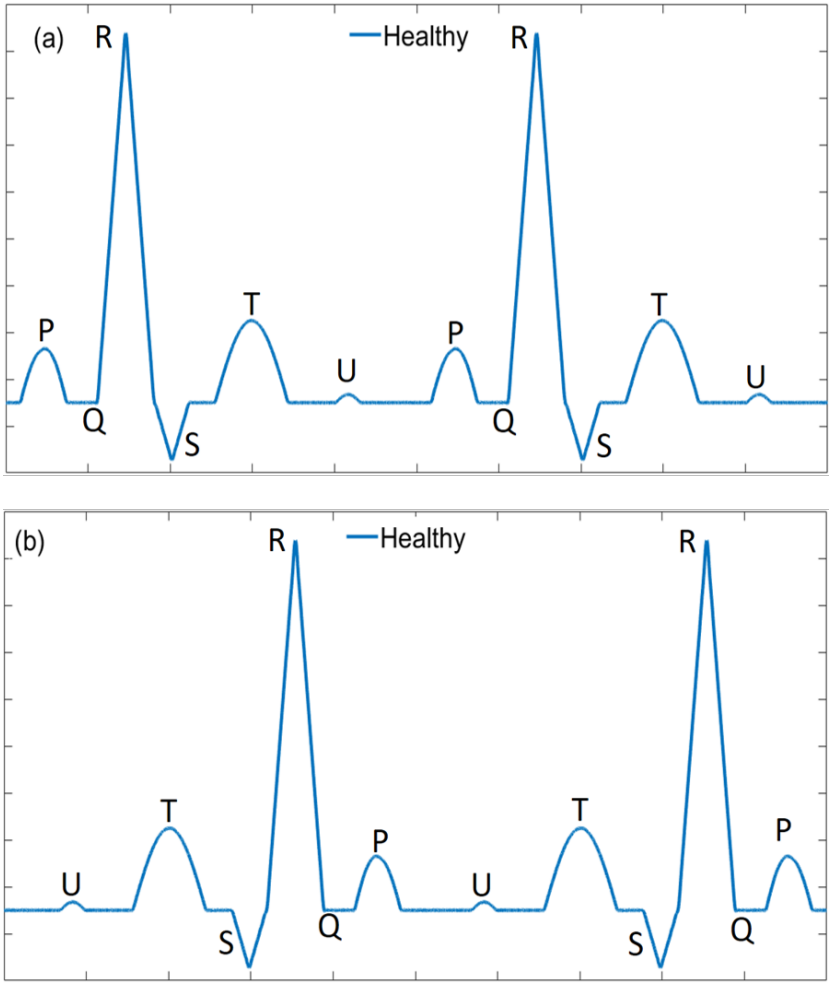

Figure 7.1: (a) Orderly behavior pattern on a normal ECG. (b) Time reversed electrocardiogram. We can write a symbolic sequence $\omega_H = \{PQRSTPQRSTU...PQRSTU\}$ that represents the different signal waves, as well as its time-reversed version as $\omega_H^r = \{UTSRQPTSRQP...UTSRQP\}$. We can see that it is clear to distinguish the arrow of time, since the waves and segments appear in strict order. This electrocardiogram was artificially generated using the algorithm proposed in [56] and represents the behavior of a normal electrocardiogram.

When we make a comparison between the string of symbols of an ECG of a healthy patient (ω_H) and that of a diseased patient (ω_{UH}), we can clearly distinguish a different typical pattern in the sequence of each patient group. This difference in the typical pattern of symbols suggests that, on average, the EPR in each group of patients differs. Furthermore, Costa and Goldberger [7] have reported that cardiac electrical activity loses temporal irreversibility with aging and in the presence of medical conditions; that is, the average EPR is expected to be higher in healthy and young patients, which can be used to evaluate the functionality of the heart using electrocardiograms. Therefore,

we propose to use the EPR as an indicator to analyze electrocardiograms coming from different patient groups. In section 10, we show that it is possible, up to some extent, to discriminate between groups of patients using our method.

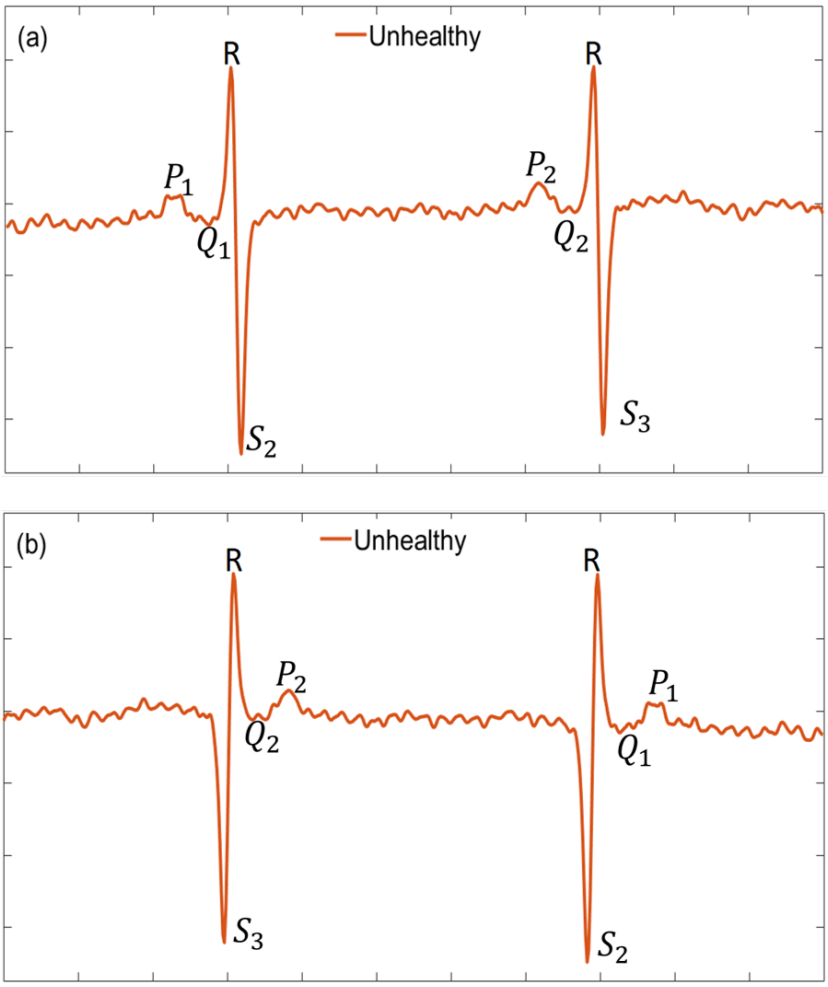

Figure 7.2: (a) Disordered behavior patterns of electrocardiograms under unhealthy conditions (atrial fibrillation). (b) Time reversed electrocardiogram. The symbolic sequence of this signal and its corresponding time-reversed version are $\omega_{UH} = \{P_2Q_3RS_2T_3PQ_2RST_2...P_2Q_3RS_3T_2\}$ and $\omega^r_{UH} = \{T_2S_3RQ_3P_2, T_2SRQ_2P, ..., T_3S_2RQ_3P_2\}$, respectively. It is more difficult to distinguish the arrow of time in ECG signals under medical conditions since they represent more disordered processes.

Up to this point, some comments regarding the concepts we are dealing with and their notation are necessary. The temporal asymmetry of a time series (electrocardiograms) indicates the time-irreversibility of the process (Cardiac Electrical Activity) that generated it. The degree of irreversibility of a process can be quantified by its entropy production rate. On the other hand, temporal asymmetry and entropy production are quantities that can be estimated directly from time series. However, making an abuse of notation, we will use the expression ¨temporal irreversibility in electrocardiograms" to

refer to the temporal irreversibility of Cardiac Electrical Activity, which, as we have just said, can be quantified through its entropy production rate.

7.2 State of art of the time-irreversibility in ECG

Here, we present a review of the state-of-the-art methodology developed so far to quantify the time-irreversibility of electrocardiograms, from a conceptual perspective, without delving into the numerical details, to focus on the importance of the time-irreversibility phenomenon for the analysis of the electrocardiographic signal.

7.2.1 Poincaré Plots based-methods

When we are interested in testing time-asymmetry in electrocardiograms, one proposal to do so is through the fluctuations of HRV, using *Poincaré plots* (PP). This graphic, in addition to being a visual tool to recognize patterns hidden in time series, is a quantitative technique, in the sense that there are different numerical tools to quantify the visual information contained in these graphs [69]. First, we describe the PP, their construction from electrocardiograms and their interpretation, which will be helpful to discuss the review of our research.

Let us consider the vector $RR := (RR_1, RR_2, ..., RR_{n-1}, RR_n)$ where RR_i is the i-th RR-interval and n is the number of heartbeats in the electrocardiogram, i.e., $n-1$ represents the number of points in the PP. From vector RR, we can define the PP as the set of ordered pairs $P_i = (RR_i, RR_{i+1})$, where $i = 1, 2, ..., n-1$ ([70], [69]); that is, the duration of the current heartbeat (RR_i) is plotted on the abscissa, while the subsequent beat (RR_{i+1}) is plotted on the ordinate (see Figure 7.3). The points above, below or on the identity line have the property $\Delta RR > 0$, $\Delta RR < 0$ or $\Delta RR = 0$, respectively, where $\Delta RR = RR_{i+1} - RR_i$; the number of points above or below the identity line is denoted as n_{up} y n_{down}, respectively. The points above or below the identity line reflect an instantaneous deceleration or acceleration of the heart rate, respectively. Since the cloud of points P_i is distributed above and below the identity line in an unbalanced way, this suggests that the heart rate pattern during acceleration is different from the deceleration pattern ([19], [18]). For each point P_i, in [20], the authors defined phase angle θ_i as $\theta_i = \arctan \frac{RR_{i+1}}{RR_i}$. Additionally, For each point P_i, it is possible to define D_i as the perpendicular distance between the i-th point and the identity line, as 1001[70]:

$$D_i = \frac{\mid RR_{i+1} - RR_i \mid}{\sqrt{2}}. \tag{7.1}$$

Different indices of time-irreversibility in the CEA have been proposed. One of them is time-asymmetry in HRV, which can be tested using PP. Employing these graphs,

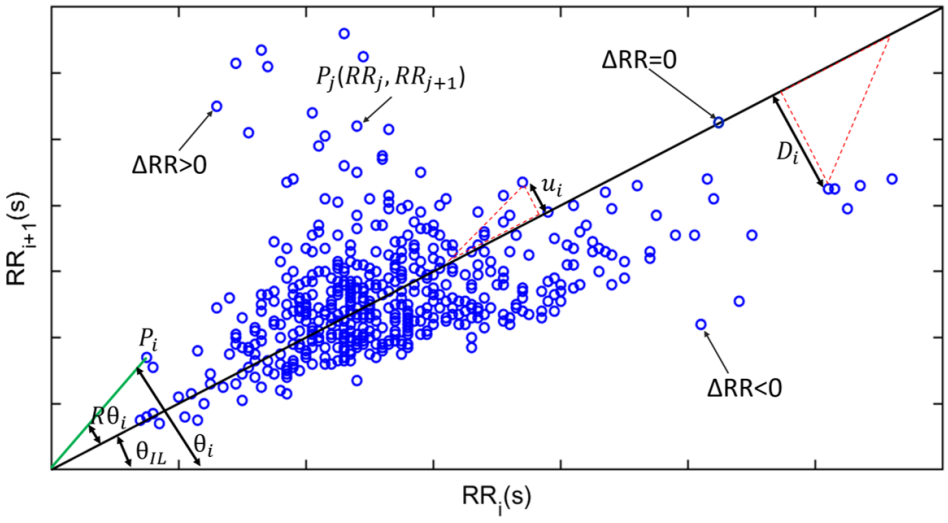

Figure 7.3: Poincaré plot. This graph allows us to visualize the asymmetric dispersion of the cloud of points, concerning the identity line. Furthermore, this asymmetry we can verify by inspection, can be quantified using the quantitative information that the graph provides us, such as the Euclidean distance D_i or the angular distance θ_i of each point P_i regarding the identity line.

different authors have proposed asymmetry indices constructed from the dispersion of the points P_i around the identity line. These asymmetry indices represent the contribution of the SNS and PNS to the irreversibility of CEA.

Frequency index I_F

In [71], the authors propose a frequency index I_F, which assigns to each point P_i in the plot the same "weight" regardless of its position on the graph. The asymmetry in the signal is measured as the percentage of the number of accelerations, concerning the total number of accelerations and decelerations of the heart rate, by:

$$I_F = \frac{n_{down}}{n_{up} + n_{down}} \times 100. \tag{7.2}$$

Distance index I_D

With the distance index I_D, proposed in [19], the weight of each point is assigned from its D_i perpendicular distance to the identity line. The asymmetry in the signal is measured by the percentage of decelerations in the heart rate, which is estimated from the distance D_i generated by the points above the identity line ($\Delta RR > 0$) with respect to the distance generated by all the points on the graph, as:

$$I_D = \frac{\sum_{i=1}^{n_{up}} u_i^2}{\sum_{i}^{n-1} D_i^2} \times 100, \tag{7.3}$$

where u_i has the same meaning as D_i but for points above the identity line.

Phase index I_{Ph}

The disadvantage of I_D is that we could find two points with the same Euclidean distance D_i but with a different angular distance θ_i, and consequently, there could exist electrocardiograms that using I_D turn out to be symmetrical, although they exhibit phase asymmetry. Consequently, in [20] they proposed the phase index I_{Ph}, which takes into account the phase asymmetry and is defined as:

$$I_{Ph} = \frac{\sum_{i=1}^{n_{up}} |R\theta_i|}{\sum_{i=1}^{n} |R\theta_i|} \times 100, \tag{7.4}$$

where $R\theta_i = \theta_{IL} - \theta_i$ and θ_{LI} is the phase angle of the identity.

Area index I_A

The indicator I_{Ph} does not consider the D_i distance of the points concerning the identity line, which represents a disadvantage in the robustness of I_{Ph}, when recordings of different duration are analyzed. In this regard, in [21] the authors report that the I_F, I_D, I_{Ph} indices exhibit sensitivity to changes in the duration of the recordings since separately, each of these indices only consider one parameter of the P_i points, namely, the frequency of points above or below the identity line (n_{up} and n_{down} respectively), their perpendicular distance D_i, or the phase angle θ_i. To complement these results, in [21], they proposed the area index I_A, which combines the information obtained from n_{up}, D_i and θ_i, of each point P_i regarding the line identity; this indicator exhibits greater robustness to variations in the duration of the electrocardiographic signal used. With I_A, the asymmetry of the HRV is estimated from the area generated by points that are located above the identity line, as:

$$I_A = \frac{\sum_{i=1}^{n_{up}} |A_i|}{\sum_{i=1}^{n} |A_i|} \times 100, \tag{7.5}$$

where $A_i = \frac{1}{2} \times R\theta_i \times r^2$; r is the radius of the sector (see Figure 7.3), while $R\theta_i$, θ_{LI} and θ_i have the definition used in the equation 7.4. I_A exhibited greater robustness to variations in the duration of the electrocardiographic signal used.

Increments-decrements patterns-based indices

In [18] the authors propose a definition of time-asymmetry which is independent of the identity line; in this proposal, to define whether a P_i point represents an increase or decrease in heart rate, its position regarding the identity line is not considered. In this new definition, the authors propose to consider two points $P_i = (RR_i, RR_{i+1})$ and $P_{i+1} = (RR_{i+1}, RR_{i+2})$, which require three consecutive RR-intervals, i.e. $\{RR_i, RR_{i+1}, RR_{i+2}\}$,

and the point P_i is classified in a set with an increasing ($\mathcal{I}$), decreasing ($\mathcal{D}$) or stable pattern ($\mathcal{N}$), regarding the cloud of points, according to:

$$\begin{aligned} P_i \in \mathcal{I}: \quad & \Big(RR_i < RR_{i+1} \wedge RR_{i+1} < RR_{i+2}\Big) \vee \\ & \Big(RR_i \geq RR_{i+1} \wedge RR_{i+1} < RR_{i+2}\Big) \vee \\ & \Big(RR_i > RR_{i+1} \wedge RR_{i+1} \leq RR_{i+2}\Big) \\ P_i \in \mathcal{D}: \quad & \Big(RR_i > RR_{i+1} \wedge RR_{i+1} > RR_{i+2}\Big) \vee . \\ & \Big(RR_i \leq RR_{i+1} \wedge RR_{i+1} > RR_{i+2}\Big) \vee \\ & \Big(RR_i < RR_{i+1} \wedge RR_{i+1} \geq RR_{i+2}\Big) \vee \\ P_i \in \mathcal{N}: \quad & RR_i = RR_{i+1} = RR_{i+2} \end{aligned} \tag{7.6}$$

Subsequently, the authors redefine I_F and I_D, to obtain:

$$I_{F_p} = \frac{n_D}{n_I + n_D} \times 100 \tag{7.7}$$

and

$$I_{D_p} = \frac{\sum_{i=1}^{n_I} u_i^2}{\sum_i^{n-1} D_i^2} \times 100, \tag{7.8}$$

respectively. In this new approach, the number of points above the identity line is equivalent to the set of points belonging to I and the set of points below the identity line is equivalent to D. Consequently, the authors substitute n_{up} for n_I and n_{down} for n_D, on equations 7.2 and 7.3, from which they obtained equations (7.7) and (7.8).

Comparison

Up to this point, we have presented a review of methods based on Poincaré plots to analyze temporal asymmetry in HRV. Intending to compare compare these results with those we obtained, we applied this methodology to four groups of patients, namely, healthy young (HY) and healthy elderly patients (HE), patients with atrial fibrillation (AF), and another with congestive heart failure (CHF), which were obtained from the *PhysioBank* database (see Section 8.2). Since these works show their results to exhibit temporal asymmetry and not for the purpose of distinguishing between different groups of patients, we make the comparison using only the average values of their results, instead of a comprehensive statistical analysis.

Figure 7.4 shows the average percentage values of the time-asymmetry indicators presented so far. We can observe that these estimators work to exhibit temporal asymmetry in the signal, but their usefulness in discriminating between patient groups needs to

be clarified; that is, we cannot distinguish a significant difference between the percentage of temporal asymmetry of the different patient groups. Furthermore, these results show some inconsistencies in the sense that in some cases (I_F, I_D, I_{F_p} and I_A), the groups of unhealthy patients exhibit higher temporal asymmetry concerning the group of young healthy patients. On the contrary, in the remaining works (I_{Ph} and I_{D_p}), the young healthy patients exhibit higher temporal asymmetry than the others. According to what was discussed in Sections 3.2 and 7.1, temporal asymmetry in the group of young healthy patients is expected to be the greatest and its value decreases under medical conditions and aging, since the electrocardiogram of a young healthy patient represents a more orderly process.

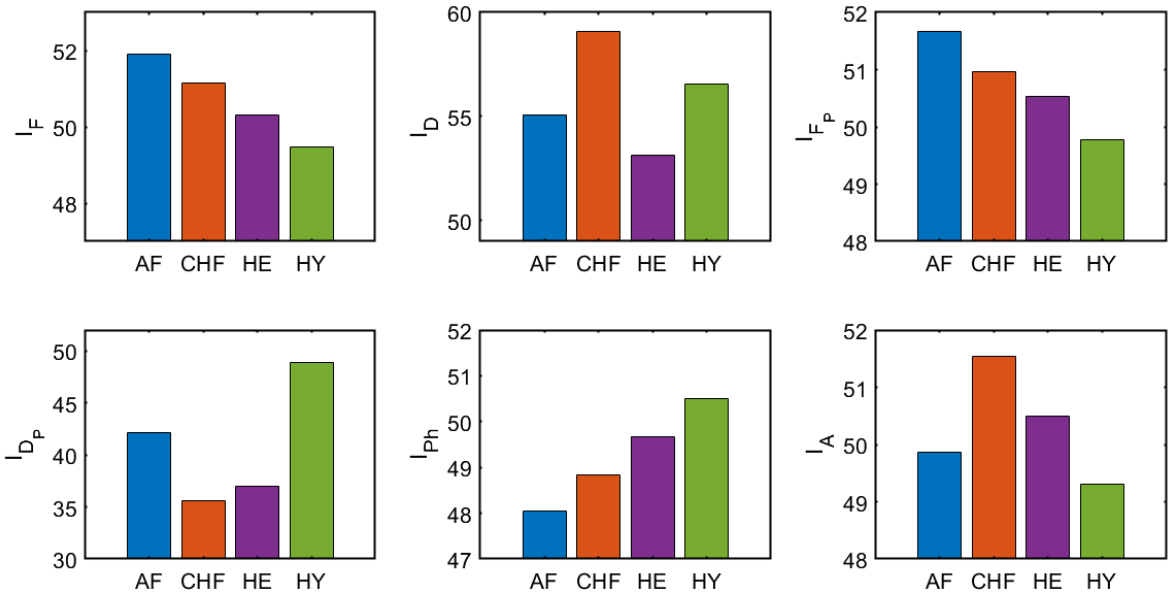

Figure 7.4: Percentage of temporal asymmetry in HRV, using Poincaré plots. We make a comparison of the average temporal asymmetry of four groups of patients. These methods allow us to exhibit temporal asymmetry in the signal, but it is not possible to distinguish a significant difference between the four groups of patients.

7.2.2 Different methods

Slope index I_S

With the same objective of estimating time-irreversibility in electrocardiograms by HRV fluctuations, different authors have proposed alternative methods to Poincaré plots. In [72] the authors proposed to estimate the time asymmetry using the first derivative of $RR := (RR_1, RR_2, ..., RR_{n-1}, RR_n)$, which they called slope asymmetry, as:

$$I_S = \frac{\sum_{i=1}^{n-1}(RR_i - RR_{i+1})^3}{(\sum_{i=1}^{n-1}(RR_i - RR_{i+1})^2)^{3/2}}. \tag{7.9}$$

Multiscale asymmetry time index I_{a_τ}

In [7] the authors propose a time-irreversibility estimator constructed from the increases and decreases of a time series at different scales $\tau \in \mathbb{N}$, under the hypothesis that if the HRV signal is a symmetric time series, the the number of increments ($RR_{i+1} - RR_i > 0$), on average, is equal to the number of decrements ($RR_{i+1} - RR_i < 0$). With this method, the time series $RR := (RR_1, RR_2, ..., RR_{n-1}, RR_n)$ is mapped to the sequence of increments and decrements $\{\gamma_i : i = 1, 2, ..., n-1\}$, where $\gamma_i = RR_{i+1} - RR_i$. To capture information on multiple time scales, the authors construct a new coarse-grained time series, taking the average within a moving window with $\tau \in \mathbb{N}$ points, as $\gamma_\tau(i) = \frac{1}{\tau}\sum_{j=0}^{\tau-1}\gamma_{i+j}$. From the probability distribution $\mathbb{P}(\gamma_\tau)$ of the variable γ_τ and for a τ fixed, the authors define $a(\tau)$ as a measure of time-irreversibility, as:

$$a(\tau) = \frac{\sum_{\gamma_\tau>0}\mathbb{P}(\gamma_\tau)\ln[\mathbb{P}(\gamma_\tau)]}{\sum_{\gamma_\tau}\mathbb{P}(\gamma_\tau)\ln[\mathbb{P}(\gamma_\tau)]} - \frac{\sum_{\gamma_\tau<0}\mathbb{P}(\gamma_\tau)\ln[\mathbb{P}(\gamma_\tau)]}{\sum_{\gamma_\tau}\mathbb{P}(\gamma_\tau)\ln[\mathbb{P}(\gamma_\tau)]}. \tag{7.10}$$

Finally, using $a(\tau)$, they propose the time-irreversibility index I_{a_τ} as the sum of the irreversibility values obtained for each value of τ, as:

$$I_{a_\tau} = \sum_{\tau=1}^{L} a(\tau). \tag{7.11}$$

The authors report that using this index, it was possible to evaluate time-irreversibility in electrocardiograms at different scales τ, and they found that values of I_{a_τ} are higher for a time series from young healthy subjects and decrease with aging or heart disease.

Multiscale asymmetry time index I_{d_τ}

Following a similar procedure of seeking to capture the imbalance between increases and decreases, in [73], the authors propose a multiscale method to measure time-asymmetry in time series based on the difference between increments and decrements, for different values of the scale $\tau \in \mathbb{N}$. First, given the vector $RR := (RR_1, RR_2, ..., RR_{n-1}, RR_n)$, they define the variable $z_i = RR_{i+\tau} - RR_i$, for $1 \leq i \leq n - \tau$. Next, the authors estimate the difference d_τ between the rate of increases and decreases by:

$$d_\tau = \frac{\sum_{z_i<0}H(-z_i) - \sum_{z_i\geq 0}H(z_i)}{n-\tau} \tag{7.12}$$

where H is the Heaviside function ($H(z_i) = 0$ if $z_i < 0$ or $H(z_i) = 1$ if $z_i \geq 0$). The time-irreversibility estimator is defined for range of scales τ as:

$$I_{d_\tau} = \sum_{\tau=1}^{L} d_\tau. \tag{7.13}$$

Entropy of differences index E_D

Given the vector $RR := (RR_1, RR_2, ..., RR_{n-1}, RR_n)$, in [22], the authors perform a symbolic encoding of the data using a uniform partition of state space $\mathbf{S}$. Let $a_1^k = a_1 a_2 ... a_k$ be a word of length k that can be formed in the sequence, that is, $a_1^k \in \mathbf{S}^k$. Next, for the probability distributions $\mathbb{P}(a_1^k)$ and $\mathbb{P}(a_k^1)$ of all k-length words that can be formed in the sequences and their inverted version in time, a_1^k and a_k^1, respectively, the authors define an irreversibility estimator based on the entropy of differences between $\mathbb{P}(a_1^k)$ and $\mathbb{P}(a_k^1)$, as:

$$E_D = -\sum_{N_d \neq 0} N_d \log N_d, \tag{7.14}$$

where N_d is the normalized difference between $\mathbb{P}(a_1^k)$ and $\mathbb{P}(a_k^1)$, defined as:

$$N_d = \frac{|\mathbb{P}(a_1^k) - \mathbb{P}(a_k^1)|}{\sum_{a_1^k \in \mathbf{S}^k} |\mathbb{P}(a_1^k) - \mathbb{P}(a_k^1)|}. \tag{7.15}$$

Natural time-based index Λ_τ

In [17] the authors propose to measure the breaking of temporal symmetry in HRV by means of the entropy change in natural time of the system. This entropy change $\Delta S = S - S^r$, is defined as the difference between the entropy S of the original sequence of RR-intervals and the entropy of the sequence reversed S in time; the time series formed by the RR-intervals is read in the natural time domain of the system. In an HRV signal, the natural time χ is introduced by assigning to the m-th heartbeat of the signal consisting of n beats, the value $\chi_m = m/n$ and the analysis is done in terms of the pair (χ_m, RR_m) , where RR_m denotes the duration of the m-th beat. S y S^r are defined respectively as:

$$S = \langle \chi \ln \chi \rangle - \langle \chi \rangle \ln \langle \chi \rangle , \tag{7.16}$$

and

$$S_R = \langle \chi \ln \chi \rangle_R - \langle \chi \rangle_R \ln \langle \chi \rangle_R , \tag{7.17}$$

where $\langle \chi \rangle = \sum_{m=1}^n p_m \chi_m$, $p_m = \frac{RR_m}{\sum_{i=1}^n RR_i}$, $\langle \chi \ln \chi \rangle = \sum_{m=1}^n p_m \chi_m \ln \chi_m$ and $\langle f(\chi) \rangle_R \equiv \sum_{m=1}^n f(\chi_m) p_{n-m+1}$. In order to evaluate ΔS at different scales τ, the authors estimated ΔS_τ for $\tau = 1, 2, \ldots, L$; τ denotes the number of successive pulses used to estimate ΔS_τ. That is, from a moving window of size τ that slides through the time series $RR = \{RR_1.RR_2, ..., RRn\}$ composed of n heartbeats, the entropy in natural time is determined for each position j of the sliding window, considering $p_m = \frac{RR_{j+m}}{\sum_{m=1}^\tau RR_{j+m}}$ for $m = 1, 2, ..., \tau$. Next, they focus on the application of the complexity measures

$$\Lambda_\tau = \frac{\sigma(\Delta S_\tau)}{\sigma(\Delta S_3)} \tag{7.18}$$

for moving window of τ length heartbeats.

Permutation method index I_O

In [74], the authors construct an irreversibility indicator based on *permutation patterns*. Broadly speaking, given a time series $X = \{X(1), X(2), ..., X(t)\}$, they first build a space windowed of size m as $X_m^\tau(i) = \{X(i), X(i + [m - (m-1)]\tau) + ... + X(i + (m-1)\tau)\}$. Next, the elements of $X_m^\tau(i)$ are sorting. For example, in ascending order as $\{X(j_1) \leq X(j_2) \leq ...X(j_m)\}$, from which they obtain a vector of ordinal patterns as $\zeta_m = (j_1, j_2, ...j_m)$, whose time-reversed version is $\zeta_m^r = (j_m, j_{m-1}, ...j_1)$. For instance, let us consider the time series $X = \{401, 805, 703, 823, 712, 505, 600, 485, 610, 570\}$, containing the duration of 10 consecutive heartbeats (in milliseconds). For $m = 4$, $i = 4$ and $\tau = 1$, we have that $X_4^1(4) = \{823, 712, 505, 600\}$, $\zeta_4 = (3, 4, 2, 1)$ and $\zeta_4^r = (1, 2, 4, 3)$. Let $\mathcal{O}^m$ be the set of all possible ordinal patterns that can be formed by sliding the m-length window over the time series X. Let $\mathbb{P}(\zeta_m)$ and $\mathbb{P}(\zeta_m^r)$ the probability distributions of ζ_m and ζ_m^r, respectively. The authors propose an irreversibility estimator given by [74]:

$$I_O = \sum_{\zeta_m \in \mathcal{O}^m} \mathbb{P}(\zeta_m) \frac{\mathbb{P}(\zeta_m) - \mathbb{P}(\zeta_m^r)}{\mathbb{P}(\zeta_m) + \mathbb{P}(\zeta_m^r)}. \tag{7.19}$$

Comparison

In Figure 7.5, we show the values of the indices constructed with additional approaches to Poincaré plots, which were obtained using the same four groups of patients as in Figure 7.4. Most of these indices (I_{a_τ},I_{d_τ},Λ_τ and I_O) exhibit a higher asymmetry in young healthy patients, which is lost under medical conditions and aging. The I_S and E_D estimators performed the poorest in distinguishing between the different groups of patients, while the Λ_τ estimator seems to show the best performance, in the sense that its value in the case of the HY group is approximately twice higher than that of AF and CHF.

7.2.3 Final comments on the review

The previous research we just discussed in this section was accomplished by analyzing merely the *RR*-intervals. Perhaps except for what was reported in [17], with none of the tests carried out have they been able to discern a clear difference between groups of patients. Additionally, results reported in preceding works were achieved using signal times ranging from 30 minutes to 24 hours, which from a practical point of view turns out to be too long. Hence, this leads us to search for new alternatives. In this thesis, we propose to perform our analysis by segmenting the signal into three different categories, namely, (1) the electrocardiographic signal, (2) *RR*-intervals and (3) joint variability signals; this allowed us to have a comprehensive analysis of the signal.

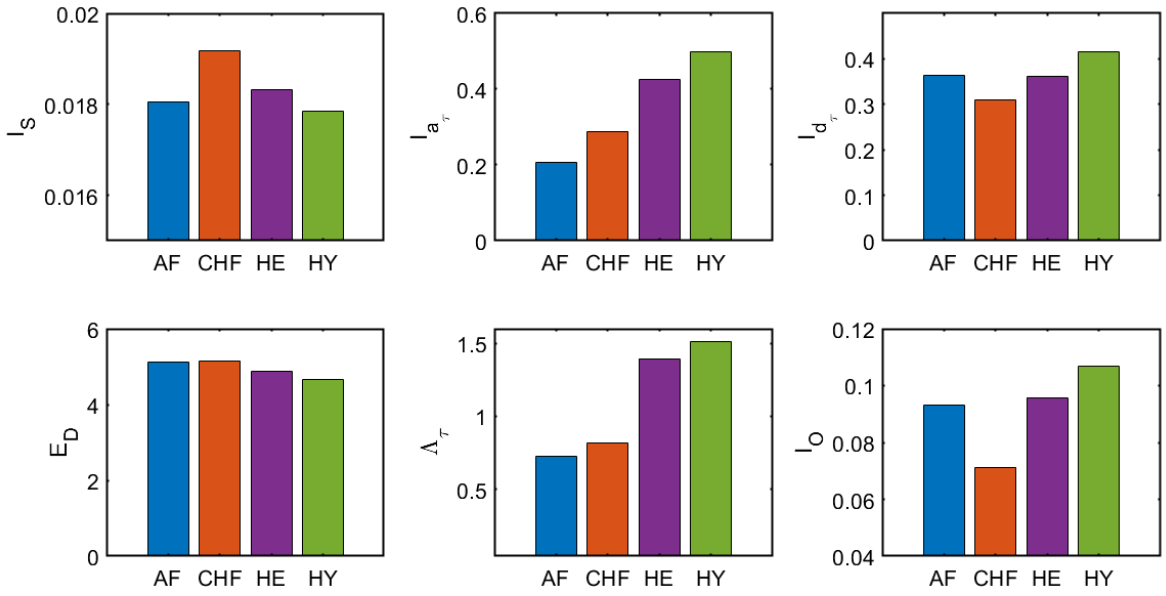

Figure 7.5: Temporal asymmetry in HRV, using different methods. Four of these methodologies are consistent (figures (b),(c), (e) y (f)) in the sense that they indicate greater irreversibility in the case of the HY group. In the case of Λ_τ, it exhibits the greatest difference between the HY group and the groups with medical conditions (AF and CHF).

7.3 Chapter summary

In this chapter, we have described the electrocardiographic signal as a time series that exhibits temporal asymmetry, which can be measured by irreversibility indicators such as Poincaré plots, permutation patterns, natural time, etc. Next, we made a comparison of the indicators found in the literature by analyzing the HRV. We found that analyzing only HRV does not take into account other signal components, such as waveform fluctuations when medical conditions are present. Therefore, in Chapter 8, we will derive other signal components and use them to study temporal irreversibility. Additionally, in the same chapter, we will analyze the data using the entropy production rate as an indicator of irreversibility.

Chapter 8

Methodology

This chapter describes the methodology followed to analyze the temporal irreversibility in electrocardiograms, which is a process consisting of different stages. An important stage of the process is the one described in Section 8.5, where we carry out an autocorrelation analysis of the data and these results supported us to assume that our data are of a Markovian nature. Each of the remaining stages are explained in detail in this chapter, except the ROC analysis, for which we devote Chapter 9.

As we discussed in Section 7.2, in the literature we can find works that use different irreversibility indicators to analyze electrocardiograms, using only the RR-intervals signal (HRV). In some of them, the authors display their results only as irreversibility test for ECGs ([71], [19], [70], [18], [23], [73]); in the other works, the authors show how to use their proposed temporal irreversibility indicators to discriminate ECGs from different groups of patients ([20], [21], [22], [7], [74], [17]). However, except for what is reported in [17], according to our knowledge, in none of these studies have they been able to discern a clear difference between groups of patients with different health conditions. Additionally, results reported in preceding works were achieved using signal times ranging from 30 minutes to 24 hours, which from a practical point of view turns out to be too long.

Improving the effectiveness of the methodology to distinguish between different groups of patients, while reducing the signal time necessary to carry out the analysis is a significant challenge that leads us to look for new alternatives. In this thesis, we propose to use EPR as an index to discriminate between electrocardiograms of different groups of patients. First, we use estimators found in the literature, namely, *Entropy Production Rate* (equation (4.3)), *Matching Time* (equation (4.7)) and *Kullback-Leibler Divergence* (equation (4.10)). Next, we introduce the *Lag Irreversibility Function* as an estimator of time-irreversibility (equation (4.12)), which has shown some advantages to discriminate ECGs from four groups of patients (see Section 10). Aiming to achieve a comprehensive analysis of the signal, we propose to analyze the electrocardiographic signal in three categories, namely, (1) the entire electrocardiographic signal, (2) heart rate variability, and (3) joint variability signals. The latter refers to jointly analyzing heart rate and the variation of wave amplitudes in each heartbeat, for which we proposed an encoding technique (see Section 8.10). When comparing with what is reported in the literature, our proposal is a more complete analysis and represents an advantage, since previous

works have reported research that only analyzes heart rate variability.

8.1 Outline

The problem of analyzing time series coming from real-life systems, such as electrocardiograms, could be considered as the problem of obtaining the symbolic representation of the time series, from which it is possible to analyze the data, similar to the inverse problem we discussed in Section 2.3.1. In this thesis, we propose a methodology to discriminate between electrocardiograms of different groups of patients, for which the symbolic representation of the signal is an essential stage. Therefore, in Section 8.6, we provide a detailed description of the procedure for the symbolic representation of electrocardiograms.

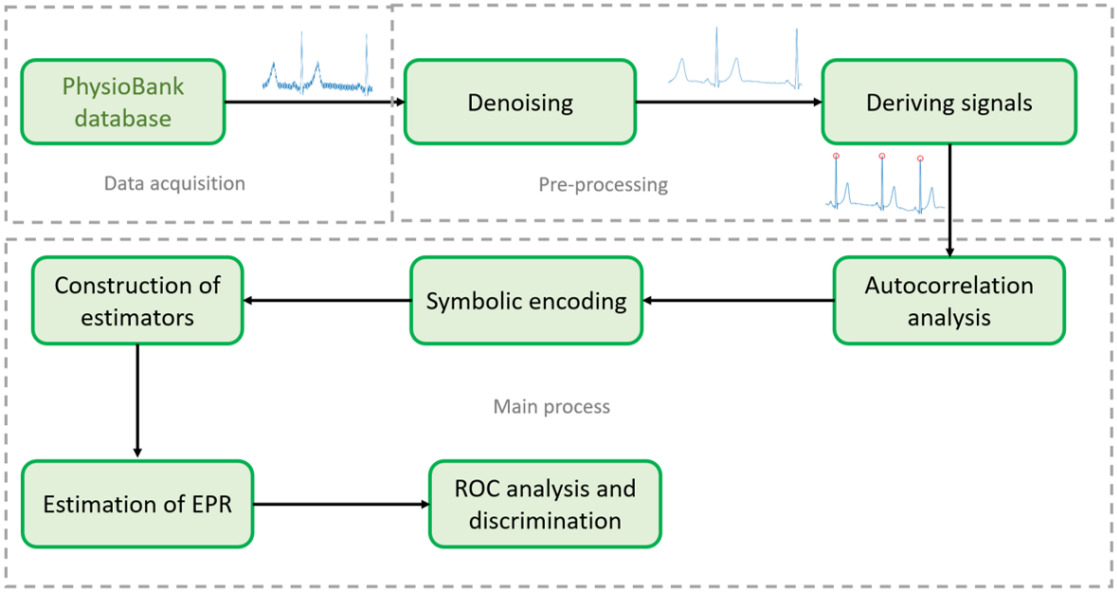

Figure 8.1: Entropy production in electrocardiograms. The analysis of electrocardiograms using our approach is a process divided into three main stages. The first stage corresponds to data acquisition, while the preprocessing stage is composed of two sub-stages, denoising and deriving signals. The main stage of the process consists of five sub-stages: autocorrelation analysis, symbolic encoding, construction of the estimators, estimation of EPR and ROC analysis.

As we mentioned above, the main purpose of this work is to use time-irreversibility as a property for discriminating two groups of healthy patients, Healthy Young (HY) and Healthy Elderly (HE), from those with medical conditions, Congestive Heart Failure (CHF) and Atrial Fibrillation (AF). However, quantifying the degree of time-irreversibility from ECG recordings is neither a direct nor a trivial task, so we propose a methodology consisting of eight stages (see Figure 8.1): (1) data acquisition, (2) denoising of the ECG signal, (3) deriving signals, (4) autocorrelation analysis, (5) symbolic encoding, (6)

construction of the estimators, (7) estimation of EPR for classification and (8) ROC analysis and discrimination. Next, we give a description of stages (1)-(6), which are the preliminary steps before presenting our main results in stages (7) and (8), which are fully described in Chapter 10 below.

8.2 Data acquisition

PhysioBank is an archive of digital recordings of physiological signals that can be used for biomedical science research [24]. This archive currently includes databases of neuronal, pulmonary, cardiac and other biomedical signals, for healthy patients and with a wide variety of medical conditions, which have important implications for public health, such as sudden cardiac death, atrial fibrillation, congestive heart failure, epilepsy and many others. Currently, *PhysioBank* contains more than 75 databases that can be freely downloaded, for which it has *PhysioToolkit*, which is a collection of software to visualize, analyze and simulate biomedical signals; in particular, *PhysioToolkit* provides *the WFDB Software Package* for *MATLAB* [75]. With this open-source toolbox, we can access more than 50 databases contained in *PhysioBank*, which include ECG, EEG, EMG, fetal ECG, PLETH (PPG), ABP, respiration, and more. This software package has 65 functions for visualization, annotation, signal processing and automated analysis, such as *rdsamp* (to read the signals in the files).

Datasets were obtained from the *PhysioBank* database, by means of the open-source WFDB Software Package, using the command *rdsamp*. HY and HE groups were selected from *FANTASIA* database [76], while CHF and AF groups were selected from the *BIDM Congestive Heart Failure* [77] and *MIT-BIH Atrial Fibrillation* [78] databases, respectively.

The Healthy Young group, as well as the Healthy Elderly group, are comprised of 20 electrocardiograms (ECGs) each, which were acquired from patients at supine rest. The sampling frequency is 250 Hz and every ECG record is 120 minutes long. It is also important to mention that the HY patient group is comprised of 10 men and 10 women aged between 21 and 34. On the other hand, the HE patient group is also comprised of 10 men and 10 women but aged between 68 and 85.

For the CHF group, the databases provide 15 ECG recordings from which, 11 correspond to men aged from 22 to 71 and 4 correspond to women aged from 54 to 63. Every ECG record in this group is 20 hours long with a sampling frequency of 250 Hz. For the AF group the database provides 25 ECG records of adult subjects [1] and each recording is 10 hours long with a sampling frequency of 250 Hz. ECG recordings for AF and CHF groups were obtained by means of ambulatory electrocardiography.

[1] No mention about the patient age is found in the database.

We point out that, although HY, HE and AF databases have 20 or more electrocardiographic recordings, CHF database contains only 15 ECG samples. Therefore, we considered 15 ECG recordings for each group, so we have homogeneity in the number of samples used. Moreover, in order to have homogeneous samples, we take the first 100 minutes of the ECGs samplings. Also, we consider 5500 heartbeats from ECGs to carry out all the estimates, which corresponds to the common length of heartbeats within all the considered sequences. In Table 8.1 we give a summary of the information described in the last paragraphs about the databases.

Patient group	Database	Recordings	Age
HY	FANTASIA	20 (10 M,10 W)	21-34
HE	FANTASIA	20 (10 M,10 W)	68-85
CHF	BIDM	15 (11 M,4 W)	22-71
AF	MIT-BIH	15	

Table 8.1: Patient groups. All signals were obtained with a sampling frequency of 250 Hz. Each group is composed of men (M) and women (W).

8.3 Denoising of the ECG signal

As we discussed in Section 6.1, when we implement methods for discriminating electrocardiograms from different groups of patients, the removal of noise in the data is a vital part of the preprocessing stage. This is not only due to the physiological oscillation of the signal but also due to the different sources of noise that the signal may present, which corrupt the signal and prevent its correct analysis. These noise sources include the power line of the equipment, respiratory movement, muscle noise, and baseline wander, among others [33]. Here, we employ one of the most used tools for filtering ECGs which is the *Discrete Wavelet Transform* (DWT) (see [32] for a review). It allows us to implement a band pass filtering by eliminating high- and low-frequency signals that do not correspond to the range of electrocardiographic signal frequencies (see Chapter 6).

The denoising process in MATLAB can be implemented using the *Wavelet Signal Denoiser* app, which is an interactive tool for visualization and denoising in signals using the *Wavelet transform* (see Chapter 6). In particular, this app provides the *wden* function, which receives the raw signal as an argument and returns a denoised version of it. To obtain the WT coefficients, the *wden* function decomposes the received signal using a specific wavelet; in our case, following the methodology proposed in [33], we use the *Symlets* wavelet family. Next, wavelet denoising consists of passing the WT

coefficients through a threshold, which removes those coefficients below a specific value. Finally, it is possible to reconstruct the signal using inverse DWT. This can be done without affecting the signal quality since its characteristics are concentrated in the highest magnitude wavelet coefficients ([33], [32]).

Figure 8.2 plots a raw ECG signal (green line) and its denoised version (red line). As we mentioned above, when we process electrocardiograms, it is important not to affect the important information of the signal. In Figure 8.2 we can see that after the denoising process, the signal preserves the significant points that interest us for the encoding process later, namely, the peak and the onsets and offsets points of each wave (see Figure 8.3). Additionally, we can see that the signal preserves the amplitude and duration of each wave.

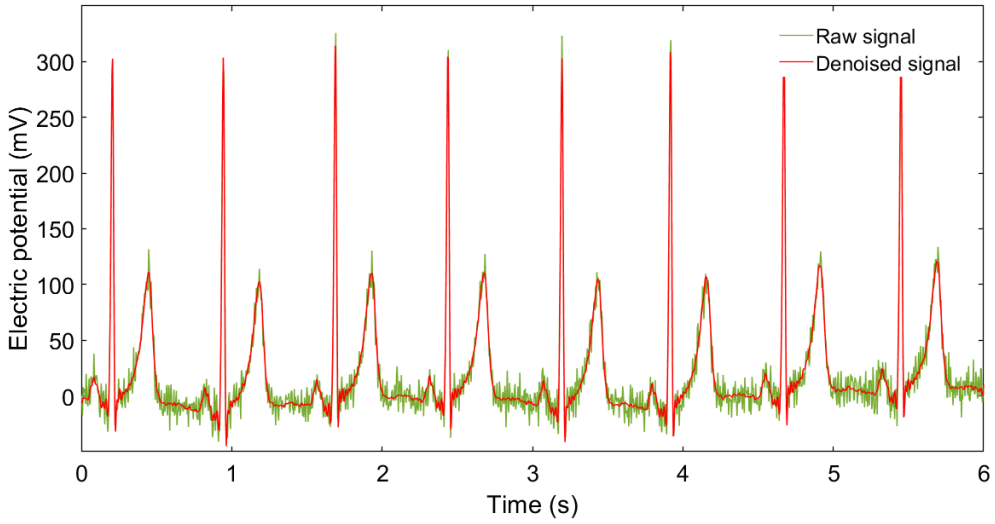

Figure 8.2: Raw and denoised signals. In this example, the raw signal exhibits high-frequency noise (green color). After the noise removal process, the clean signal (red color) preserves the characteristic points of the electrocardiogram.

8.4 Deriving signals

In addition to the electrocardiographic signal, the other components under study were obtained using the NeuroKit2 package, which is The Python Toolbox for Neurophysiological Signal Processing ([79]). This tool allows to detect the components of the electrocardiographic signal. In particular, we can locate the onsets and peaks of the P, R and T waves (see Figure 8.3(a)), using the *ecg-delineated* command.

Next, using the onsets and peaks of P, R and T waveforms, we compute the waveform amplitude through the difference between the voltage at its onset point and its peak. Specifically, the wave amplitude is defined as $W_{peak} - W_{onset}$, where W_{onset} is the voltage at the starting point of the wave and W_{peak} is the voltage that reaches the peak

of the wave. For example, for the i-th heartbeat, the R-wave amplitude is given by $RW_i = RW_{peak_i} - RW_{onset_i}$; we repeat the procedure analogously for the P and T waves (see Figure 8.3(b)). Regarding the RR intervals, it is possible to obtain them using the `hrv` function of *Neurokit*.

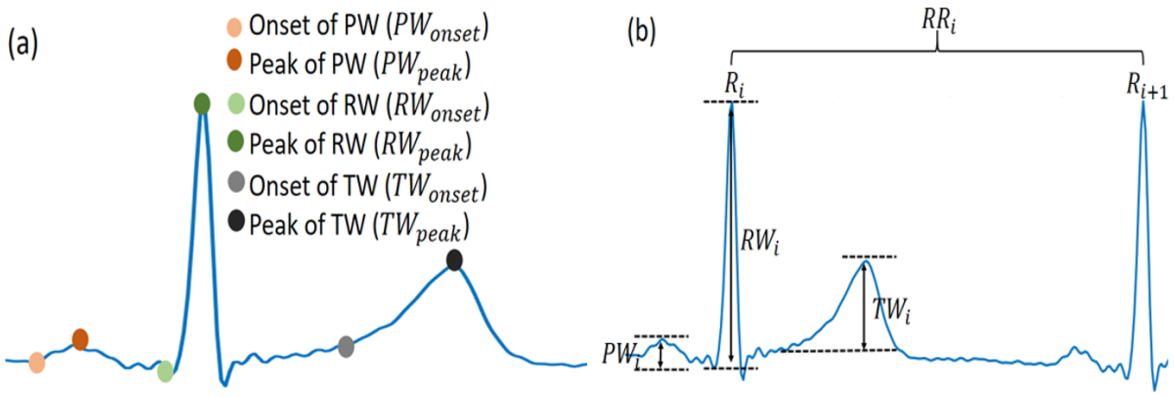

Figure 8.3: Components of the ECG signal. The amplitudes of waves P, R and T, at the i-th heartbeat, are obtained by means of $PW_i = PW_{peak_i} - PW_{onset_i}$, $RW_i = RW_{peak_i} - RW_{onset_i}$ and $TW_i = TW_{peak_i} - TW_{onset_i}$, respectively.

This definition of wave amplitude gives us four time series, namely, $PW = \{PW_i : i = 1, 2, \ldots, n\}$, $RW = \{RW_i : i = 1, 2, \ldots, n\}$, $TW = \{TW_i : i = 1, 2, \ldots, n\}$ and $RR = \{RR_i : i = 1, 2, \ldots, n\}$, where $n = 5\,500$, is the number of heartbeats contained in data. These quantities are those that, in Section 10.4, we refer to as *variability signals*. Moreover, the electrocardiographic signal itself is a signal under study of the form $x = (x_1, \ldots, x_N)$, where N corresponds to the recorded signal time.

8.5 Markovianity of the electrocardiographic signal

In Section 2.3, we discussed that the time series we are working with (electrocardiographic signal) can be considered as a realization of a stochastic process. In particular, we assume that our data are realizations of Markov processes, which can be tested by cross-correlating the signal with itself, considering a temporal lag τ. Therefore, in this section, we first show the *autocorrelation function* (ACF) of the electrocardiographic signal and of the variability signals we analyze in this work. This will serve as background to present the assumptions of the Markov model of the signal.

In Figure (8.4), we show the ACF of each of the variability signals with a version of itself lagged τ units in time, that is, we show the ACF of the pairs of signals $(RR_t, RR_{t+\tau})$, $(PW_t, PW_{t+\tau})$, $(RW_t, RW_{t+\tau})$ and $(TW_t, TW_{t+\tau})$. We can see that the signals in all cases show similar autocorrelation properties. For example, for the RR-intervals signal (see Figure (8.4)(a)), the highest autocorrelation value of $|\rho_{(RR_t, RR_{t+\tau})}(\tau)| \approx 0.5$ is obtained

with $\tau = 1$. For values of $2 \leq \tau \leq 5$ the function quickly approaches zero, while for $\tau > 5$, we have $|\rho_{(RR_t, RR_{t+\tau})}(\tau)| \approx 0$. On the other hand, as we saw in Section 2.4, if $|\rho_{(RR_t, RR_{t+\tau})}(\tau)| = 1$, then there are constants $\beta_1, \beta_2 \in \mathbb{R}$ such that $RR_{t+\tau} = \beta_1 RR_t + \beta_2$, that is, we can derive $RR_{t+\tau}$ from RR_t. This suggests that when $|\rho_{(RR_t, RR_{t+\tau})}(\tau)| > 0$ (significantly different from zero), we have an rough measure to forecast RR at time $t + \tau$ from its value at time t. In our analysis of the RR_t and $RR_{t+\tau}$ signals, in the four groups of patients, we have that $|\rho_{(RR_t, RR_{t+\tau})}(1)| > |\rho_{(RR_t, RR_{t+\tau})}(\tau)|$, for $\tau = 2, 3, ...20$, that is, the highest autocorrelation is found for $\tau = 1$. This suggests that this signal has the highest degree of memory for $\tau = 1$, which in turn can be interpreted as the signal being of Markovian nature. We have similar results for the other three variability signals in Figures (8.4)(b), (8.4)(c) and (8.4)(d).

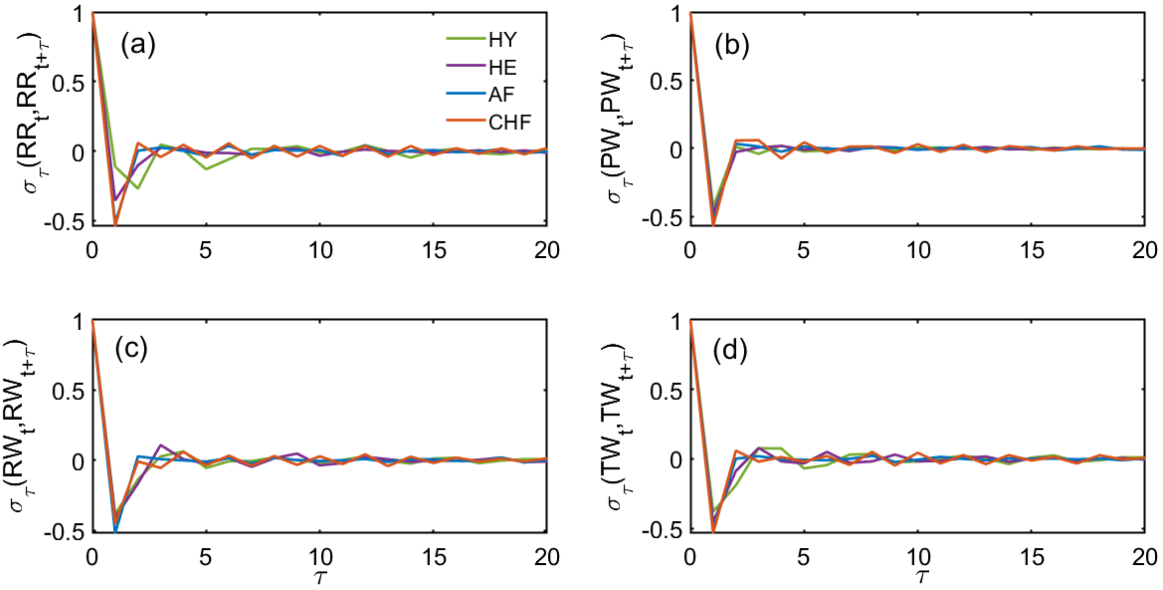

Figure 8.4: Autocorrelation function of variability signals. Each ACF was obtained by cross-correlating each variability signal with itself (using 5000 heartbeats), for lags of $\tau = 1, ..., 20$. The values shown in this figure are the average of 15 subjects in each group.

In Figure 8.5, we display the ACF of the electrocardiographic signal with a version of itself lagged ι units in time; that is, we show the ACF of the signals $(ECG_t, ECG_{t+\iota})$. We can see that ACF exhibits non-zero values for $\iota = 1, 2, ..., 8$ and for values of $\iota > 8$ we have that $|\rho_{(ECG_t, ECG_{t+\iota})}(\iota)| \approx 0$, for the four groups of patients. However, as in the case of variability signals, we can see that $|\rho_{(ECG_t, ECG_{t+\iota})}(1)| > |\rho_{(ECG_t, ECG_{t+\iota})}(\iota)|$, for $\iota = 2, 3, ...20$, that is, the highest degree of memory is obtained for $\iota = 1$. Since there is a more significant correlation for $\iota = 1$, here we only study the memory of the previous step ($\iota = 1$), which is related to the markovianity of the electrocardiographic signal.

The ACF results provide us with the necessary arguments to assume Markovianity in the electrocardiographic signal. Next, we present the assumptions of the signal Markov model, with transition matrix P:

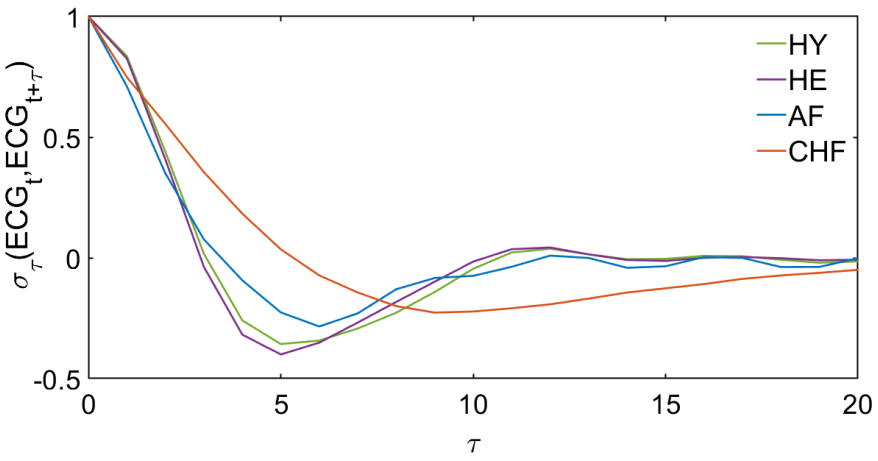

Figure 8.5: Autocorrelation function of the electrocardiographic signal. Each ACF was obtained by cross-correlating the electrocardiographic signal with itself (using 100 minutes), for lags of $\iota = 1, ..., 20$. The values shown in this figure are the average of 15 subjects in each group.

1. Stationary Markov process.
2. Irreducible Markov process.
3. Positive recurrent Markov P process.
4. Aeriodic Markov process.
5. The length of the signals is large enough, such that the convergence of the law of large numbers in equation (2.14) is achieved. This condition allows us to obtain the invariant probability distribution π of the process using $\pi = P\pi$, from which we can estimate the EPR of the process using equation (4.3); this invariant probability distribution π is unique in an ergodic Markov process that is irreducible, aperiodic, and positive recurrent.

8.6 Encoding

Let us recall that the data under study is a discrete sequence of the form $x = x_1, \ldots, x_N$, corresponding to 100 minutes of ECG recordings sampled at 250 Hz. That gives us a 1500000-long discrete vector for each one of the samples we analyze.

In order to avoid spurious non-stationary characteristics, in the case of variability signals, once we have obtained the PW, RW, TW and RR vectors, we consider the differences between consecutive entries, eliminating the non-stationary characteristics. For instance, in the case of the RR intervals, we consider the time series of differences $\delta = (\delta_1, \ldots, \delta_{n-1})$, where n is the total number of heartbeats in our samples and $\delta_i = RR_{i+1} - RR_i$ is the difference between the $(i+1)$-th and the i-th heartbeats

duration (see Figure 8.6); we repeat the procedure analogously for the PW, RW and TW vectors. Specifically, for the RR intervals, P-wave, R-wave, and T-wave, their respective difference time series are given by $\Delta RR = \{\Delta RR_i : \Delta RR_i = RR_{i+1} - RR_i, i = 1, 2, \ldots, n-1\}$, $\Delta PW = \{\Delta PW_i : \Delta PW_i = PW_{i+1} - PW_i, i = 1, 2, \ldots, n-1\}$, $\Delta RW = \{\Delta RW_i : \Delta RW_i = RW_{i+1} - RW_i, i = 1, 2, \ldots, n-1\}$ and $\Delta TW = \{\Delta TW_i : \Delta TW_i = TW_{i+1} - TW_i, i = 1, 2, \ldots, n-1\}$. We call these signals *variability signal differences*, according to the signal being studied, i.e., in the cases of the RR intervals and PW (P-wave amplitude), they are called *RR-interval differences signal* and *PW differences signal*, respectively. Regarding the ECG signals, after the process of denoising, we proceed similarly to the variability signals, eliminating non-stationary characteristics. That is, we consider the vector $y = (y_1, \ldots, y_{N-1})$ where $y_i = x_{i+1} - x_i$, for $i = 1 \ldots, N-1$; vector y will be called *ECG differences signal* (see Figure 8.7).

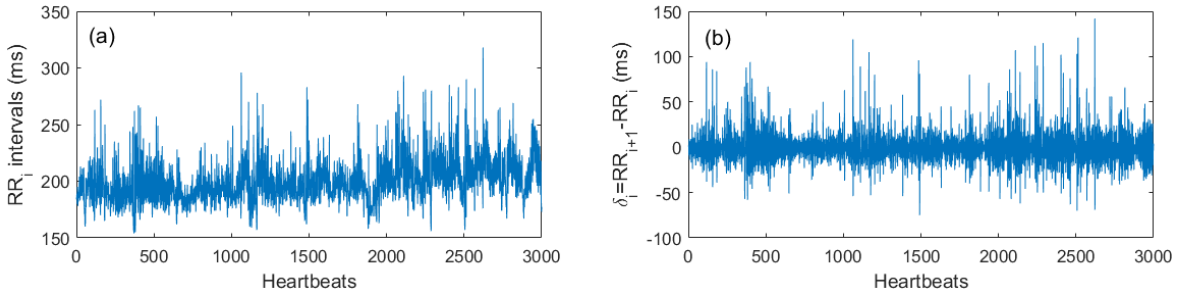

Figure 8.6: (a) Original RR-intervals signal. (b) RR-intervals signal differences.

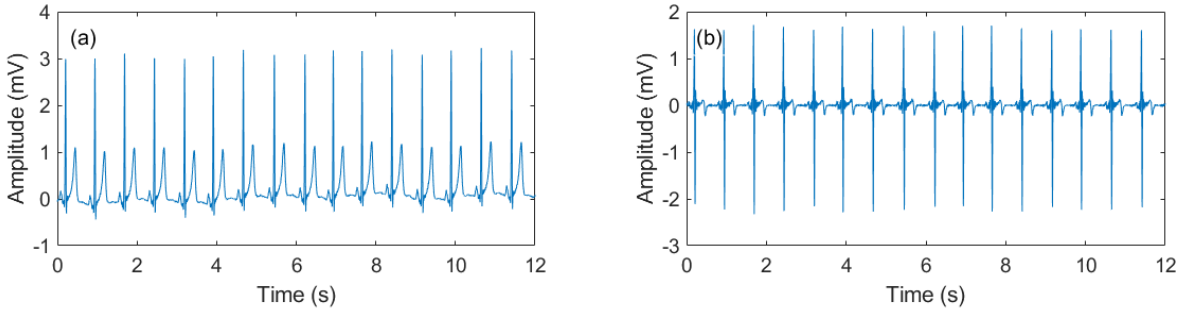

Figure 8.7: (a) Original ECG signal. (b) ECG signal differences.

Once we have our vectors y and δ, we encode them by partitioning the state space of the time series. An intuitive encoding technique was proposed in [8], which considers a uniform state space partition. However, this uniform partition does not consider the typical signal fluctuations. In order to capture these fluctuations inherent to physiological processes, we propose different partitions composed of elements with non-uniform sizes. That is, we consider a "center cell" around the mean μ value of the time series, and the size of the partition element is defined using the standard deviation σ of the data and fitted by means of a parameter γ. Considering non-uniform size for the elements of

the partition represents a novelty in the literature and we show that our method has advantages compared with previous works.

Let us consider $\kappa = 2j+1$, for $j \in \mathbb{N}$. Now, let $A = \{1, \ldots, \kappa\}$ be the alphabet of size κ and whose symbols will represent the labels of elements of the partition. Given a signal y (respectively δ), one considers its mean value μ and its standard deviation σ, which will be used for our method. Using the 'center cell' of the data, we carry out the partition of the state space of the time series. That cell is considered to be centered at μ (see Figure 8.8, for an example with $j = 2$). We construct its width employing the standard deviation σ, modulated by a parameter γ_1. We proceed with building up symmetrically from this center cell to both sides. The second layer of cells is defined analogously, by considering an interval centered at μ, but now with another width that is modulated by the parameter γ_2 (satisfying $\gamma_2 > \gamma_1$). So the second layer will be defined by subtracting the previous layer (in this case, the center cell) to the new obtained interval. Thus, the second layer will be composed by the segments $(\mu - \gamma_2\sigma, \mu - \gamma_1\sigma) \cup (\mu + \gamma_1\sigma, \mu + \gamma_2\sigma)$. We continue in this way until we reach the most external layer which is defined by taking $\mu \pm \gamma_j$ and that considers the segments $(-\infty, \mu - \gamma_j\sigma)$ and $(\mu + \gamma_j\sigma, \infty)$ from the other side. It is important to mention that by this construction we keep the number of parameters low, but at the same time we let the layers to vary its width. This feature is relevant for our method since represents a novelty concerning the existent literature. Its importance relies in the fact that, by letting vary the width of the intervals, one can detect in a better way the typical fluctuations of the data and take into account the transitions between different behaviors of the time series. This turns to be important for the estimation of the entropy production as we will see below. So, for instance, by letting γ_1 be large, then small fluctuations around the mean value will not be noticed. On the contrary, if we make γ_1 very small, then large fluctuations will be missed. That is why, here we perform an exploratory study to find the values of the parameters that allow us to better discriminate the groups of patients using the time-asymmetry of the data sequences.

Given a fixed partition, to generate a symbolized sequences $\omega(y)$ corresponding to the data sequences y, we label the atoms as follows:

$$\omega(y_i) := \begin{cases} 1 & \text{if and only if } \ y_i \in (-\infty, \mu - \gamma_j\sigma], \\ 2 & \text{if and only if } \ y_i \in (\mu - \gamma_j\sigma, \mu - \gamma_{j-1}\sigma], \\ \vdots & \qquad\qquad \vdots \\ j+1 & \text{if and only if } \ y_i \in (\mu - \gamma_1\sigma, \mu + \gamma_1\sigma), \\ \vdots & \qquad\qquad \vdots \\ \kappa & \text{if and only if } \ y_i \in [\mu + \gamma_j\sigma, \infty). \end{cases}$$

Observe that the label $j+1$ is assigned to the center cell, the label 1 to the first atom at

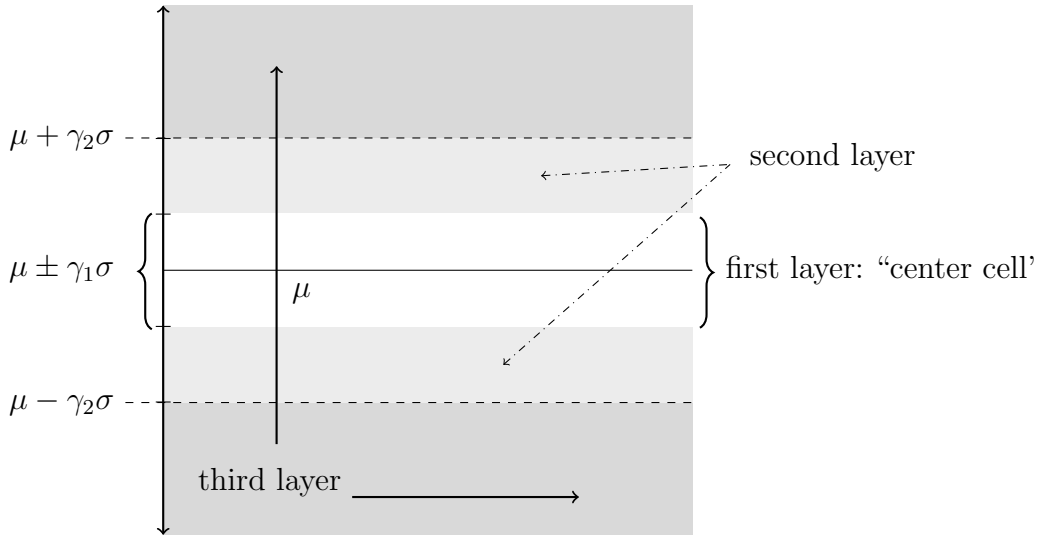

Figure 8.8: Schematic diagram for the build up of the partition for $j = 2$. The cells can be expanded or contracted based on an adjustment of the γ parameter values.

the bottom and the label increases up to κ (see Figure 8.9). The procedure is analogous (*mutatis mutandis*) for the case of $\omega(\delta)$ (variability signals).

In Figure 8.9, we provide an illustrative example of simbolization for $j = 2$, that is, for $\kappa = 5$. In this case, the labels of the elements of the partition are given as follows:

i) Label 1 for $(-\infty, \mu - \gamma_2\sigma]$,

ii) Label 2 for $(\mu - \gamma_2\sigma, \mu - \gamma_1\sigma]$,

iii) Label 3 for $(\mu - \gamma_1\sigma, \mu + \gamma_1\sigma)$,

iv) Label 4 for $[\mu + \gamma_1\sigma, \mu + \gamma_2\sigma)$,

v) Label 5 for $[\mu + \gamma_2\sigma, \infty)$.

So, we end up with the symbolic space $\Omega = A^N$ (where $N = n - 1$, for ECGs and $N = m - 1$, for the variability signals sequences) containing the symbolic sequences $\omega(y)$ for each sample y, and $\omega(\delta)$ for each sample δ.

In order to have a comprehensive analysis of the signal, we will perform numerical tests to find the best possible values of the parameter γ_j. This means that we will present our results for different partitions and an exploration of the size of the intervals in the partition.

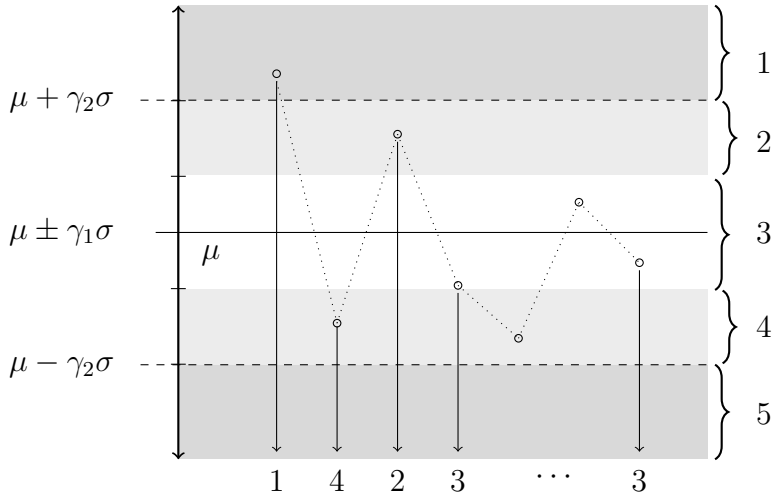

Figure 8.9: Schematic diagram of the symbolization procedure for $j = 2$. The symbols in the sequence are assigned according to the partition in which the value of the signal signal y (or δ) falls.

8.7 Joint encoding

Considering that the variability signals are not necessarily independent and represent different stages of a heartbeat, we performed a joint encoding of these signals. This procedure allows us to jointly analyze the fluctuations of the RR intervals and the amplitudes of the P, R and T waves.

Using the methodology described in Section 8.6, with the same approach of considering a non-uniform size of the partition elements, in this section we consider the simplest case of partitioning the state space, which is the ternary partition, but implementing two signals jointly, using the following rule. Given two variability signals differences $\delta^1 = (\delta_1^1, \ldots, \delta_{n-1}^1)$ (with parameters μ_1 and σ_1) and $\delta^2 = (\delta_1^2, \ldots, \delta_{n-1}^2)$ (with parameters μ_2 and σ_2), their joint symbolic sequence can be obtained by means of (see Figure 8.10):

$$\omega(\delta_i^1, \delta_i^2) = \begin{cases} 1 & \text{if and only if} \quad \delta_i^1 \in [\mu_1 + \gamma\sigma_1, \infty) & \wedge & \delta_i^2 \in [\mu_2 + \gamma\sigma_2, \infty), \\ 2 & \text{if and only if} \quad \delta_i^1 \in [\mu_1 + \gamma\sigma_1, \infty) & \wedge & \delta_i^2 \in (\mu_2 - \gamma\sigma_2, \mu_2 + \gamma\sigma_2), \\ 3 & \text{if and only if} \quad \delta_i^1 \in [\mu_1 + \gamma\sigma_1, \infty) & \wedge & \delta_i^2 \in (-\infty, \mu_2 - \gamma\sigma_2], \\ 4 & \text{if and only if} \quad \delta_i^1 \in (\mu_1 - \gamma\sigma_1, \mu_1 + \gamma\sigma_1) & \wedge & \delta_i^2 \in [\mu_2 + \gamma\sigma_2, \infty), \\ 5 & \text{if and only if} \quad \delta_i^1 \in (\mu_1 - \gamma\sigma_1, \mu_1 + \gamma\sigma_1) & \wedge & \delta_i^2 \in (\mu_2 - \gamma\sigma_2, \mu_2 + \gamma\sigma_2), \\ 6 & \text{if and only if} \quad \delta_i^1 \in (\mu_1 - \gamma\sigma_1, \mu_1 + \gamma\sigma_1) & \wedge & \delta_i^2 \in (-\infty, \mu_2 - \gamma\sigma_2], \\ 7 & \text{if and only if} \quad \delta_i^1 \in (-\infty, \mu_1 - \gamma\sigma_1] & \wedge & \delta_i^2 \in [\mu_2 + \gamma\sigma_2, \infty), \\ 8 & \text{if and only if} \quad \delta_i^1 \in (-\infty, \mu_1 - \gamma\sigma_1] & \wedge & \delta_i^2 \in (\mu_2 - \gamma\sigma_2, \mu_2 + \gamma\sigma_2), \\ 9 & \text{if and only if} \quad \delta_i^1 \in (-\infty, \mu_1 - \gamma\sigma_1] & \wedge & \delta_i^2 \in (-\infty, \mu_2 - \gamma\sigma_2], \end{cases} \tag{8.1}$$

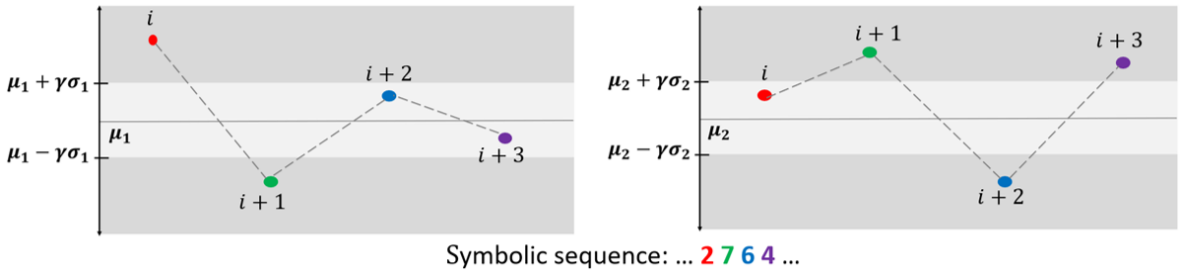

Figure 8.10: Diagram of the joint coding of time series. Given two variability signals differences $\delta^1 = (\delta^1_1, \ldots, \delta^1_{n-1})$ and $\delta^2 = (\delta^2_1, \ldots, \delta^2_{n-1})$, the symbolic sequence is generated depending on the partitions in which the i-th elements of each time series jointly fall. In our diagram, each color represents the i-th site in both time series jointly. For example, the $i+1$-th position of the symbolic sequence is assigned the symbol 7, because the $i+1$-th point of time series δ^1 falls in partition $(-\infty, \mu_1 - \gamma\sigma_1]$, while the i-th point of time series δ^2 falls in partition $[\mu_2 + \gamma\sigma_2, \infty)$, according the mapping (8.1).

8.8 Construction of the estimators

Once we have finished the symbolic encoding process of the data, the next step is to build the Markov model that approximates the process. After that, we continue to build up the estimators for the entropy production rate we defined in Section 4.1. Firstly, using equation (4.2), the transition probabilities P_{ij} were directly estimated from the data sequences of size n. This allows us to get an approximation for the transition matrix P. Next, we compute the invariant probability distribution for each subject by finding the left eigenvector of the corresponding estimated matrix. Finally, we estimate the Entropy Production Rate $\widehat{e}_p$, for every electrocardiogram of each group of patients, using equation (4.3).

Regarding the Kullback-Leibler Divergence Estimator $\widehat{D}_{n,k}$ (see Equation (4.9)), once we have our symbolic sequence $\omega(y)$ (or respectively, $\omega(\delta)$), we need first to find the set of all k-words a^k_1, that occur within the sequence $\omega(y)$ (or $\omega(\delta)$) and their respective time-reversed versions (a^1_k). Further, we estimate the empirical probabilities of all a^k_1 and a^1_k. This is done using equation (4.8) for the words and their time-reversed versions. As a final step, we estimate the KLD $\widehat{D}_{n,k}$, for all the ECG and variability signal sequences of each group of patients, using equation (4.9). We remind that, when k and n are large enough, then one can obtain good estimations. As provided by the Ornstein-Weiss theorem [54], one should have that n is exponentially larger than k in order to assure the convergence of the estimations. This represents a disadvantage when dealing with short data sequences. Here, for both cases (ECG and variability signals sequences), we use $k = 3$, that is, words of length 3. For longer words, the statistics of the appearance of the words is poor due to the size of the sequences, especially for the variability signals.

In the case of the *Lag-irreversibility function*, given a symbolic sequence $\omega(y)$ (or

respectively, $\omega(\delta)$), we have estimated the joint probability functions $\mathbb{P}(x_t = s_i; x_{t+\tau} = s_j)$ and $\mathbb{P}(x_t = s_j; x_{t+\tau} = s_i)$, for $\tau = 1, \dots 20$, using equations (4.11a) and (4.11b), respectively. Once we have the joint probability function, we directly plug them into equation (4.12), which in turn provides us with the estimated *lag irreversibility function*, $\widehat{L}(\tau)$.

Finally, for the Matching time estimator, given the set $\mathscr{M}$ made up of m finite symbolic sequences $\omega(y)$ (or respectively, $\omega(\delta)$) of the data, we first find the matching time ℓ^+ and the time-reverse matching time ℓ^- for each of the m sequences, using equations (3.15) and (3.16), respectively. This allows us to construct the sets $\mathscr{L}^+$ and $\mathscr{L}^-$ composed of all ℓ^+ and ℓ^-, respectively. Once we have the sets $\mathscr{L}^+$ and $\mathscr{L}^-$, we estimate the entropy of the sequence ($\widehat{h}$) and the entropy of the process reversed in time ($\widehat{h}^r$), using equations (4.6a) and (4.6b), respectively. In the case of our data, to estimate $\widehat{h}$ and $\widehat{h}^r$, we have that $n_i = n_j$ for all the i, j sequences in $\mathscr{M}$, that is, all sequences have the same length. Finally, we estimate the EPR of the process by substituting $\widehat{h}$ and $\widehat{h}^r$ in equation (4.7).

8.9 Chapter summary

This chapter has described the methodology followed for the analysis of temporal irreversibility in electrocardiograms. Although we tried to give as much detail as possible, this could not always be achieved. For example, in Section 8.8, where we discuss the estimation process, we only give a general description of the algorithm implemented, without stopping to explain the different functions used for the calculations, some of which are previously programmed in MATLAB, while others were programmed by ourselves. In Chapter 10 we will show the results obtained by analyzing the electrocardiograms using the methodology explained here. To evaluate the efficiency of this proposed methodology, we performed a ROC analysis of the results, which is the subject of the Chapter 9.

Chapter 9

Receiver operating characteristics graphs: ROC analysis

The Receiver Operating Characteristic (ROC) analysis, or *ROC analysis*, is a graphical method that is used to visualize and evaluate the efficiency of a binary classifier. In particular, in the area of medicine, ROC analysis has been widely used in medical decision making and diagnostic tests (see for example [80], [81], [82]). In this section we provide the theoretical framework necessary to carry out the ROC analysis of our results in Chapter 10.

9.1 ROC analysis

Let us consider the set $J = \{j_1, j_2, \ldots, j_m\}$ formed by all possible instances, $U = \{\mathbf{Y}, \mathbf{N}\}$ the set of hypothesized classes and $u = \{\mathbf{p}, \mathbf{n}\}$ the set of true classes. The mapping $R : J \to U$ defines a classification model or classifier, that is, a classifier maps the set of all possible instances to the set of predicted classes. This means that, given an instance j_i and a threshold value $\lambda \in \mathbb{R}$ above which, instances can be classified as positive, there are four possible outcomes. If the instance is classified as positive by the model ($j_i > \lambda$, that is $j_i \in \mathbf{Y}$) and it actually is positive ($j_i \in \mathbf{p}$), it is counted as true positive (TP); it is counted as a false negative (FN) if the model classifies it as negative ($j_i \leq \lambda$), but it is truly positive ($j_i \in \mathbf{p}$). If the instance is classified as negative by the model ($j_i \leq \lambda$, that is $j_i \in \mathbf{N}$) and it actually is negative ($j_i \in \mathbf{n}$), it is counted as a true negative (TN); it is counted as a false positive (FP) if the model classifies it as positive ($j_i > \lambda$), but it is genuinely negative ($j_i \in \mathbf{n}$) ([83], [84]). In Figure 9.1 we show a diagram of this data distribution.

From a classifier and these four possible outcomes, we can build a *confusion matrix* like the one shown in Figure 9.2, which represents the arrangement of the possible instances in J and is the basis for the ROC analysis. In Figure 9.2 we show the equations of the main metrics that can be estimated from the positive and negative instances. In particular, the *true positive rate* (h) is [83]:

$$h := \frac{\text{positives correctly classified}}{\text{Total positives}} = \frac{1}{P} \sum_{i=1}^{P+N} \mathbb{1} \left[j_i > \lambda \right], \tag{9.1}$$

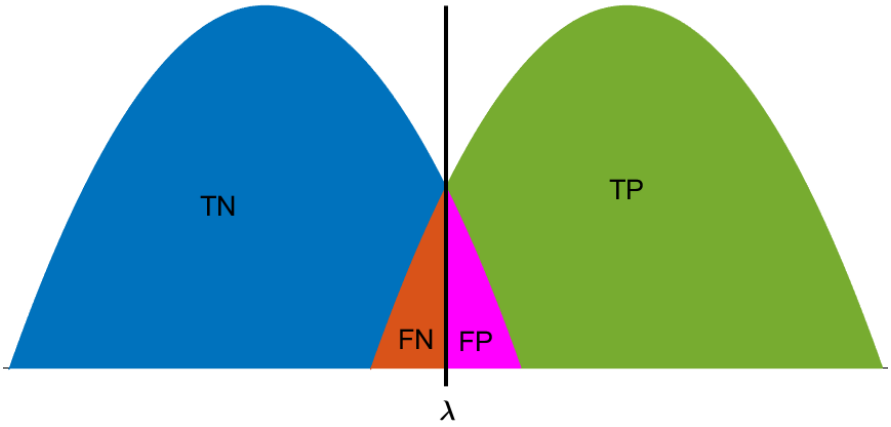

Figure 9.1: ROC analysis: data distribution. The green curve represents true positive (TP) cases and the blue curve represents true negative (TN) cases. All cases of true positives below the threshold λ are classified as false negatives (FN), while cases of true negatives above the threshold are classified as false positives (FP).

where $\mathbb{1}[j_i > \lambda]$ is the identity function, which is equal to 1 whenever $j_i > \lambda$, otherwise it is equal to zero.

The *false positive rate* (g) is [83]:

$$g := \frac{\text{negatives incorrectly classified}}{\text{Total negatives}} = \frac{1}{N}\sum_{i=1}^{P+N} \mathbb{1}[j_i \leq \lambda], \tag{9.2}$$

where $\mathbb{1}[j_i \leq \lambda]$ is the identity function, which is equal to 1 whenever $j_i \leq \lambda$, otherwise it is equal to zero.

Actual class

Hypothesized class		**p**	**n**	
	Y	True positive	False positive	true positive rate=$\frac{TP}{P}$
	N	False negative	True Negative	false positive rate=$\frac{FP}{N}$
	total	P	N	

Figure 9.2: Confusion matrix.

9.2 ROC space

From the information provided by the confusion matrix, it is possible to construct a two-dimensional graph whose axes x and y are the false positive rate (g) and the true positive rate (h), respectively. This graph is known as *ROC space* (see Figure 9.3). Depending on the area in which each point (h, g) falls in the ROC space, it has a different interpretation. For example, the point $(0, 0)$ represents a classifier that never issues positive classifications, that is, with this classifier there are never false positive errors. The opposite case is represented by the point $(1, 1)$, which always returns positive classifications, that is, with this classifier there are never false negative errors. The particular case of the point $(0, 1)$ represents a classifier that is correct 100% of the time, that is, all positive classifications actually are true positives [83].

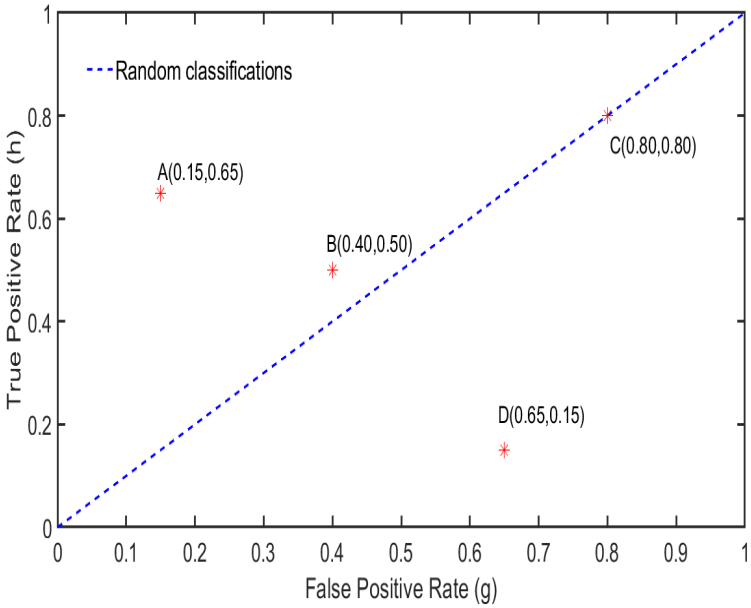

Figure 9.3: ROC space. Points in ROC space are considered best on the northwest side of the graph, since the true positive rate is higher and the false negative rate is lower in that zone.

When we apply ROC analysis to analyze data arising from practical topics such as medical sciences, the above cases rarely happen and consequently there is no interest in analyzing them. In Figure 9.3, we depict points A, B, C, and D of the ROC space, which are most commonly encountered in data analysis. It can be said that the ROC space is better on the upper left-hand side of the graph (true positive rate increases and false positive rate decreases), that is, the points in this area make positive classifications only when there is strong evidence and it makes them incur fewer false positive errors. Point A gives predictions with fewer occurrences of false positives than point B. Point C represents random classifications because it is located on the identity line. For example, if the classification model returns 80% of instances as positive, its false positive rate will

also increase to 80%, generating the point $(0.80, 0.80)$. When we have a point that is located in the lower right-hand triangle of the ROC space, as in the case of point D, it will show a confusion matrix opposite to that of point A and its predictions must be inverted to produce points in the left-hand upper triangle [83].

Each point in the ROC space describes a discrete classifier that assigns each instance a decision regarding the class it belongs to, but these points do not give information about the performance of the classifier, that is, the individual points in the ROC space do not provide information of the effectiveness of the classification decision made by the classifier. This problem can be addressed using *ROC curves* ([85], [83]).

9.3 ROC curve

By using discrete classifiers like those that produced points A, B, C, and D, we obtain a single classification decision, that is, we obtain a single point in the ROC space. To construct a ROC curve, we first choose a threshold value, above (or below) which, instances can be classified as positive (or negative). This allows us to take advantage of the regularity of classifications through threshold values, that is, any instance that is classified as positive for a certain threshold value, will be positive for higher (or lower) threshold values. In this way, we can sort the instances under analysis and move up the ordered data set, classifying each instance and updating TP and FP at the same time. The result of this series of steps is a vector with the points of the ROC curve (see Figure 9.4), generated by a linear scan of the data previously ordered. With this procedure, there is a single point in the ROC space for each threshold value. Although it is theoretically possible to take threshold values in the interval $(-\infty, \infty)$, in the analysis of data generated by real-life systems, such cases do not have an important meaning, since a very high threshold value (trending to infinity) produces the point $(0, 0)$ and a very low threshold value (trending to minus infinity) produces $(1, 1)$, which represent classifiers with no positive classifications and classifiers with all positive classifications, respectively ([83], [84]).

9.4 Area under an ROC curve

When we are interested in evaluating the efficiency of a classifier to distinguish between two classes, it is necessary to be able to interpret the information depicted in the ROC curve, as a scalar value that represents the performance of the classifier. A common method to obtain such a scalar is to calculate the *Area Under the ROC Curve* (AUC). In the case of discrete data, the AUC can be computed using a polynomial approximation ([83], [86]). Let $R : J \to U$ be a classifier and $J = \{j_1, j_2, \ldots, j_m\}$

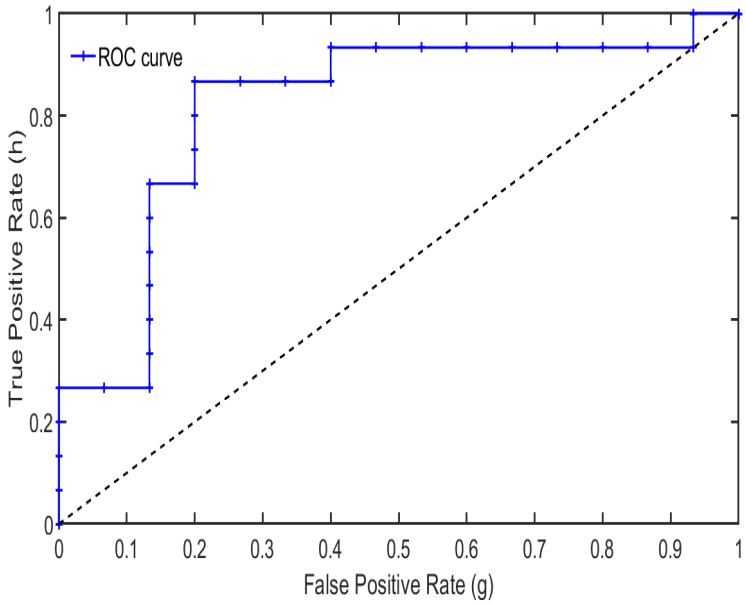

Figure 9.4: ROC curve. An example of a ROC curve formed in the upper left triangle of the graph, which represents the type of graph we want to work with. This is because the ROC curves in the lower right triangle indicate that the data is being analyzed incorrectly.

be the set of all possible instances (both defined as before), which can be segmented into the set of negative ($\mathbf{n}$) and positive samples ($\mathbf{p}$), that is, $\mathbf{n} = \{j_1^0, j_2^0, \ldots, j_{m_1}^0\}$ and $\mathbf{p} = \{j_1^1, j_2^1, \ldots, j_{m_2}^1\}$, respectively, where $m = m_1 + m_2$. The AUC of the classifier R can be estimated from the Mann-Whitney-Wilcoxon test, which tests whether positives instances are ranked higher than negatives, using ([87], [88]):

$$AUC := \frac{\sum_{j_i^0 \in \mathbf{n}} \sum_{j_j^1 \in \mathbf{p}} \mathbb{1}\left[R(j^0) < R(j^1)\right]}{|\mathbf{n}| \cdot |\mathbf{p}|}, \tag{9.3}$$

where $\mathbb{1}\left[R(j^0) < R(j^1)\right]$ is the identity function, which is equal to 1 whenever $R(j^0) < R(j^1)$. From a statistical point of view, the AUC can be interpreted as the probability that a classifier R can discriminate between a positive and a negative instance when both are selected randomly.

Broadly speaking, we can have three cases when estimating AUC. The first of them happens when there is no intersection between both data curves (Figure 9.5i.(a)), therefore, we will have $AUC = 1$ (Figure 9.5ii.(a)). This means that the classifier can distinguish or classify between the two classes in 100% of cases. The second case occurs when there is a partial overlap of the data (Figure 9.5i.(b)), and as a consequence, there are cases of false positives and false negatives, that is, errors are made. These errors are minimized or maximized for each threshold value λ. In this case, the AUC values fall in the interval $0.5 < AUC < 1$, which is very common in practical situations (Figure 9.5ii.(b)). For example, if $AUC = 73$, we can interpret that the classifier is effective

up to 73% of the cases. The worst situation occurs when the data completely overlap (Figure 9.5i.(c)), resulting in $AUC = 0.5$ (Figure 9.5ii.(c)). In this case, the classifier cannot distinguish between either class at all.

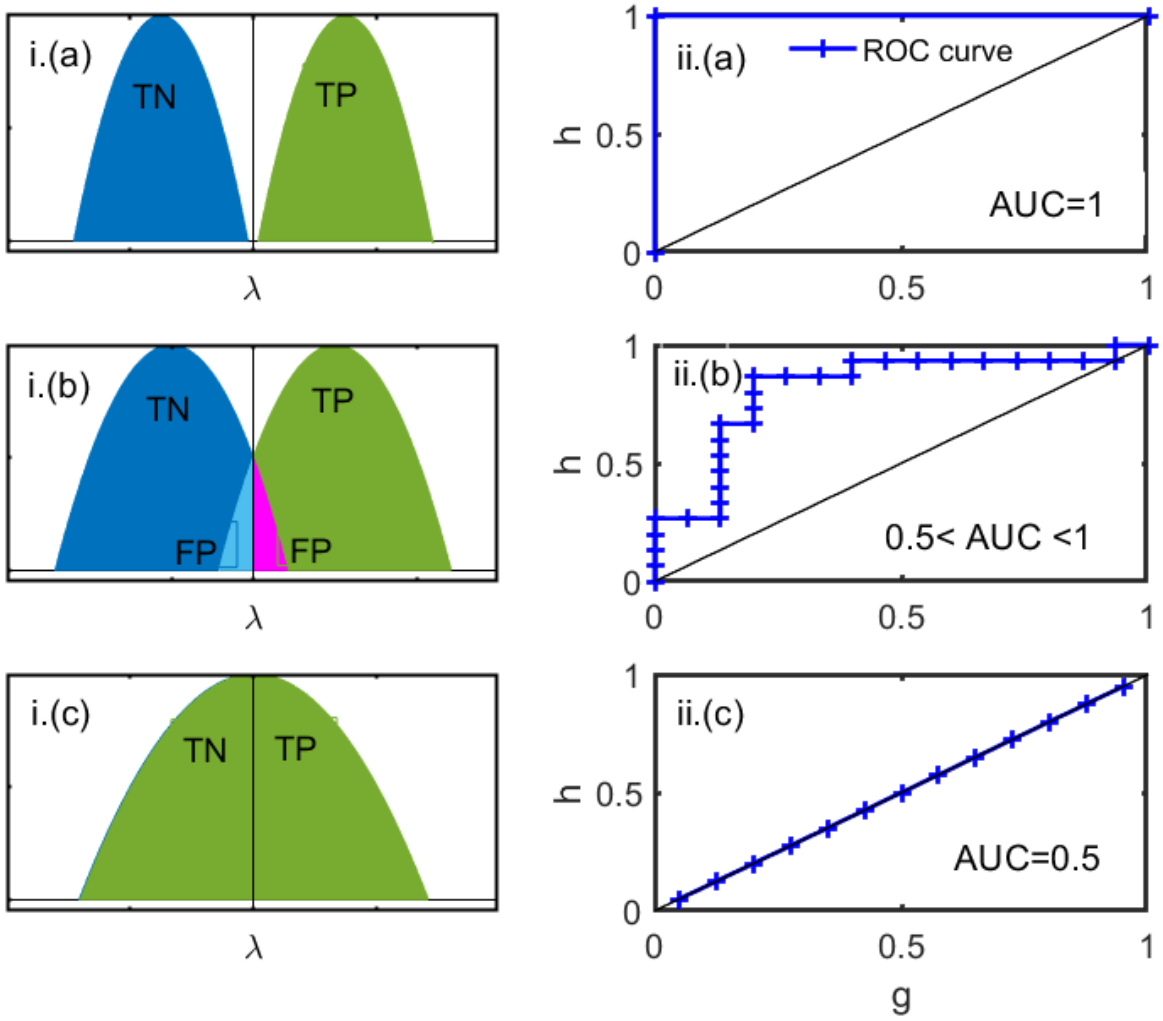

Figure 9.5: Three general cases of ROC data analysis. (a) There is no overlapping of the data, it is the ideal case. (b) There is a partial overlap of the data distribution and cases of false positives and false negatives are generated. (c) The distributions of the data overlap completely.

For the sake of clarity, the ROC curve can be interpreted according to the following intervals [89]:

- $AUC = 0.50$: the classifier does not have discriminative capacity.
- $AUC \in (0.50, 0.60]$:bad classifier.
- $AUC \in (0.60, 0.75]$:regular classifier.
- $AUC \in (0.75, 0.90]$:good classifier.
- $AUC \in (0.90, 0.97]$:very good classifier.
- $AUC \in (0.97, 1.0]$:excellent classifier.

9.5 Chapter summary

As we have seen throughout this chapter, ROC analysis is a powerful tool for analyzing the efficiency of a classifier to distinguish between two classes. In Chapter 10, we will show the results of using ROC analysis to evaluate the efficiency of our methodology to discriminate between electrocardiograms from different groups of patients.

Chapter 10

Results and discussion

In this Chapter, we estimate time-irreversibility in electrocardiograms. We propose to analyze the electrocardiographic signal in three different categories, namely, (1) the electrocardiographic signal, (2) RR-intervals and (3) joint variability signals, which allowed us to have a comprehensive analysis of the signal. After the data encoding process is completed, following the procedure discussed in Section **??**, we directly use the symbolic sequences of these signals to construct the time-irreversibility estimators, for which we assume that the signal presents a Markovian nature (see Section 8.5). We estimate the time-irreversibility of the ECG signal using the estimators empirically constructed from the data, namely, the Entropy Production Rate $\widehat{e}_p$ (equation 4.3), the Kullback-Leibler Divergence $\widehat{D}$ (equation 4.10), the Matching time $\widehat{M}$ (equation 4.7) and the Lar-irreversibility function $\widehat{L}(\tau)$ (equation 4.12).

We separate our results into three parts. First, we show the results by analyzing the electrocardiographic signal (Section 10.1). Later on, we analyze the HRV (Section 10.2) and make a comparison between the performance of the electrocardiographic signal and the HRV to discriminate between the four groups of patients (AF, CHF, HE and HY), through a ROC analysis of the results (Section 10.3). Finally, in Section 10.4, we display the results of analyzing the joint variability signals using the LI function, introduced in Section 3.3.4.

The results shown in this chapter are based on the following previously published material:

- MALDONADO, Cesar; MERINO–NEGRETE, Nazul. Irreversibility indices as discriminators of heart conditions from electrocardiographic signals. Physica A: Statistical Mechanics and its Applications, 2024, vol. 637, p. 129584.
- MERINO-NEGRETE, Nazul; MALDONADO, Cesar; SALGADO-GARCÍA, Raúl. Sorting ECGs by lag irreversibility. Physica D: Nonlinear Phenomena, 2024, vol. 459, p. 134022.

10.1 Time-irreversibility in electrocardiographic signal

First, we estimate the EPR of the ECG signals. In figures 10.1, 10.2 and 10.3, we show the values of the estimators $\widehat{e}_p$, $\widehat{D}$ and $\widehat{M}$, respectively, which were empirically

estimated from the symbolized ECG differences signal of 100 minutes ($n = 1500000$) long and using the three different partitions we already have specified. The results shown in these figures correspond to the average value obtained with 15 subjects for each group. For each size of the partition ($\kappa = 3, 5, 7$), we make an exploratory study to find the best values for γ_j. This is done for the four groups of patients (as we have described in Section **??**).

Figure 10.1, shows that the EPR is higher for the two groups of healthy subjects (HE and HY) than in the other two groups with medical conditions (CHF and AF), having the highest value the group of healthy young patients, for all the tested partitions and for all the tested parameters. We point out that for γ_1 larger than 2.5 it is expected to have no conclusive results since most data falls into the central cell with high probability.

For the simplest case, $\kappa = 3$, one has the best discrimination between the groups of patients for γ_1 between 0.8 and 1.2. Furthermore, for $\kappa = 5$, we see that in the HY and HE groups, the EPR is found to have values in a range from ≈ 0.04 to ≈ 0.06, compared with both AF and CHF subjects which are in a range from ≈ 0.007 to ≈ 0.014. For $\kappa = 7$ one can obtain different values for AF which are in a range from ≈ 0.012 to ≈ 0.021 and for CHF the values are found between ≈ 0.012 and ≈ 0.020. Based on these results, the condition that provides better discrimination between different groups is to use a partition with seven symbols (i.e. $\kappa = 7$) and parameters values of $\gamma_1 = 0.8$, $\gamma_2 = 3$ and $\gamma_3 = 4.25$. Therefore, in the case of EPR, we propose to employ this collection of parameter values to discriminate electrocardiographic signals coming from group of patients under different medical conditions.

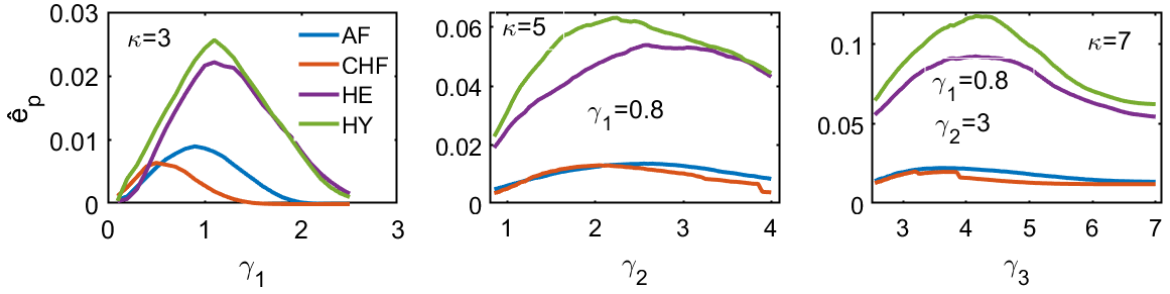

Figure 10.1: Average entropy production rate in symbolized ECG differences signals for different partitions with $\kappa = 3, 5, 7$ as a function of the parameters γ_j. In the case of $\kappa = 5$, $\gamma_1 = 0.8$ is the value we kept constant to make the corresponding calculations for different values of γ_2. Regarding $\kappa = 7$, $\gamma_1 = 0.8$ and $\gamma_2 = 3$ are the values we kept constant to make the corresponding calculations for different values of γ_3.

Next, in Figure 10.2 we show the estimated Kullback-Leibler Divergence (KLD) in ECG signals. From now on, $\widehat{D}_{n,k}$ will be denoted only as $\widehat{D}$, since we use words of length three ($k = 3$) for all cases; it is important to mention that one would require much more data to make the estimations for longer words. We obtain our results for

the same conditions as for EPR. This means that we study the same three different number of the partitions, that is, we consider $\kappa = 3, 5, 7$. We observe that it is possible to distinguish between healthy subjects and unhealthy patients, which is a consistent result regarding the EPR.

For $\kappa = 3$ and $\gamma_1 = 1.5$, we have the best result, in the sense that one can better discriminate between groups, that is, for young and elderly healthy subjects we have $\widehat{D} \approx 0.0108$ and $\widehat{D} \approx 0.00738$, respectively, while for the AF group $\widehat{D} \approx 0.0025$ and for the CHF group we have $\widehat{D} \approx 0.0014$. For $\kappa = 5$ the best result was obtained using $\gamma_2 = 3$ given that $\gamma_1 = 1.5$, and for $\kappa = 7$ the best selection of parameters is $\gamma_3 = 5$, given that $\gamma_1 = 1.5$ and $\gamma_2 = 3$. This means that using the average value of the KLD, these parameter values allow us to have the greatest difference between the groups of healthy and sick patients.

Let us emphasize that the KLD estimator was built from the empirical frequency of 3-words and that for short dataset sequences the fluctuations are typically large. Thus, as we have already said, aiming to achieve a better estimations using words of length four or longer, it is necessary to carry out the estimation procedure employing longer dataset sequences.

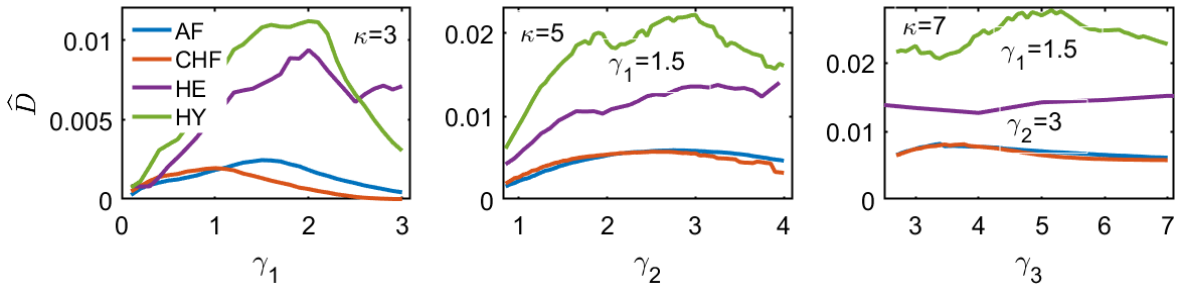

Figure 10.2: Average Kullback-Leibler Divergence in symbolized ECG differences signals, for different partitions with $\kappa = 3, 5, 7$ as a function of the parameters γ_j.

Finally, Figure 10.3 shows that the Matching time estimator allows us to discriminate between healthy subjects (young and elderly) and unhealthy patients, for the same three different number of atoms in the partitions ($\kappa = 3, 5, 7$). For the case $\kappa = 7$ using $\gamma_1 = 1.6$, $\gamma_2 = 3$ and $\gamma_3 = 5$, we have the best discrimination, that is, for the HY group, the value of the estimator ($\widehat{M} > 0.22$) is approximately two times greater than the groups of ill patients ($\widehat{M} \approx 0.11$ for the CHF group).

We emphasize that discriminating between the two healthy groups (HY and HE) or between the two ill groups of patients (AF and CHF) becomes a difficult task, given that in all cases, each pair of groups show very similar values (in average) for the irreversibility indices under study.

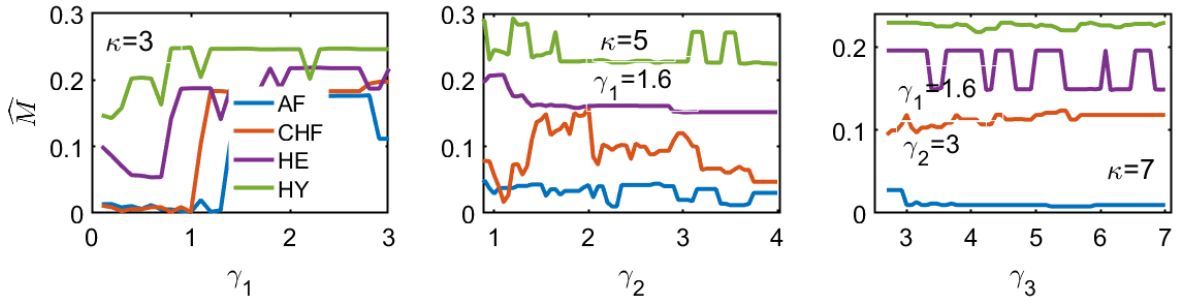

Figure 10.3: Average matching time in symbolized ECG differences signals, for different partitions with $\kappa = 3, 5, 7$ as a function of the parameters γ_j.

10.2 Time-irreversibility in HRV

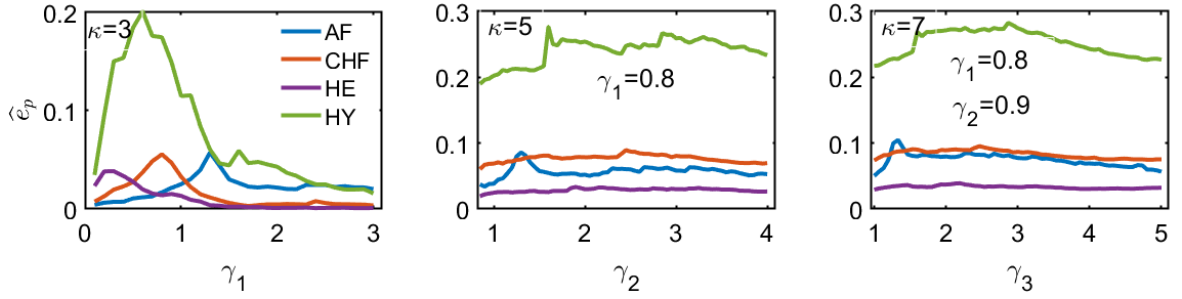

Figure 10.4: Average entropy production rate for symbolized RR-interval differences signals (using 5,500 heartbeats, that is, $n = 5,500$), for different partitions ($\kappa = 3, 5, 7$) as a function of the parameter γ_j.

Aiming to achieve a comprehensive comparison, in this thesis, we study the *RR*-interval sequences, since most of the existent works (see for example [19], [20], [21], [7]) dealing with time-irreversibility features in the electrocardiographic signal analyze the HRV from the the *RR*-interval sequences. Figure 10.4 displays the empirical EPR for the symbolized *RR*-interval differences signal, obtained using the same methodology described above.

We obtain compatible results with those obtained for the EPR in ECG signals. This means that the EPR is higher in healthy young patients than in those with medical conditions. However, when we analyze the *RR*-interval sequences using the methodology applied to the analysis of the electrocardiographic signal, these estimators fail to discriminate the group of healthy elderly patients from those who exhibit medical conditions. Furthermore, according to what was reported in [7], it is expected that, on average, the EPR in the healthy elderly group is higher compared to the ill patient groups. Therefore, given that analyzing the HRV with this methodology, we do not have conclusive results to discriminate between the group of healthy elderly patients from those with medical conditions, in Section 10.3, the ROC analysis will focus on discussing

the obtained results when analyzing the HY, AF and CHF groups. Later, in Section 10.4, we will discuss the obtained results with the proposed Lag-irreversibility estimator (see Section 3.3.4), with which it is possible to discriminate between the four groups of patients.

Regarding the unhealthy groups, granted that the difference between them was not statistically significant, the values of EPR were slightly larger for patients with CHF than for those with AF. We believe that, due to the properties of the *RR*-intervals sequence and the nature of these medical conditions, some of them can be better detected than others using this signal. For instance, *RR*-intervals fluctuations are lower in patients with CHF than in patients with AF, since the latter exhibit high variation in heartbeat frequency [55]. In this context, concerning the EPR and its usefulness for analyzing groups of patients with these medical conditions, further research must be done.

Figure 10.4 shows that in a partition of $\kappa = 3$ atoms and $\gamma_1 = 8/10$ one has that the healthy patients have an EPR of ≈ 0.1745, while the CHF group shows an EPR ≈ 0.0556, and the AF group an EPR ≈ 0.0170. For $\kappa = 5$ and $\gamma_1 = 0.8$, the parameter γ_2 which gives the most distinguishable results between the groups (excluding the group HE) is $\gamma_2 = 0.9$, giving values of the EPR ≈ 0.2277 for the HY group, ≈ 0.0608 for CHF and ≈ 0.0246 for the AF group. And finally, for $\kappa = 7$ with the previous mentioned optimal values for γ_1 and γ_2, one obtains the most distinguishable results for $\gamma_3 = 1$. That is, ≈ 0.2463 for HY, ≈ 0.0770 for CHF and ≈ 0.0445 for AF (see Figure 10.4).

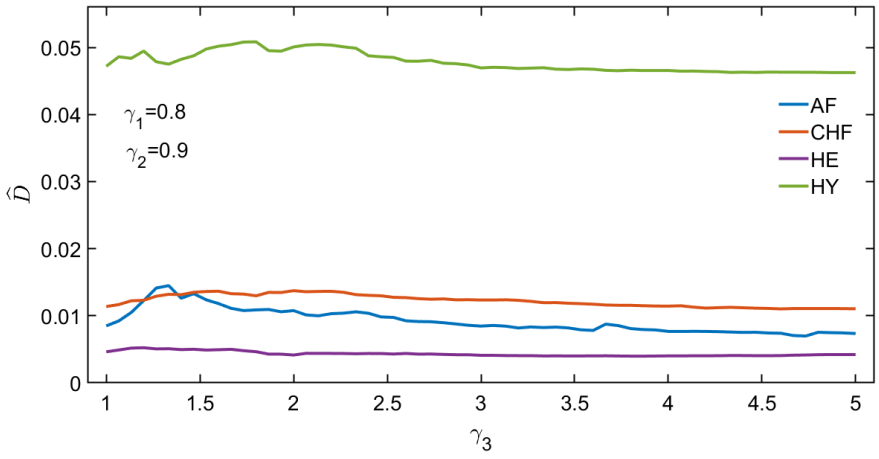

Figure 10.5: Average Kullback-Leibler divergence based-entropy production rate for symbolized RR-interval differences signals, for a partition with $\kappa = 7$, as a function of the parameter γ_3.

Figure 10.5 displays the estimated KLD in the *RR*-interval sequences using a partition with $\kappa = 7$.

For this signal, with the KLD estimator, we do not achieve convincing results employing a few partitions ($\kappa = 3$ and 5), since we obtain large fluctuations of the frequencies of 3-words empirically estimated. Hence, we show the results of the KLD estimator considering a partition with $\kappa = 7$ and taking the values for the parameters

$\gamma_1 = 0.8$ and $\gamma_2 = 0.9$, as in the case for the EPR, above. Observe that the results are compatible with those obtained for the EPR. Distinguishable values are obtained for $\gamma_3 = 1$, that is, a $\widehat{D} \approx 0.048$ for the HY group, ≈ 0.0127 in the case of CHF, and ≈ 0.0089 for the AF subjects. We can see that using RR-interval sequences it is also possible to discriminate between healthy and unhealthy subjects, although these results are less conclusive than those obtained with the electrocardiographic signal.

Regarding the Matching time, we do not obtain conclusive results for any size of the partition ($\kappa = 3, 5, 7$). We consider this to be due to the length of the RR-interval differences signals and longer sequences are required to obtain good estimates.

10.3 ECG signal vs HRV: comparison and ROC Analysis

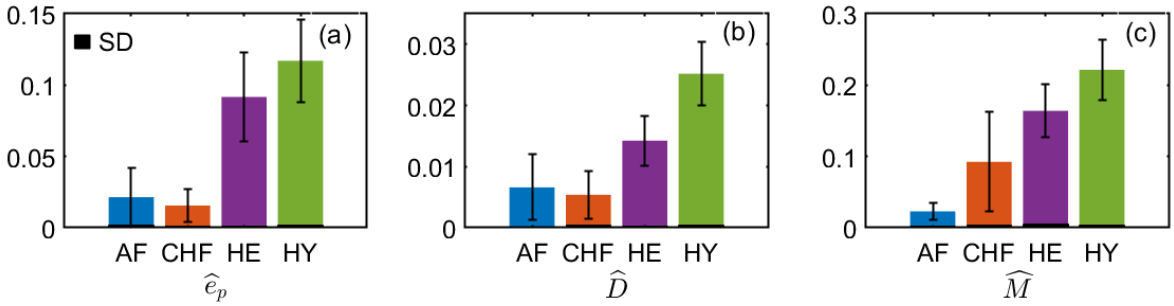

Figure 10.6: Estimated $\widehat{e}_p$ (a), $\widehat{D}$ (b) and $\widehat{M}$ (c) in average and their respective standard deviation bar, for symbolized sequences of ECG differences (for $\kappa = 7$). In the case of the Kullback-Leibler divergence estimator, the selected length of the words was $k = 3$. Additionally, in black, we plot the average results of our method applied to shuffled data (SD).

As a summary, in Figure 10.6 we make a comparison of the estimated average EPR using the symbolized ECG signal. We also plot, in black bars, the results of our method applied to shuffled data (SD); this means that before starting the encoding process of the original data (the ECG signal), they were subjected to a randomization process, which eliminates their original structure. The results show values very close to zero, which means that the EPR values obtained come from the irreversible nature of the data and are not a consequence of the methodology or estimator used. We can see that under our methodology using these three estimators, in the case of the ECG signals, we can discriminate the healthy patients (young and elderly) from the unhealthy ones. Furthermore, regarding the EPR estimated from the ECGs, we obtain quite satisfactory results using only 20 minutes of signal, which, from a practical point of view, represents an advantage over the existent literature, in which the used signals range from 30 minutes to 24 hours (see for instance [17, 22, 90]). In Figure 10.7 we do the same

for the case of RR-interval differences signals. We can observe that by applying the same methodology to both signals (ECG signal and RR-interval differences signal), it is possible to discriminate between the group of young healthy patients and the groups with unhealthy patients, since in all cases, EPR is at least two times higher in the HY group compared to the AF and CHF groups. However, for the case of the RR-interval differences signal, this methodology does not give conclusive results when we want to discriminate between the group of healthy elderly patients from the unhealthy ones. As we said previously, in Section 10.4, we will discuss the results obtained with the Lag-irreversibility estimator, with which it is possible to have more evident discrimination between these two groups of patients.

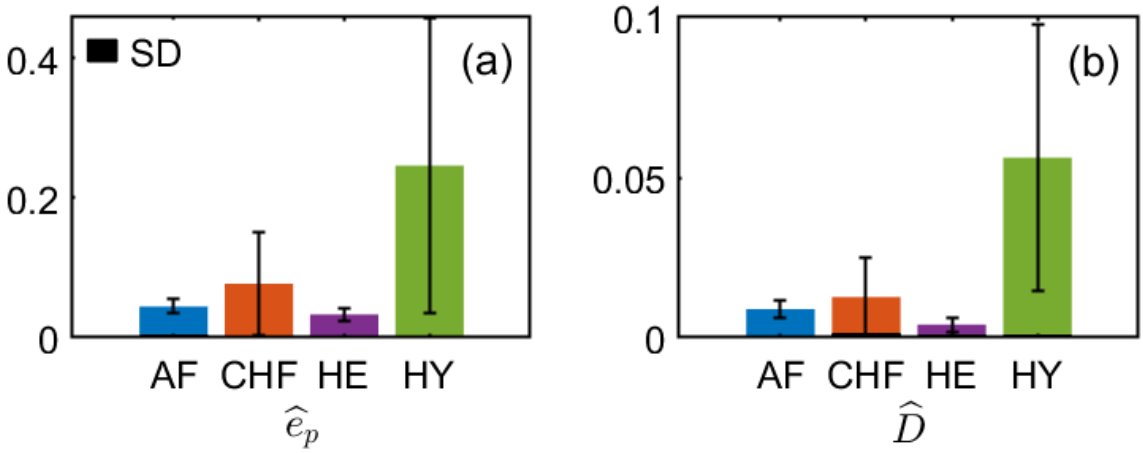

Figure 10.7: Estimated $\widehat{e}_p$ (a) and $\widehat{D}$ (b) in average and their respective standard deviation bar, for symbolized sequences of RR-interval differences ($\kappa = 7$). In the case of the Kullback-Leibler divergence estimator, the selected length of the words was $k = 3$. Additionally, in black, we plot the average results of our method applied to shuffled data (SD).

Next, we perform the ROC analysis on our method (see Chapter 9). This evaluates the accuracy of our methodology in distinguishing between groups of patients under different medical conditions, using time-irreversibility indices as a discrimination tool. To build the ROC curve, we choose a threshold value of EPR, and above that value, the patient is predicted as a negative instance (healthy, for example) and below the value, as a positive instance (unhealthy). For each threshold value, one obtains a number of TP and TN instances and their respective errors (false positive or false negative). Next, we assess the accuracy of our method for discriminating between pairs of patient groups, namely, HY vs AF, HY vs CHF, AF vs CHF and finally, HY vs both AF or CHF, which we denote by UHG (unhealthy in general). Under this analysis, one can quantitatively evaluate the performance of the method by means of the AUC, which takes values in the range of $[0, 1]$. The closer the values of AUC are to 1, the greater the efficiency of the method to discern between the two evaluated groups ([83], [86]). As we specified previously, given that we do not have conclusive results with the healthy

elderly patients, we did not include the HE group in our ROC analysis of the pairs of groups of patients, and we leave its respective ROC analysis for Section 10.4.2.

In Figure 10.8 we show the ROC curve for the obtained results using the EPR of the ECG signals for each pair of the three groups we have considered. We show the ROC curves for the results obtained in the three different partitions defined in Section 8.6. We obtain values close to 1 for our estimators, for instance, for the case of the EPR on ECG, using a partition of $\kappa = 3$, one obtains values of $AUC > 0.92$ discriminating between HY and AF groups. For HY vs CHF, one obtains $AUC > 0.94$, and $AUC > 0.93$ for the discrimination between healthy patients and any of the two diseased groups. These values are interpreted as "very good tests" (see Section 9.4). The values increase for partitions with more atoms. For instance, for $\kappa = 7$, one has $AUC > 0.96$ for HY vs AF using a threshold value of 0.0511. For HY vs CHF, one has $AUC > 0.98$ using a threshold value of 0.0513 and $AUC > 0.97$ for HY vs UHG using a threshold value of 0.0534. The threshold value mentioned above provides us with the optimal operating point of the ROC curve, i.e., it is the threshold value at which we can obtain the highest efficiency for discriminating between the two groups under analysis. Concerning the ROC analysis to discriminate between the two groups of unhealthy patients, we can see that the method yields results with a lower precision of approximately 60% (see Table 10.1). This represents a challenging problem that needs to be addressed with further research, since our methodology does not seem to be good enough to distinguish between these two groups of patients.

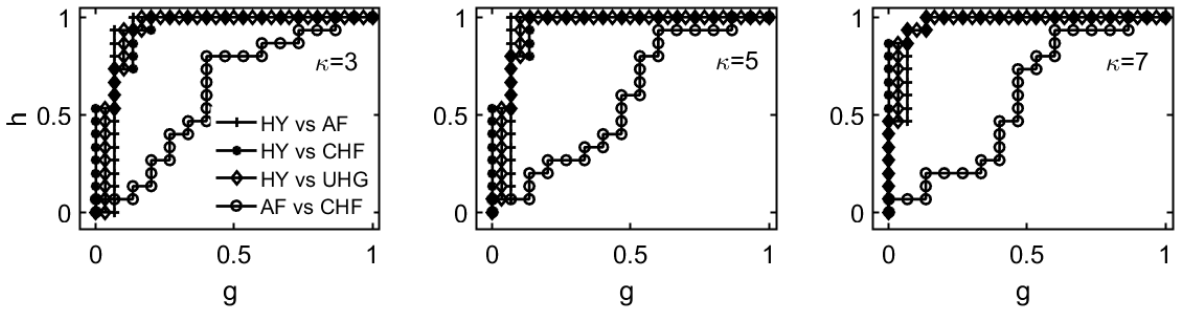

Figure 10.8: ROC curve for the EPR method for discriminating ECG signals.

Regarding the KLD estimator, the ROC analysis yielded comparable results (see Figure 10.9). For instance, for a symbolic encoding with $\kappa = 3$ one has $AUC > 0.98$ discriminating between HY and AF, $AUC > 0.94$ for HY vs CHF and $AUC > 0.96$ for HY vs UHG. These are very good results, also concerning the existent literature. Similar results were obtained for $\kappa = 5$. For $\kappa = 7$ one has a $AUC > 0.95$ for HY vs AF using a threshold value of 0.0162, $AUC > 0.98$ for HY vs CHF using a threshold value of 0.0163 and $AUC > 0.96$ for HY vs UHG using a threshold value of 0.0162 (see Table 10.1). As we have previously pointed out, the method fails to discriminate between the two diseased groups, having $AUC > 0.59$, only.

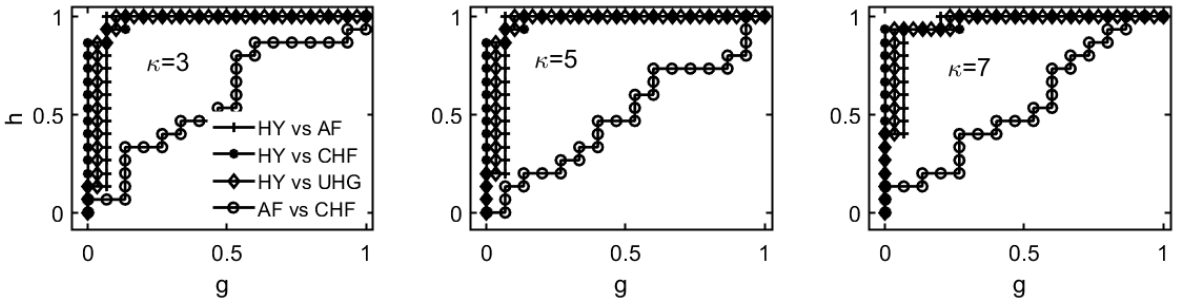

Figure 10.9: ROC curve for the KLDB method for discriminating ECG signals.

In the case of the Matching Time, the best results were obtained with $\kappa = 7$ (see Figure 10.10). That is, one has a $AUC > 0.81$ for HY vs AF using a threshold value of 0.079, $AUC > 0.75$ for HY vs CHF using a threshold value of 0.161 and $AUC > 0.71$ for HY vs UHG using a threshold value of 0.137 (see Table 10.1).

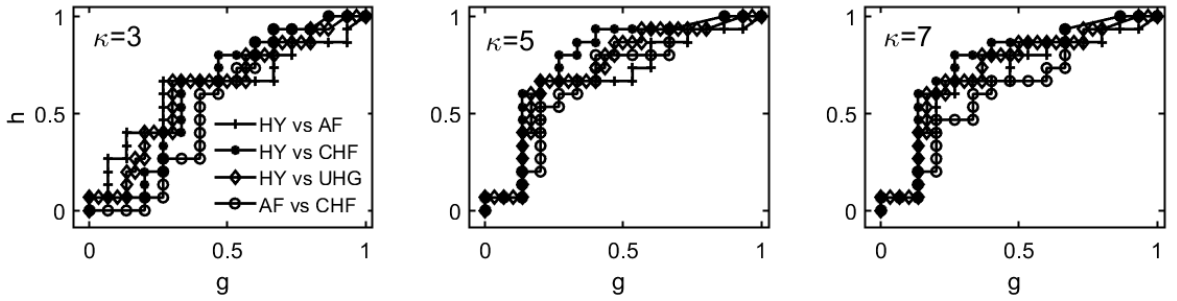

Figure 10.10: ROC curve for the MT method for discriminating ECG signals.

We observe outstanding results using the estimators $\widehat{e}_p$ and $\widehat{D}$, and we have less conclusive results with $\widehat{M}$ in the ECG signals. According to our literature review, our methodology applied to the analysis of the electrocardiographic signal yields better results than most of the researches found in the literature. Additionally, in order to have an exhaustive investigation and for comparison purposes with other results available, we performed ROC analysis of the results obtained by analyzing the RR-interval sequences. Figure 10.11 displays the ROC curves using the three different partitions schemes for the EPR in RR-interval sequences.

When estimating the EPR using RR-interval signals, we have that the best performance is obtained for $\kappa = 7$. One has that $AUC > 0.72$ for HY vs AF using a threshold value of 0.0512, $AUC > 0.81$ for HY vs CHF and $AUC > 0.74$ for discriminating between HY and UHG, both of them using a threshold value of 0.0596. These are interpreted as "good tests". These results show that using the HRV signal it is possible to distinguish between the group of young healthy patients and those with a medical condition, although the percentage of effectiveness is lower than in the case of the ECG signal. Analogous to what was obtained in the previous cases, the methodology does not show good results for discriminating between the AF and CHG groups, in which

one obtains that $AUC > 0.66$, only.

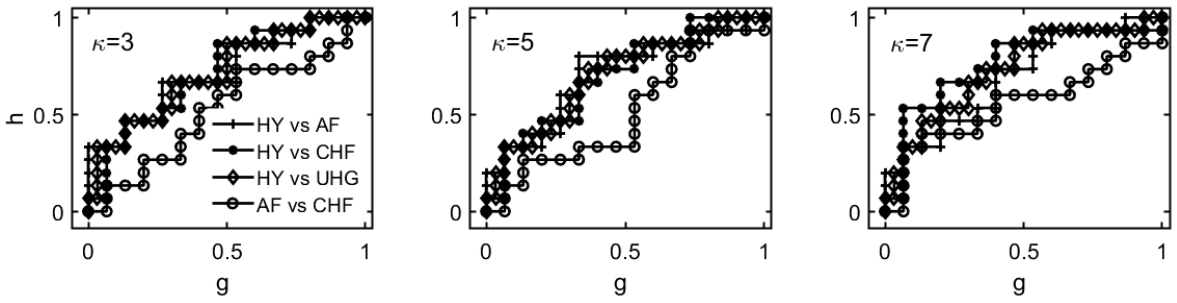

Figure 10.11: ROC curve for the EPR method for discriminating RR-interval sequences.

Additionally, we compute the ROC curve for the KLD method using RR-interval signals with a partition of the state space with $\kappa = 7$ as we did in the previous section, see Figure 10.12. We obtain that in this case $AUC > 0.77$ for HY vs AF with a threshold of 0.0219, $AUC > 0.84$ for HY vs CHF using a threshold of 0.0111 and $AUC > 0.81$ for HY vs UHG using a threshold value of 0.0166.

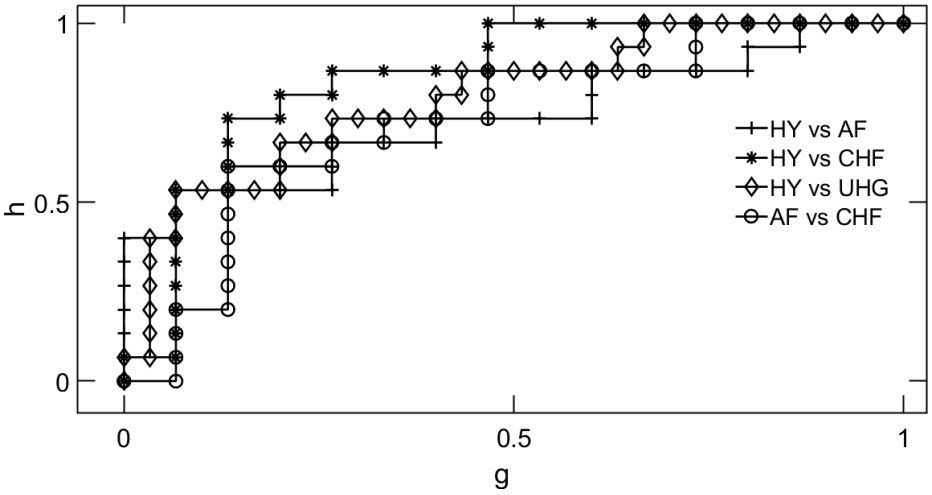

Figure 10.12: ROC curve for the KLD method for discriminating RR-interval sequences.

We collect quantitative results in Table 10.1 for the area under the ROC curve, for each pair of groups for which we tested our methodology. This is done for both time series (ECG signal and RR-intervals) and the three estimators ($\widehat{e}_p$, $\widehat{D}$ and $\widehat{M}$) under study. The results show that using our methodology, it is possible to distinguish the group of young healthy subjects from those with medical conditions, with a high percentage of effectiveness. For the analysis of the ECG signals these results are slightly more accurate when we use the estimator $\widehat{e}_p$ and less conclusive with $\widehat{M}$. For the RR-interval signals, we have the best results with the estimator $\widehat{D}$, although in that case, we need to consider a partition with a larger number of atoms. In Table 10.1, we show the obtained values with a partition of a number of atoms equal to $\kappa = 7$, which is the one we finally suggest.

	AUC				
	ECG			HRV	
	$\widehat{e}_p$	$\widehat{D}$	$\widehat{M}$	$\widehat{e}_p$	$\widehat{D}$
HY vs AF	0.960	0.951	0.7978	0.7233	0.7718
HY vs CHF	0.9867	0.9822	0.7578	0.8144	0.8489
HY vs UHG	0.9733	0.9667	0.7178	0.7408	0.8133
AF vs CHF	0.6422	0.5931	0.6333	0.6656	0.7333

Table 10.1: Area under the ROC curve, using a partition of $\kappa = 7$.

For practical reasons, we would like to use as less signal recording as possible and still be able to discriminate between the three groups of patients with our method. In Figure 10.13, we plot the AUC as a function of time, for the symbolized ECG differences signals; (a) in the case of the estimator $\widehat{e}_p$, (b) for the estimator $\widehat{D}$ and (c) for the estimator $\widehat{M}$. We observe that values of AUC near 0.9 can be reached using approximately 20 minutes of signal in the case of the estimator $\widehat{e}_p$. This represents an advantage over other methods that use very long sequences.

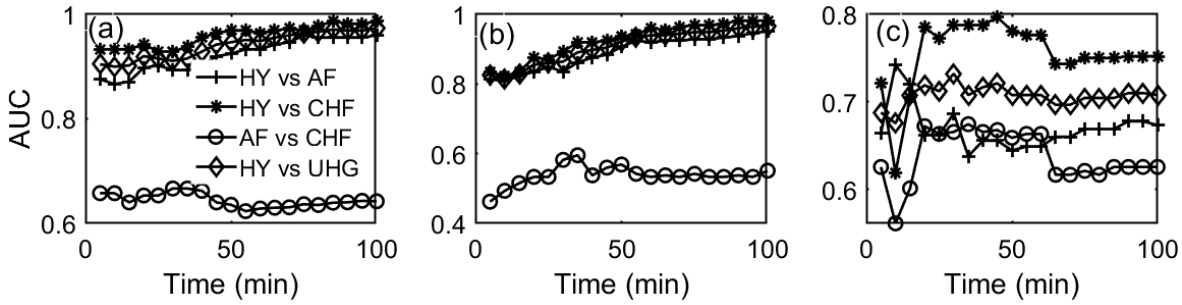

Figure 10.13: AUC for different values of length of the recording and the comparisons of pairs of patient groups, using the symbolized ECG differences signals and the three estimators (for $\kappa = 7$). (a) in the case of the estimator $\widehat{e}_p$, (b) for the estimator $\widehat{D}$ and (c) for the estimator $\widehat{M}$.

In Figure 10.14, we plot the AUC as a function of time, for the symbolized RR-interval differences signals; (a) in the case of the estimator $\widehat{e}_p$ and (b) for the estimator $\widehat{D}$. We observe that nearly the maximum values of AUC for each pair of groups were achieved using 5500 heartbeats. Nonetheless, in this case, we expect that one would be able to improve the results applying the present methodology in longer sequences. So, we suggest that further research should be done in this direction.

The results suggest that, under our methodology, it is possible to discern between young healthy patients group and unhealthy ones, using data sequences of 20-30 minutes of electrocardiographic signal. This is because with our methodology, an efficiency greater than 90% ($AUC > 0.90$) can be achieved with this signal time, according to Figure 10.13 and Table 10.1. We suggest as an adequate partition that with $\kappa = 7$ and whose atoms

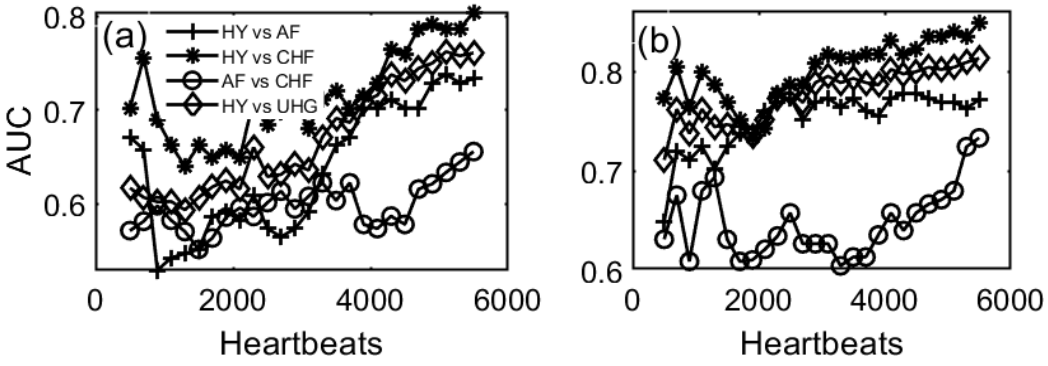

Figure 10.14: AUC for different values of length of the recording and the comparisons of pairs of patient groups, using the symbolized RR-interval differences signals (for $\kappa = 7$). (a) in the case of the estimator $\widehat{e}_p$ and (b) for the estimator $\widehat{D}$

have sizes according to the values of the parameters $\gamma_1 = 0.8$, $\gamma_2 = 3$ and $\gamma_3 = 4.25$, for the case of the EPR estimator. For the KLD estimator, we suggest considering blocks of size 3, using a partition with $\kappa = 7$ and the sizes of the atoms scaled by the parameters $\gamma_1 = 1.5$, $\gamma_2 = 3$ and $\gamma_3 = 5$. Finally, for the MT estimator, the best results were achieved considering a partition with $\kappa = 7$ and $\gamma_1 = 1.6$, $\gamma_2 = 3$ and $\gamma_3 = 5$.

10.4 Time-irreversibility in variability signals

As we saw in Section 10.2, using the HRV as a signal, the methodology used with the estimators of EPR found in the literature, does not give conclusive results when we try to distinguish between the four groups of patients. That is, with this signal, it was not possible to discriminate the healthy elderly group from groups with medical conditions. Aiming to improve these results, we proposed an encoding technique that allows us a joint analysis of any pair of variables obtained in each heartbeat (see Section 8.10). With this encoding technique, in each heartbeat we derive information about the oscillation of two important variables of the ECG signal, namely, the duration of the heartbeat (duration of the RR-interval) and the amplitude of the P, R and T waves; as we saw in Section 8.4, we call these variables *variability signals*. The joint encoding technique is important since each variability signal represents different stages of each heartbeat. Additionally, we use the lag irreversibility function, which was introduced in Chapter 3, to discriminate between four groups of patients with different health conditions. First, in Section 10.4.2 we show the results of analyzing the variability signals individually. Next, in Section 10.4.3 we show the results of analyzing the variability signals jointly. We do this using an empirical estimation of the joint probabilities, as described in Section 8.8.

Since $\widehat{L}(\tau)$, the estimator of the LI function, can be estimated for different time scales τ, in Section 10.4.1 we first find the optimal value of γ, from which we estimate

the LI function of single variability signals (Section 10.4.2) and joint variability signals (Section 10.4.3) as a function of τ.

10.4.1 Fixing the value of γ

In Figure 10.15 we show the values of the LI function for single variability signals, for different values of γ and $\tau = 1$. In this figure we can see that the RR-interval differences signal (ΔRR) exhibits a higher value of LI for the HY group and it decreases with aging and disease. Furthermore, we see from the latter that a suitable choice for the parameter is $\gamma = 3/10$, in the sense that it allows a better discrimination between groups, i.e., for healthy young subjects the LI value (≈ 0.01832) is more than three times higher than the LI value for CHF (≈ 0.00526) and about five times higher than the LI value for AF group (≈ 0.00354). For healthy elderly subjects its LI value (≈ 0.00614) is approximately 16% higher than for CHF (≈ 0.00526) and 73% higher than for AF (≈ 0.00354). Finally, the LI value in AF is roughly 48% higher respect the CHF group. From these results we suggest that $\gamma = 3/10$ is a suitable choice to estimate $\widehat{L}(\tau)$ as a function of τ (see Section 10.4.2 below). Additionally, we plot the results of our method applied to shuffled data (SD), which shows values very close to zero as expected. As we said before, this means that the LI function values obtained come from the irreversible nature of the data and are not a consequence of the methodology or estimator used.

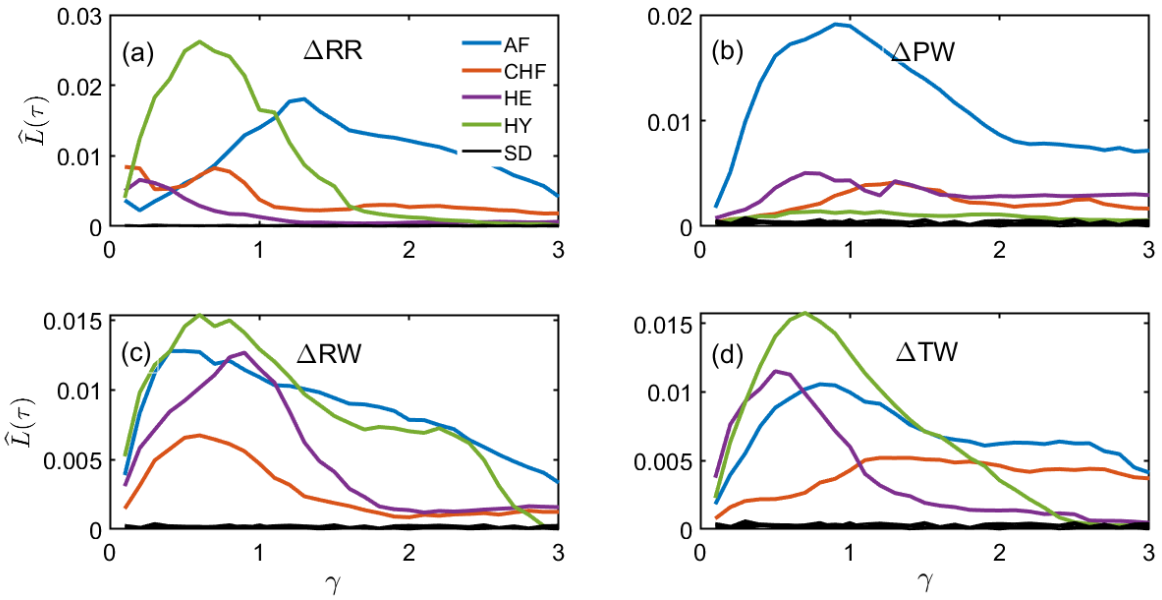

Figure 10.15: Lag-irreversibility function of single variability signals, for different values of γ and for $\tau = 1$. (a) For ΔRR signal, (b) for the P-wave variability signal ΔPW, (c) for the R-wave variability signal ΔTW and (d) for the T-wave variability signal ΔRW.

The main advantage of the LI function is found in the case of the joint variability signals. We carry out the same exploratory study, that is, we estimate LI function for $\tau = 1$

and different values of γ, which we show in Figure 10.16. We can see that joint encoding cases involving RR-interval differences signal $((\Delta RR, \Delta PW), (\Delta RR, \Delta RW), (\Delta RR, \Delta TW))$ allows better and consistent discrimination between groups of healthy patients from those with some adverse health condition. For example, for the case $(\Delta RR, \Delta PW)$, the LI value of the healthy young group is ≈ 0.0421, which is four times greater than that for the CHF group (≈ 0.0106) and two times greater than the value for the AF group (≈ 0.0207), while the LI value of the group HE (≈ 0.0356) is three times greater than that for the CHF group and two times greater than the value for the AF group. Similar results are obtained for $(\Delta RR, \Delta RW), (\Delta RR, \Delta TW)$. All these results were obtained using $\gamma = 3/10$ for the three cases (see Table 10.2 below). Accordingly, we will use that value to estimate $\widehat{L}(\tau)$ as a function of τ, in Section 10.4.3.

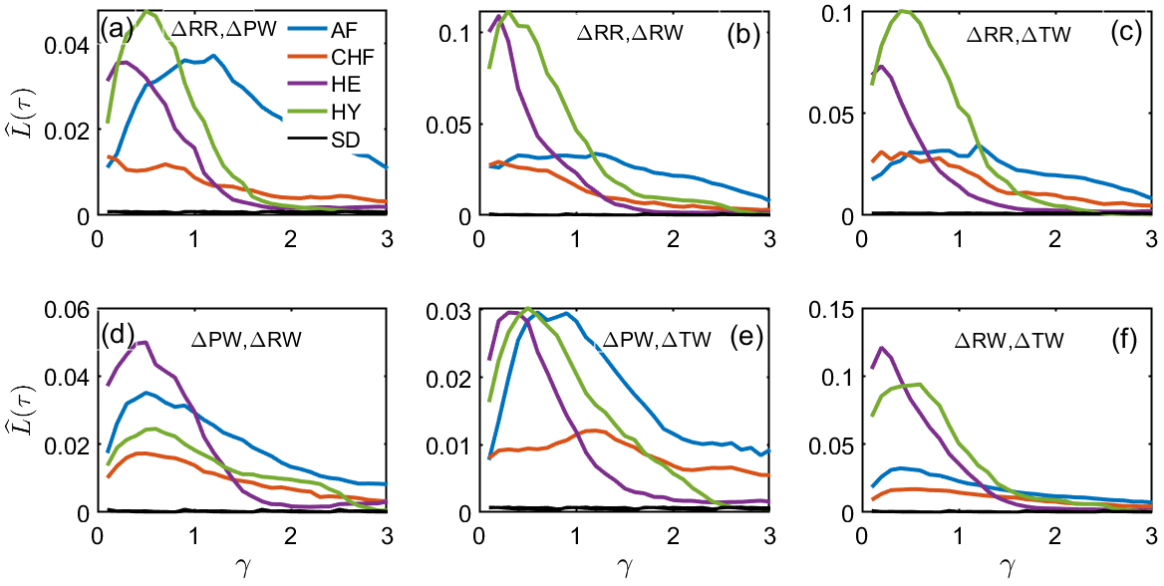

Figure 10.16: Lag-irreversibility function of joint variability signals differences, for different values of γ and for $\tau = 1$. There are six possible pair joint signals: (a) (ΔRR, ΔPW), (b) (ΔRR, ΔRW), (c) (ΔRR, ΔTW), (d) (ΔPW, ΔRW), (e) (ΔPW, ΔTW) and (f) (ΔRW, ΔTW).

10.4.2 Lag-irreversibility of single variability signals

In Figure 10.17 we can see the LI function of all the single variability signals differences as a function of τ. We can see in Figure 10.17(a) that the LI function of ΔRR signal for the HY group is larger than for the other groups. The latter means that LI function of the RR-intervals signal might be used as a tool for discriminating between healthy young individuals from the other individuals under study. However, we can see in Figure 10.17(a) that by individually encoding each variability signal, this estimator does not seem to yield conclusive results to separate the healthy elderly group from the

	ΔRR,ΔPW	ΔRR,ΔRW	ΔRR,ΔTW
HY	0.04217	0.11155	0.09455
HE	0.03566	0.09478	0.06762
CHF	0.01063	0.02748	0.02745
AF	0.02075	0.02993	0.02519
$\widehat{L}(\tau = 1)$ and $\gamma = 3/10$			

Table 10.2: $\widehat{L}(1)$ values for joint variability signals differences (ΔRR,ΔPW), (ΔRR,ΔRW) and (ΔRR,ΔTW) using parameter $\gamma = 3/10$. The obtained values for the $\widehat{L}(1)$ function are consistent with the hypothesis that healthy patients exhibit higher values than unhealthy subjects.

two groups with medical conditions, as happened with the EPR and KLD estimators. Additionally, in Figure 10.17 (b), (c) and (d), we observe that the LI function of ΔPW, ΔRW and ΔTW, respectively, does not allow us to achieve consistent results, since it is expected that the group of young healthy patients exhibits the highest irreversibility values, according to what was reported in [7]. Aiming to obtain results that allow us to discriminate between the four groups of patients, we jointly analyze the variability signals in the following Section.

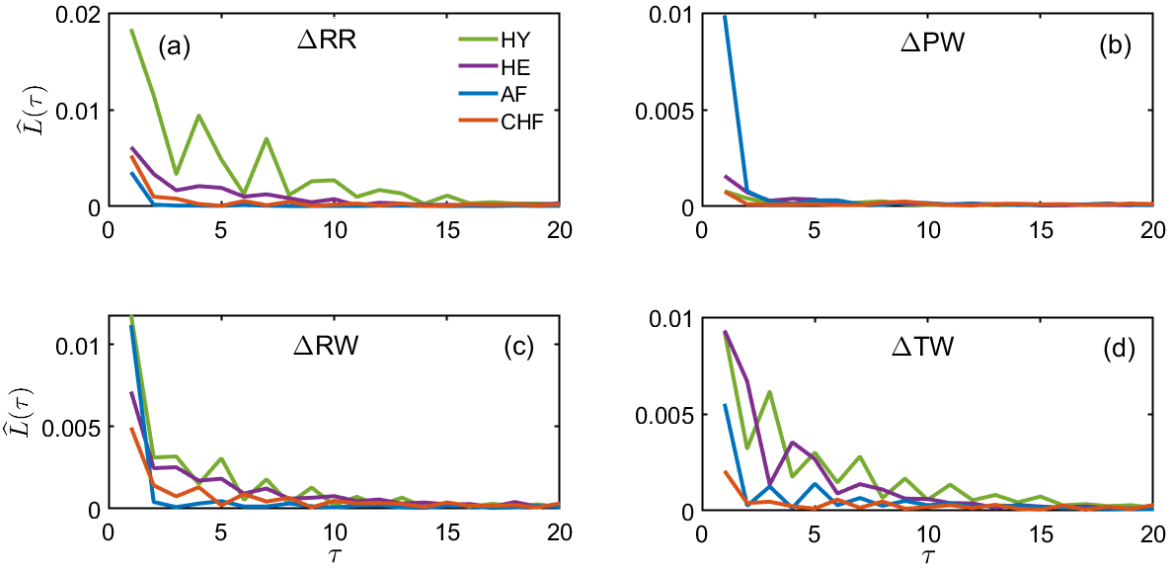

Figure 10.17: Lag-irreversibility function of single variability signals differences. We show the estimated LI functions, $\widehat{L}(\tau)$, for (a) RR-interval differences signal, (b) PW differences signal, (c) RW differences signal and (d) TW differences signal. This figure suggests that $\widehat{L}(\tau)$ for the ΔRR signal might be used as a discriminator of healthy patients from the other groups.

10.4.3 Lag-irreversibility of joint variability signals

Provided that the LI function of a single variability signal differences gives concluding results only for the ΔRR signal, we go further and consider a joint variability signal study. We expect that the joint analysis provides us with information related to the irreversible properties of the process that cannot be drawn by individually analyzing a single variability signal. This is because variability signals are not necessarily independent, since they represent different stages of the cardiac cycle.

In Figure 10.18 we can see the resulting LI functions estimated from the six cases of pair variability signals differences: (a) (ΔRR, ΔPW), (b) (ΔRR, ΔRW), (c) (ΔRR, ΔTW),(d) (ΔPW, ΔRW), (e) (ΔPW, ΔTW) and (f) (ΔRW, ΔTW). In order to estimate the LI function, we first performed the symbolic encoding scheme described in Section 8.10. For every pair of variability signals differences, we obtained a symbolic time series made up of nine symbols, which we used to estimate the LI function using the method described in Section 8.8. In every panel of Figure 10.18 we show the average LI function for every case of joint encoding. We can qualitatively observe in that figure that almost all cases allow us to distinguish between healthy individuals (young and elderly) from those individuals with an adverse health condition. A clear exception is observed in Figure 10.18(d) where the analysis of the pair (ΔPW, ΔRW) fails to achieve satisfactory discrimination between health conditions. Next, in section 10.4.4, we test the performance of this methodology of discrimination by quantifying its accuracy using ROC analysis (see Chapter 9).

10.4.4 ROC analysis

In this section, we perform the ROC analysis of our results (see Chapter 9). We use this methodology to discriminate between eight pairs of patient groups, namely, HY vs AF, HY vs CHF, HY vs UHG, HY vs HE, HE vs AF, HE vs CHF, HE vs UH and AF vs CHF; the group UHG (unhealthy group), is made up of patients exhibiting any of the adverse health conditions, AF or CHF. On the other hand, for practical reasons, we are interested in having the highest value of AUC, using the shortest signal time as possible. Consequently, in Figure 10.19, we show the AUC values as a function of time (heartbeats), for the eight pairs of patient groups and the six encoding cases.

In Figure 10.19, we can see that with cases (ΔRR, ΔPW), (ΔRR, ΔRW) and (ΔRR, ΔTW), which involve RR-interval differences signal (ΔRR), it is possible to distinguish more clearly between the two groups of healthy patients (HY and HE) and those with medical conditions. Specifically, the two pairs of groups that show the greatest area under the curve (AUC$>$ 0.80) are HY vs AF, HY vs CHF and HY vs UHG, i.e., the methodology makes it possible to better distinguish between the group of healthy young patients from those with any of the medical conditions. The two pairs of groups

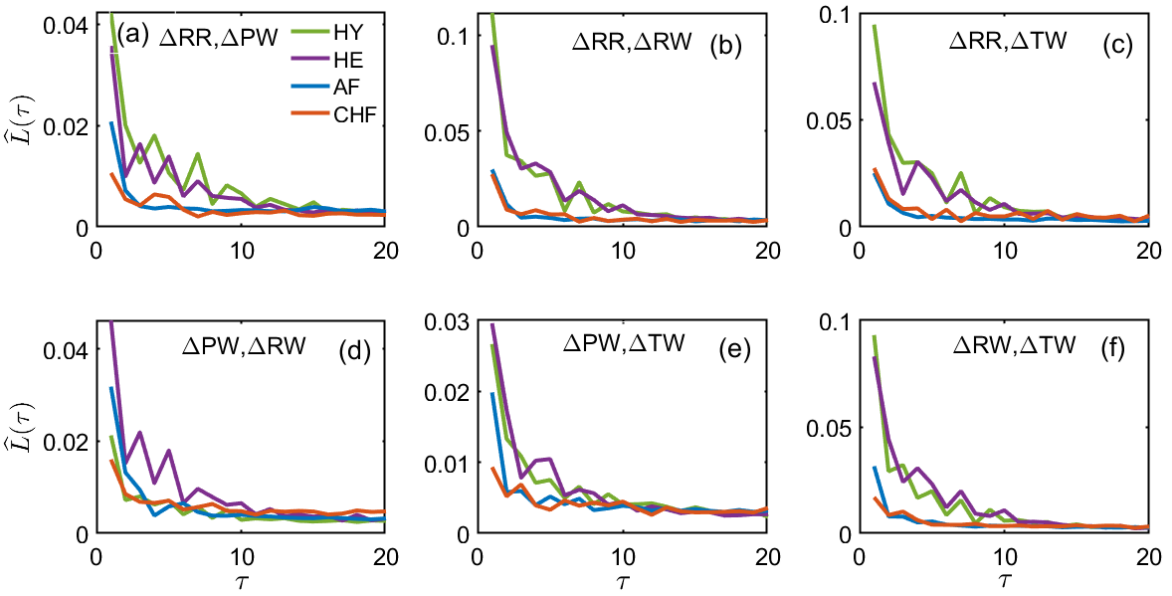

Figure 10.18: Lag-irreversibility functions of joint variability signals differences. We show the estimated LI function of joint signal, i.e., we consider two signals obtained from an ECG to obtain the LI function. (a) (ΔRR, ΔPW), (b) (ΔRR, ΔRW), (c) (ΔRR, ΔTW),(d) (ΔPW, ΔRW), (e) (ΔPW, ΔTW) and (f) (ΔRW, ΔTW). This encoding procedure results in a time series with a states space of nine symbols (see Section **??**).

that yield the lowest AUC value (≈ 5.5) are HY vs HE and AF vs CHF. In cases (ΔRR, ΔRW) and (ΔRR, ΔTW), the maximum AUC values (> 0.8) can be obtained using approximately 3 000 heartbeats. Regarding cases (ΔPW, ΔRW), (ΔPW, ΔTW) and (ΔRW, ΔTW), they yield AUC values similar to the previous cases, but to distinguish between the unhealthy groups. Explicitly, the case (ΔPW, ΔTW) allows reaching AUC values close to 0.8, to distinguish between the two groups with medical conditions.

The results described above are shown quantitatively in Tables 10.3 and 10.4, which show the AUC values obtained when using the full signal (5 500 heartbeats). We can see that values close to 0.80 or greater are reached with pairs HY vs CHF, HY vs AF and HY vs UHG, when joint encoding includes RR-interval differences signal ((ΔRR, ΔPW), (ΔRR, ΔRW), (ΔRR, ΔTW)). In other words, we can say that, within the accuracy of our statistical analysis, this methodology is good enough for distinguishing between these groups of patients (up to 80% of the analyzed cases). An interesting case not yet reported in the literature is the group of HE patients. We see that our methodology makes it possible to discriminate this group from healthy young or individuals with AF or CHF up to 70% of the analyzed cases (AUC> 0.70). As mentioned above, these maximum AUC values can be achieved using approximately 3 000 heartbeats, which, in real time, is approximately 25-30 minutes of electrocardiographic signal.

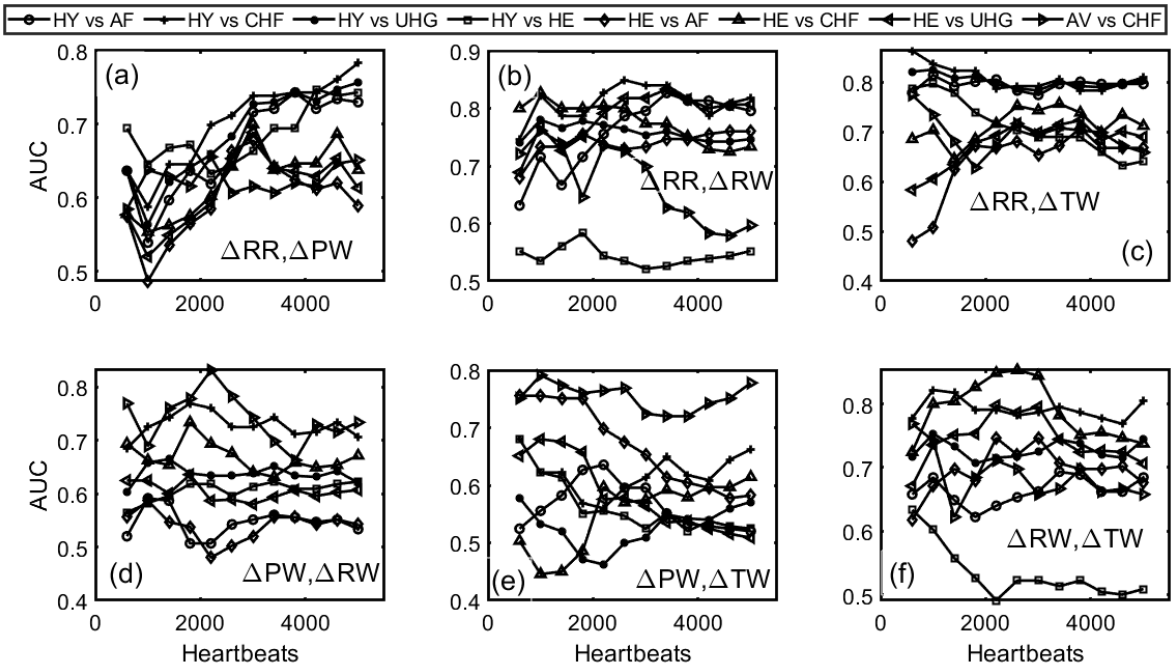

Figure 10.19: AUC as a function of time for the joint variability signal analysis, for (a) (ΔRR, ΔPW), (b) (ΔRR, ΔRW), (c) (ΔRR, ΔTW), (d) (ΔPW, ΔRW), (e) (ΔPW, ΔTW) and (f) (ΔRW, ΔTW).

	AUC		
	$\Delta RR, \Delta PW$	$\Delta RR, \Delta RW$	$\Delta RR, \Delta TW$
HY vs AF	0.7300	0.8266	0.7966
HY vs CHF	0.7833	0.8488	0.8300
HY vs UHG	0.7566	0.7466	0.8033
HY vs HE	0.7433	0.5722	0.6611
HE vs AF	0.6200	0.7600	0.6677
HE vs CHF	0.6866	0.7733	0.7344
HE vs UHG	0.6133	0.8066	0.7011
AF vs CHF	0.6511	0.6188	0.6988

Table 10.3: Area under the ROC curve for joint variability signals with ΔRR, using $\tau = 1$. One can see from this table that under our method using signals with ΔRR one can obtain a good discrimination between healthy groups (HY and HE) and the unhealthy groups (AF, CHF and UH).

	AUC		
	$\Delta PW, \Delta RW$	$\Delta PW, \Delta TW$	$\Delta RW, \Delta TW$
HY vs AF	0.5333	0.5200	0.6844
HY vs CHF	0.7333	0.6622	0.8044
HY vs UHG	0.6422	0.5711	0.7444
HY vs HE	0.6222	0.5244	0.5088
HE vs AF	0.5555	0.5822	0.7022
HE vs CHF	0.6711	0.6144	0.7555
HE vs UHG	0.6066	0.5377	0.7244
AF vs CHF	0.7333	0.7777	0.6666

Table 10.4: Area under the ROC curve for joint variability signals, using $\tau = 1$. Despite the fact that the results using variability signals without considering the ΔRR signal are not completely conclusive, one can still have a good discrimination between HY and CHF groups using $(\Delta RW, \Delta TW)$ joint variability signals, or even discriminating between AF and CHF group using $(\Delta PW, \Delta TW)$ joint variability signals, for instance.

Chapter 11

Final remarks

In this thesis, we study the time-irreversibility of Cardiac Electrical Activity. Expressly, we use the entropy production rate in the electrocardiographic signal to discriminate between four groups of patients: HY, HE, AF and CHF. We propose to analyze the signal in three different categories, namely, (1) the electrocardiographic signal, (2) RR-intervals signal and (3) joint variability signals, for which we proposed an encoding method. After the data encoding process is completed, we directly use the symbolic sequences of these signals to empirically construct the entropy production rate estimators found in the literature ($\widehat{e}_p$, $\widehat{D}$ and $\widehat{M}$).

In the case of the electrocardiographic signal, we show that, under this scheme, these estimators exhibited good results in separating the 4 groups of patients. However, when we analyze the RR-intervals, the results show that these estimators do not give conclusive results to discriminate between the group of healthy elderly subjects from the two ill groups. Aiming to improve these results, we proposed an encoding technique that allows us to derive additional information in each heartbeat, namely, the duration of the heartbeat and the amplitude of the P, R and T waves. In addition, we introduced a time-irreversibility indicator, the so-called *Lag Irreversibility Function*, which allows us to analyze any pair of variables obtained in electrocardiograms. We show that this methodology allows discrimination in the four groups of patients.

In order to provide a quantitative study of the accuracy of our results, we apply the ROC analysis to our methodology to discriminate between different groups of patients. According to this analysis, we obtain a very good performance. Our method has the feature that we let the partition have atoms of different sizes in the symbolization procedure. Another difference with related research is that we start the construction of the partition centered at the mean value of the time series itself and selecting the best set of parameters permits us to detect the typical fluctuations of the signals. A practical advantage of our method, with respect to similar methods in the literature, is that we obtain satisfactory results using around 20 to 30 minutes of signal recordings.

We point out that for the case of the RR-interval sequences, one observes that a 5500-heartbeats-long signal might not be a sufficiently large data sequence for having conclusive results. However, it is still valid for the discrimination of the healthy group from the diseased patients, which can be attained up to a certain level of accuracy. As a matter of discussion, we think that the method applied to RR-interval sequences and

ECG signals are, somehow, complementary in the sense that in the case of the ECG signals, the CHF group shows lower irreversibility features, while the AF group does for the case of the *RR*-interval signals.

As a final comment, we should mention that *Lag Irreversibility Function* is a function depending on the time delay (i.e., the lag). This characteristic distinguishes it from most irreversibility measures documented in existing literature. Consequently, comparing this approach with other measures becomes a challenging task. Nevertheless, for our research, what truly matters in comparing time-irreversibility indices, is their efficacy in categorizing ECG signals from different health conditions based on their time-irreversibility property. The actual assessment of the *Lag Irreversibility Function* performance is accomplished through ROC analysis. In principle, any time-irreversibility index (for example, those we can found in Ref. [16]) could be employed to determine whether the signals extracted from electrocardiograms are reversible or not, aiming to accomplish electrocardiograms classification based on health condition. However, according to what we discussed in Section 7.2, some indices may prove more or less successful in classifying electrocardiograms solely based on the irreversibility property. This serves as an initial step in comparing our technique with others outlined in the current literature.

11.1 Future directions

We hope that the results obtained in this thesis can enrich the literature on electrocardiogram analysis using the temporal irreversibility approach. Furthermore, we hope that our future work will also allow us to obtain information with which it is possible to predict medical conditions. In this context, during the development of this research, a series of ideas emerged that make it possible to improve its scope.

11.1.1 State of the art

Although in this thesis we reproduce the methodology proposed so far to analyze electrocardiograms using the temporal irreversibility approach, a statistical evaluation of the performance of each of these methodologies is needed, which is not easy work. Considering practical aspects, this analysis should show which estimator allows us to obtain more evident discrimination between the different groups of patients and the one that allows these results to be obtained using the shortest amount of signal possible (sampling time).

11.1.2 Encoding techniques

In this thesis, we encode the data from the electrocardiographic signal and the variability signals. In principle, we could conduct an experimental design to test different combinations of variables (intervals, segments, duration and amplitude of the waves) that can be obtained from the ECG for data encoding. However, different medical conditions could allow us to reduce the number of tests and provide us with new insights. For example, analyze data based on QT and RR intervals. This is because in a normal heartbeat, the QT interval should measure less than half the length of the previous RR interval [57]. This suggests that we could encode the data considering fluctuations in the QT interval with respect to the RR interval. Furthermore, in normal sinus rhythm, the PP interval is equal to the RR interval, which is altered in the presence of some arrhythmias [55]. This represents an opportunity to encode ECG from these variables.

11.1.3 Scope of the results

Our results include threshold values of the entropy production with which the maximum AUC values are obtained, that is, the threshold values that allow us to discriminate between pairs of patient groups best. A complementary work is to obtain electrocardiograms of healthy people with the same medical conditions (AF and CHF) and evaluate the prediction capacity of our results when using the threshold values obtained.

11.1.4 Open-source libraries

Develop open-source libraries to implement our algorithm in MATLAB and Python. Furthermore, in the context of future applications, if the results are satisfactory, an interesting work would be to optimize the computational algorithms developed, so that they can be programmed into smart devices.

11.1.5 Analysis of electroencephalograms

On the one hand, in [91] the authors use the permutations-based time irreversibility to characterize electroencephalographic signals. On the other hand, the lag irreversibility function can be used to evaluate irreversibility in discrete time series, regardless of their source. In this context, the analysis of electroencephalograms arises as an application area. A proposed work would be to use the LI Function as a tool for discrimination between electroencephalograms of different groups of patients and then evaluate the effectiveness of the results obtained and make a comparison with the existing methodology.

11.1.6 Properties of $L(\tau)$

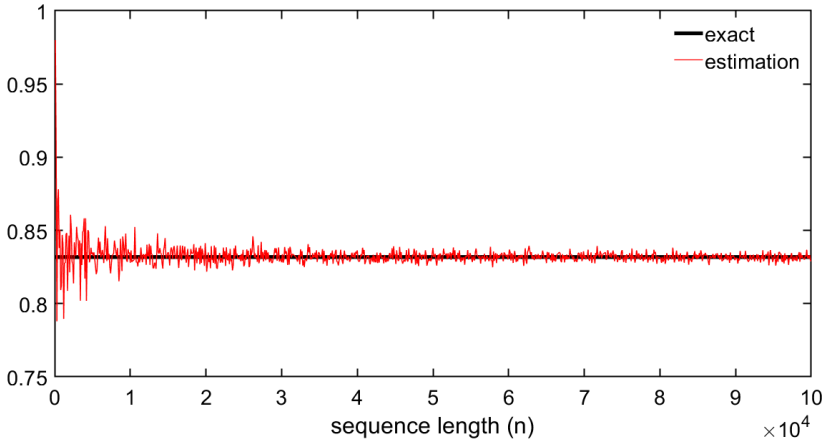

Figure 11.1: EPR in a Markov process, whose transition matrix is given by the equation 3.25. In black we show the exact value of the EPR for $p = 0.80$ and in red we show the value estimated using the $\widehat{L}(\tau)$ estimator, for $\tau = 1$ and $n = 100000$.

The simulations in Figure 4.1(d) show numerical evidence that the proposed irreversibility estimator, $L(\tau)$, is equal to zero, for all τ, when the process is reversible. Therefore, proof that $L(\tau) = 0$ for all τ if and only if the process is reversible is an unfinished problem. Additionally, Figure 11.1 shows numerical evidence that $L(\tau)$, converges to the enropy production rate and therefore, an interesting work would be to study such convergence from a rigorous point of view.

Bibliography

[1] C. Maes and K. Netočnỳ, "Time-reversal and entropy," *Journal of statistical physics*, vol. 110, pp. 269–310, 2003.

[2] P. Gaspard, "Time-reversed dynamical entropy and irreversibility in markovian random processes," *Journal of Statistical Physics*, vol. 117, no. 3-4, pp. 599–615, 2004.

[3] F. S. Gnesotto, F. Mura, J. Gladrow, and C. P. Broedersz, "Broken detailed balance and non-equilibrium dynamics in living systems: a review," *Reports on Progress in Physics*, vol. 81, no. 6, p. 066601, 2018.

[4] R. Salgado-García, "Time-irreversibility test for random-length time series: The matching-time approach applied to dna," *Chaos: An Interdisciplinary Journal of Nonlinear Science*, vol. 31, no. 12, p. 123126, 2021.

[5] M. Gilson, E. Tagliazucchi, and R. Cofré, "Entropy production of multivariate ornstein-uhlenbeck processes correlates with consciousness levels in the human brain," *Phys. Rev. E*, vol. 107, p. 024121, Feb 2023.

[6] R. Cofré and C. Maldonado, "Information entropy production of maximum entropy markov chains from spike trains," *Entropy*, vol. 20, no. 1, 2018.

[7] M. Costa, A. L. Goldberger, and C.-K. Peng, "Broken asymmetry of the human heartbeat: loss of time irreversibility in aging and disease," *Physical Review Letters*, vol. 95, no. 19, p. 198102, 2005.

[8] C. Daw, C. Finney, and M. Kennel, "Symbolic approach for measuring temporal "irreversibility"," *Physical Review E*, vol. 62, no. 2, p. 1912, 2000.

[9] A. Porporato, J. Rigby, and E. Daly, "Irreversibility and fluctuation theorem in stationary time series," *Physical Review Letters*, vol. 98, no. 9, p. 094101, 2007.

[10] E. Roldán and J. M. R. Parrondo, "Entropy production and kullback-leibler divergence between stationary trajectories of discrete systems," *Physical Review E*, vol. 85, p. 031129, Mar 2012.

[11] E. Roldán and J. M. R. Parrondo, "Estimating dissipation from single stationary trajectories," *Phys. Rev. Lett.*, vol. 105, p. 150607, Oct 2010.

[12] J. H. Martínez, J. L. Herrera-Diestra, and M. Chavez, "Detection of time reversibility in time series by ordinal patterns analysis," *Chaos: An Interdisciplinary Journal of Nonlinear Science*, vol. 28, no. 12, 2018.

[13] L. Lacasa, A. Nunez, É. Roldán, J. M. Parrondo, and B. Luque, "Time series irreversibility: a visibility graph approach," *The European Physical Journal B*, vol. 85, pp. 1–11, 2012.

[14] J.-R. Chazottes and F. Redig, "Testing the irreversibility of a gibbsian process via hitting and return times," *Nonlinearity*, vol. 18, no. 6, p. 2477, 2005.

[15] R. Salgado-Garcia and C. Maldonado, "Estimating entropy rate from censored symbolic time series: A test for time-irreversibility," *Chaos: An Interdisciplinary Journal of Nonlinear Science*, vol. 31, no. 1, 2021.

[16] M. Zanin and D. Papo, "Algorithmic approaches for assessing irreversibility in time series: Review and comparison," *Entropy*, vol. 23, no. 11, p. 1474, 2021.

[17] N. Sarlis, S.-R. Christopoulos, and M. Bemplidaki, "Change δs of the entropy in natural time under time reversal: Complexity measures upon change of scale," *Europhysics Letters*, vol. 109, no. 1, p. 18002, 2015.

[18] C. K. Karmakar, A. Khandoker, J. Gubbi, and M. Palaniswami, "Defining asymmetry in heart rate variability signals using a poincaré plot," *Physiological measurement*, vol. 30, no. 11, p. 1227, 2009.

[19] P. Guzik, J. Piskorski, T. Krauze, A. Wykretowicz, and H. Wysocki, "Heart rate asymmetry by poincaré plots of rr intervals," 2006.

[20] C. Karmakar, A. Khandoker, and M. Palaniswami, "Phase asymmetry of heart rate variability signal," *Physiological measurement*, vol. 36, no. 2, p. 303, 2015.

[21] C. Yan, P. Li, L. Ji, L. Yao, C. Karmakar, and C. Liu, "Area asymmetry of heart rate variability signal," *Biomedical engineering online*, vol. 16, no. 1, pp. 1–14, 2017.

[22] F. Hou, X. Huang, Y. Chen, C. Huo, H. Liu, and X. Ning, "Combination of equiprobable symbolization and time reversal asymmetry for heartbeat interval series analysis," *Physical Review E*, vol. 87, no. 1, p. 012908, 2013.

[23] C. Cammarota and E. Rogora, "Time reversal, symbolic series and irreversibility of human heartbeat," *Chaos, Solitons & Fractals*, vol. 32, no. 5, pp. 1649–1654, 2007.

[24] A. L. Goldberger, L. A. Amaral, L. Glass, J. M. Hausdorff, P. C. Ivanov, R. G. Mark, J. E. Mietus, G. B. Moody, C.-K. Peng, and H. E. Stanley, "Physiobank,

physiotoolkit, and physionet: Components of a new research resource for complex physiologic signals," *Circulation*, vol. 101, no. 23, pp. e215–e220, 2000.

[25] R. M. Feldman and C. Valdez-Flores, *Applied probability and stochastic processes*, vol. 2. Springer, 2010.

[26] G. A. Pavliotis, *Stochastic processes and applications*. Springer, 2016.

[27] R. Durrett and R. Durrett, *Essentials of stochastic processes*, vol. 1. Springer, 2012.

[28] D. Gusak, A. Kukush, A. Kulik, Y. Mishura, and A. Pilipenko, "Theory of stochastic processes," *Problem Books in Math. Springer, New York*, 2010.

[29] J. Jacod and P. Protter, *Probability essentials*. Springer Science & Business Media, 2004.

[30] U. R. Acharya, S. M. Krishnan, J. A. Spaan, and J. S. Suri, *Advances in cardiac signal processing*, vol. 8. Springer, 2007.

[31] A. Gacek and W. Pedrycz, *ECG signal processing, classification and interpretation: a comprehensive framework of computational intelligence*. Springer Science & Business Media, 2011.

[32] P. S. Addison, "Wavelet transforms and the ecg: a review," *Physiological measurement*, vol. 26, no. 5, p. R155, 2005.

[33] B. N. Singh and A. K. Tiwari, "Optimal selection of wavelet basis function applied to ecg signal denoising," *Digital signal processing*, vol. 16, no. 3, pp. 275–287, 2006.

[34] S. P. Singh and S. Urooj, "Wavelets: biomedical applications," *International Journal of Biomedical Engineering and Technology*, vol. 19, no. 1, pp. 1–25, 2015.

[35] G. E. Box, G. M. Jenkins, G. C. Reinsel, and G. M. Ljung, *Time series analysis: forecasting and control*. John Wiley & Sons, 2015.

[36] J. M. Amigó, K. Keller, and V. A. Unakafova, "Ordinal symbolic analysis and its application to biomedical recordings," *Phil. Trans. R. Soc. A*, vol. 373, no. 2034, p. 20140091, 2015.

[37] R. H. Shumway, D. S. Stoffer, and D. S. Stoffer, *Time series analysis and its applications*, vol. 3. Springer, 2000.

[38] T. M. Cover, *Elements of information theory*. John Wiley & Sons, 1999.

[39] W. Greiner, L. Neise, and H. Stöcker, *Thermodynamics and statistical mechanics*. Springer Science & Business Media, 2012.

[40] Y. A. Cengel, M. A. Boles, and M. Kanoğlu, *Thermodynamics: an engineering approach*, vol. 5. McGraw-hill New York, 2011.

[41] K. Gritsalak, "States of matter. solid , liquid and gas vector on white background. urlhttps." Accessed May 27, 2024. https://www.dreamstime.com/states-matter-solid-liquid-gas-vector-white-background-states-matter\-solid-liquid-gas-vector-image110701771.

[42] "Estados fÍsicos da Água e suas mudanÇas. urlhttps." Accessed May 23, 2024. https://www.overleaf.com/project/659f939a26edb8b655292c38.

[43] É. Roldán, *Irreversibility and dissipation in microscopic systems*. Springer, 2014.

[44] É. Roldán and J. M. Parrondo, "Estimating dissipation from single stationary trajectories," *Physical review letters*, vol. 105, no. 15, p. 150607, 2010.

[45] A. Lawrance, "Directionality and reversibility in time series," *International Statistical Review/Revue Internationale de Statistique*, pp. 67–79, 1991.

[46] P. Gaspard, "Time-reversed dynamical entropy and irreversibility in markovian random processes," *Journal of statistical physics*, vol. 117, pp. 599–615, 2004.

[47] D. Andrieux, P. Gaspard, S. Ciliberto, N. Garnier, S. Joubaud, and A. Petrosyan, "Thermodynamic time asymmetry in non-equilibrium fluctuations," *Journal of Statistical Mechanics: Theory and Experiment*, vol. 2008, no. 01, p. P01002, 2008.

[48] C. Maes, "The fluctuation theorem as a Gibbs property," *Journal of Statistical Physics*, vol. 95, no. 1-2, pp. 367–392, 1999.

[49] A. Antos and I. Kontoyiannis, "Convergence properties of functional estimates for discrete distributions," *Random Structures & Algorithms*, vol. 19, no. 3-4, pp. 163–193, 2001.

[50] I. Kontoyiannis, "Asymptotic recurrence and waiting times for stationary processes," *Journal of Theoretical Probability*, vol. 11, pp. 795–811, 1998.

[51] N. Merino-Negrete, C. Maldonado, and R. Salgado-García, "Sorting ecgs by lag irreversibility," *Physica D: Nonlinear Phenomena*, vol. 459, p. 134022, 2024.

[52] A. Antos and I. Kontoyiannis, "Convergence properties of functional estimates for discrete distributions," *Random Structures & Algorithms*, vol. 19, no. 3-4, pp. 163–193, 2001.

[53] C. Maldonado and N. Merino-Negrete, "Irreversibility indices as discriminators of heart conditions from electrocardiographic signals," *Physica A: Statistical Mechanics and its Applications*, vol. 637, p. 129584, 2024.

[54] P. C. Shields, *The ergodic theory of discrete sample paths*, vol. 13 of *Graduate Studies in Mathematics*. Providence, RI: American Mathematical Society, 1996.

[55] A. L. Goldberger, Z. D. Goldberger, and A. Shvilkin, *Goldberger's Clinical Electrocardiography*. Elsevier, ninth edition ed., 2018.

[56] R. Karthik, "Ecg simulation using matlab." Accessed May 29, 2024. `https://www.mathworks.com/matlabcentral/fileexchange/10858-ecg-simulation-using-matlab`.

[57] T. B. Garcia, *12-lead ECG: The art of interpretation*. Jones & Bartlett Learning, 2015.

[58] O. C. Mimenza, "Las 13 partes del corazón humano (y sus funciones). urlhttps." Accessed May 29, 2024. `https://psicologiaymente.com/salud/partes-del-corazon`.

[59] M. K. Lahiri, P. J. Kannankeril, and J. J. Goldberger, "Assessment of autonomic function in cardiovascular disease: Physiological basis and prognostic implications," *Journal of the American College of Cardiology*, vol. 51, no. 18, pp. 1725–1733, 2008.

[60] E. Buccelletti, E. Gilardi, E. Scaini, L. Galiuto, R. Persiani, A. Biondi, F. Basile, N. G. Silveri, *et al.*, "Heart rate variability and myocardial infarction: systematic literature review and metanalysis," *Eur Rev Med Pharmacol Sci*, vol. 13, no. 4, pp. 299–307, 2009.

[61] F. Lombardi, "Origin of heart rate variability and turbulence: an appraisal of autonomic modulation of cardiovascular function," *Frontiers in physiology*, vol. 2, p. 95, 2011.

[62] U. Rajendra Acharya, K. Paul Joseph, N. Kannathal, C. M. Lim, and J. S. Suri, "Heart rate variability: a review," *Medical and biological engineering and computing*, vol. 44, pp. 1031–1051, 2006.

[63] J. Piskorski and P. Guzik, "The structure of heart rate asymmetry: deceleration and acceleration runs," *Physiological measurement*, vol. 32, no. 8, p. 1011, 2011.

[64] P. Guzik, B. Bychowiec, J. Piskorski, A. Wegrzynowski, T. Krauze, R. Schneider, P. Liszkowski, A. Wykretowicz, B. Wierusz-Wysocka, and H. Wysocki, "Heart rate

variability by poincaré plot and spectral analysis in young healthy subjects and patients with type 1 diabetes," *Folia Cardiol*, vol. 12, no. suppl D, pp. 64–67, 2005.

[65] P. K. Stein, P. P. Domitrovich, H. V. Huikuri, R. E. Kleiger, and C. Investigators, "Traditional and nonlinear heart rate variability are each independently associated with mortality after myocardial infarction," *Journal of cardiovascular electrophysiology*, vol. 16, no. 1, pp. 13–20, 2005.

[66] U. Meyerfeldt, N. Wessel, H. Schütt, D. Selbig, A. Schumann, A. Voss, J. Kurths, C. Ziehmann, R. Dietz, and A. Schirdewan, "Heart rate variability before the onset of ventricular tachycardia: differences between slow and fast arrhythmias," *International journal of Cardiology*, vol. 84, no. 2-3, pp. 141–151, 2002.

[67] V. Houshyarifar and M. C. Amirani, "Early detection of sudden cardiac death using poincaré plots and recurrence plot-based features from hrv signals," *Turkish Journal of Electrical Engineering & Computer Sciences*, vol. 25, no. 2, pp. 1541–1553, 2017.

[68] F. Shaffer and J. Ginsberg, "An overview of heart rate variability metrics and norms," *Frontiers in public health*, vol. 5, p. 258, 2017.

[69] A. H. Khandoker, C. Karmakar, M. Brennan, M. Palaniswami, and A. Voss, *Poincaré plot methods for heart rate variability analysis*. Springer, 2013.

[70] J. Piskorski and P. Guzik, "Geometry of the poincaré plot of rr intervals and its asymmetry in healthy adults," *Physiological measurement*, vol. 28, no. 3, p. 287, 2007.

[71] A. Porta, S. Guzzetti, N. Montano, T. Gnecchi-Ruscone, R. Furlan, and A. Malliani, "Time reversibility in short-term heart period variability," in *2006 Computers in Cardiology*, pp. 77–80, IEEE, 2006.

[72] C. L. Ehlers, J. Havstad, D. Prichard, and J. Theiler, "Low doses of ethanol reduce evidence for nonlinear structure in brain activity," *Journal of Neuroscience*, vol. 18, no. 18, pp. 7474–7486, 1998.

[73] M. D. Costa, C.-K. Peng, and A. L. Goldberger, "Multiscale analysis of heart rate dynamics: entropy and time irreversibility measures," *Cardiovascular Engineering*, vol. 8, no. 2, pp. 88–93, 2008.

[74] W. Yao, W. Yao, and J. Wang, "Equal heartbeat intervals and their effects on the nonlinearity of permutation-based time irreversibility in heart rate," *Physics Letters A*, vol. 383, no. 15, pp. 1764–1771, 2019.

[75] I. Silva and G. B. Moody, "An open-source toolbox for analysing and processing physionet databases in matlab and octave," *Journal of open research software*, vol. 2, no. 1, 2014.

[76] N. Iyengar, C. Peng, R. Morin, A. L. Goldberger, and L. A. Lipsitz, "Age-related alterations in the fractal scaling of cardiac interbeat interval dynamics," *American Journal of Physiology-Regulatory, Integrative and Comparative Physiology*, vol. 271, no. 4, pp. R1078–R1084, 1996.

[77] D. S. Baim, W. S. Colucci, E. S. Monrad, H. S. Smith, R. F. Wright, A. Lanoue, D. F. Gauthier, B. J. Ransil, W. Grossman, and E. Braunwald, "Survival of patients with severe congestive heart failure treated with oral milrinone," *Journal of the American College of Cardiology*, vol. 7, no. 3, pp. 661–670, 1986.

[78] G. Moody, "A new method for detecting atrial fibrillation using rr intervals," *Computers in Cardiology*, pp. 227–230, 1983.

[79] D. Makowski, T. Pham, Z. J. Lau, J. C. Brammer, F. Lespinasse, H. Pham, C. Schölzel, and S. A. Chen, "Neurokit2: A python toolbox for neurophysiological signal processing," *Behavior research methods*, pp. 1–8, 2021.

[80] A. Amyar, R. Modzelewski, H. Li, and S. Ruan, "Multi-task deep learning based ct imaging analysis for covid-19 pneumonia: Classification and segmentation," *Computers in biology and medicine*, vol. 126, p. 104037, 2020.

[81] A. Y. Hannun, P. Rajpurkar, M. Haghpanahi, G. H. Tison, C. Bourn, M. P. Turakhia, and A. Y. Ng, "Cardiologist-level arrhythmia detection and classification in ambulatory electrocardiograms using a deep neural network," *Nature medicine*, vol. 25, no. 1, pp. 65–69, 2019.

[82] M. Pahar, M. Klopper, R. Warren, and T. Niesler, "Covid-19 cough classification using machine learning and global smartphone recordings," *Computers in Biology and Medicine*, vol. 135, p. 104572, 2021.

[83] T. Fawcett, "An introduction to roc analysis," *Pattern recognition letters*, vol. 27, no. 8, pp. 861–874, 2006.

[84] J. Davis and M. Goadrich, "The relationship between precision-recall and roc curves," in *Proceedings of the 23rd international conference on Machine learning*, pp. 233–240, 2006.

[85] G. Forman, "A method for discovering the insignificance of one's best classifier and the unlearnability of a classification task'," in *Proc. First Internat. Workshop*

on Data Mining Lessons Learned (DMLL-2002). Available from: http://www. purl. org/NET/tfawcett/DMLL-2002/Forman. pdf, Citeseer, 2002.

[86] S. J. Mason and N. E. Graham, "Areas beneath the relative operating characteristics (roc) and relative operating levels (rol) curves: Statistical significance and interpretation," *Quarterly Journal of the Royal Meteorological Society: A journal of the atmospheric sciences, applied meteorology and physical oceanography*, vol. 128, no. 584, pp. 2145–2166, 2002.

[87] T. Calders and S. Jaroszewicz, "Efficient auc optimization for classification," in *European conference on principles of data mining and knowledge discovery*, pp. 42–53, Springer, 2007.

[88] J. A. Hanley and B. J. McNeil, "The meaning and use of the area under a receiver operating characteristic (roc) curve.," *Radiology*, vol. 143, no. 1, pp. 29–36, 1982.

[89] J. M. Pérez and P. P. Martin, "La curva roc," *Medicina de Familia. SEMERGEN*, vol. 49, no. 1, p. 101821, 2023.

[90] P. A. Varotsos, N. V. Sarlis, E. S. Skordas, and M. S. Lazaridou, "Identifying sudden cardiac death risk and specifying its occurrence time by analyzing electrocardiograms in natural time," *Applied Physics Letters*, vol. 91, no. 6, p. 064106, 2007.

[91] W. Yao, J. Dai, M. Perc, J. Wang, D. Yao, and D. Guo, "Permutation-based time irreversibility in epileptic electroencephalograms," *Nonlinear Dynamics*, vol. 100, pp. 907–919, 2020.

Annex

Publications and academic activities

Articles

1. MALDONADO, Cesar; MERINO–NEGRETE, Nazul. Irreversibility indices as discriminators of heart conditions from electrocardiographic signals. Physica A: Statistical Mechanics and its Applications, 2024, vol. 637, p. 129584.

2. MERINO-NEGRETE, Nazul; MALDONADO, Cesar; SALGADO-GARCÍA, Raúl. Sorting ECGs by lag irreversibility. Physica D: Nonlinear Phenomena, 2024, vol. 459, p. 134022.

3. MERINO–NEGRETE, Nazul; MALDONADO, Cesar. Time irreversibility in electrocardiograms: review and comparison (**in progress**).

Conferences and symposiums

- Merino Negrete, Nazul; Maldonado Ahumada, César. *Producción de entropía en la variabilidad del ritmo cardíaco*. LXIV Congreso Nacional de Física, del 04 al 08 de octubre de 2021.
- Merino Negrete, Nazul; Maldonado Ahumada, César. *Producción de entropía en la variabilidad del ritmo cardíaco*. 54 Congreso Nacional de la Sociedad Matemática Mexicana, del 18 al 22 de octubre de 2021.
- Merino Negrete, Nazul; Maldonado Ahumada, César. *Irreversibilidad temporal de la Actividad Eléctrica Cardíaca*. LXV Congreso Nacional de Física, del 02 al 07 de octubre de 2022.
- Merino Negrete, Nazul.*Reconocimiento de patrones en series de tiempo financieras*. Seminario de Probabilidad y Aplicaciones, 26 de octubre de 2022.
- Merino Negrete, Nazul. *Asimetría temporal de la actividad eléctrica cardíaca*. Simposio de Análisis de Señales y Modelación Estocástica, 04 de diciemre de 2023.

Divulgation activities as workshopper

- Merino Negrete, Nazul. *Nieve Científica*. Taller para 68 alumnos de nivel preescolar, el 22 de junio del 2022.
- Merino Negrete, Nazul. *fractales*. Puertas abiertas (IPICYT), 27 de octubre de 2022.

- Merino Negrete, Nazul. *La célula y sus partes*. Taller para 110 alumnos de nivel preescolar en la Escuela Francisco Gabilondo Soler Cri cri, el 28 de febrero del 2023.
- Merino Negrete, Nazul. *Eliminación de ruido en señales biomédicas*. Liga de la ciencia (IPICYT), del 03 de junio al 08 de julio de 2023.
- Merino Negrete, Nazul. *Matemáticas y el universo: fractales*. Noche de estrellas 2023, el 25 de noviembre del 2023.
- Merino Negrete, Nazul. *Fluidos mágicos*. Taller para 120 alumnos de nivel preescolar en la Escuela Sor Juana Inés de la Cruz, el 25 de abril del 2024
- Merino Negrete, Nazul. *Fluorescencia con luz ultravioleta*. Día internacional de la niña y la mujer en la ciencia, el 11 de febrero del 2024